A Thesis for the Degree of Doctor of Philosophy

Characteristics of Transcriptional Regulator OxyR2 and Flavohemoglobin HmpA in Survival Strategies of a Foodborne Pathogen *Vibrio vulnificus* under Oxidative Stress

산화 스트레스 노출 조건에서 식중독 세균
패혈증비브리오균의 전사조절자 **OxyR2** 와
플라보헤모글로빈 **HmpA** 의 특성을 통한 생존전략 규명

February, 2020

Dukyun Kim

The Graduate School
Seoul National University
Department of Agricultural Biotechnology

Characteristics of Transcriptional Regulator OxyR2 and Flavohemoglobin HmpA in Survival Strategies of a Foodborne Pathogen *Vibrio vulnificus* under Oxidative Stress

산화 스트레스 노출 조건에서 식중독 세균 패혈증비브리오균의 전사조절자 **OxyR2** 와 플라보헤모글로빈 **HmpA** 의 특성을 통한 생존전략 규명

지도교수 최 상 호

이 논문을 농학박사학위논문으로 제출함

2019 년 12 월

서울대학교 대학원

농생명공학부

김 덕 윤

김덕윤의 박사학위논문을 인준함

2019 년 12 월

위 원 장 _____(인)

부위원장 _____(인)

위 원 _____(인)

위 원 _____(인)

위 원 _____(인)

Abstract

Characteristics of Transcriptional Regulator OxyR2 and Flavohemoglobin HmpA in Survival Strategies of a Foodborne Pathogen *Vibrio vulnificus* under Oxidative Stress

Dukyun Kim

The Graduate School

Seoul National University

Department of Agricultural Biotechnology

Vibrio vulnificus is an opportunistic human pathogen whose infection can cause diseases such as life-threatening septicemia and gastroenteritis. Oxidative and nitrosative stresses, induced respectively by reactive oxygen species (ROS) and reactive nitrogen species (RNS) from the host innate immune system, threaten the survival of invading bacteria by damaging the bacterial cellular components. Therefore, for *V. vulnificus*, coping with oxidative and nitrosative stresses is crucial not only for the survival in the host but also for establishing a successful infection in

the host environment.

In this study, to understand the strategy of *V. vulnificus* to cope with oxidative stress, I analyzed the structural characteristics and mechanism of OxyR2 at the molecular level. *V. vulnificus* has two OxyRs, OxyR1 and OxyR2, which belong to the LysR-type transcriptional regulator family. Between the two OxyRs, OxyR2 recognizes relatively lower levels of H_2O_2 than OxyR1 does. OxyR2 has two conserved redox-sensing cysteines (peroxidatic and resolving cysteine). When the peroxidatic cysteine in OxyR2 are oxidized by H_2O_2, they form an intermolecular disulfide bond, and the resulting activated OxyR2 induces the transcription of *prx*2 encoding the antioxidant protein Prx2, which scavenges H_2O_2. A biochemical study identified a third redox state of OxyR2 in which the sensing cysteine of OxyR2 becomes overoxidized due to high concentrations of H_2O_2 and results in a *S*-sulfonated cysteine (Cys-SO_3H). Such modification deterred the transcription of *prx*2. These results demonstrated that OxyR2 tightly regulates the expression of *prx*2 through a three-state redox switch, thereby preventing futile production of *prx*2 in the cells when exposed to high levels of H_2O_2 sufficient to inactivate Prx2. In addition, the crystal structure of OxyR2 was determined. It was found that the substitution of the conserved Gly in other OxyRs to Glu204 in *V. vulnificus* OxyR2 causes a flipped

conformation of the peptide bond before the Glu204 residue, which then results in the rigid conformation of His 205 side chain. This conformational property of OxyR2 in *V. vulnificus* leads to the high H_2O_2 sensitivity of the protein. The peptide bond around Glu204 affects the structural rigidity of His205, which is interacting with H_2O_2. This structural characteristic of OxyR2 enables its high sensitivity to H_2O_2, which is the basis of the regulator's function.

To further understand the bacterium's survival strategies against nitrosative stress, the transcriptome change following exposure to NO was analyzed using RNA sequencing. The analysis revealed 551 differentially expressed genes upon exposure to NO. Among the genes upregulated upon exposure to NO, *VvhmpA* was identified to be the most greatly induced at the transcription level. Biochemical studies have revealed that that *Vv*HmpA is an NO-inducible flavohemoglobin containing equimolar amounts of heme and FAD. Enzyme kinetics experiments revealed that *Vv*HmpA effectively decomposes NO. Interestingly, the K_M and k_{cat} values of *Vv*HmpA for NO at 37 °C, the temperature encountered in the host, were greater than those at 30 °C, indicating that *Vv*HmpA detoxifies high levels of NO effectively during host infection. To examine the function of *Vv*HmpA in more detail, a mutant

lacking the *VvhmpA* gene was constructed. Compared with the wild type, the *VvhmpA* mutant barely decomposed exogenously supplied NO, and the growth of the *VvhmpA* mutant was impaired in the presence of NO. These result demonstrated that *Vv*HmpA contributes to the NO defense mechanism of *V. vulnificus*. In addition, the *VvhmpA* mutant showed a significant decrease in cytotoxicity toward the NO-producing macrophage RAW 264.7 cells as well as reduced survival near the RAW 264.7 cells. Furthermore, the mouse lethality of *VvhmpA* mutant was significantly attenuated compared with that of the wild type. In conclusion, *Vv*HmpA plays an important role in the bacterium's survival in the host and pathogenesis by decomposing host-derived NO.

The present study on OxyR2 and *Vv*HmpA of *V. vulnificus* adds to our understanding of the bacterial defense mechanism against the host-derived oxidative and nitrosative stresses. Further investigation into this subject area may contribute to achieving effective control of *V. vulnificus* in the future.

Keywords: *Vibrio vulnificus*, Oxidative stress, OxyR2, *Vv*HmpA

Student Number: 2016-35411

Contents

List of Figures

List of Tables

Chapter I.

Background

I-1. *Vibrio vulnificus*

Vibrio vulnificus is a Gram-negative, curved rod-shaped bacterium, which is motile with a single polar flagellum. It belongs to the *Vibrio* genus in the *Vibrionaceae* family, and like other organisms in the family, *V. vulnificus* is a facultative anaerobe capable of fermentation. However, its ability to ferment lactose is a distinctive feature from other members of the *Vibrio* genus (Strom and Paranjpye, 2000). The bacterium occurs naturally in estuarine and marine environment worldwide and thus contaminates seafood like oysters (Hor *et al*., 1995; Horseman and Surani, 2011; Wright *et al*., 1996). *V. vulnificus* is usually found in waters with temperature between 9 and 31 °C. The water temperatures above 18 °C and salinities between 15 and 25 parts per thousand (ppt) have been reported as a preferred habitat. Salinities at or greater than 30 ppt will substantially reduce the growth of *V. vulnificus* regardless of the water temperature (Horseman and Surani, 2011). Although the number of *V. vulnificus* in estuarine waters is below 10 colony forming unit (CFU)/ml, it becomes concentrated in molluscan shellfish (10^5 CFU/g of tissue) because of their filter-feeding method for obtaining food (Oliver, 2015). Interestingly, *V. vulnificus*

cells enter dormancy state and fail to grow on the rich media at temperature below 13°C. This state is commonly referred to as the “viable but nonculturable” state. In the case of *V. vulnificus*, resuscitation to culturable state occurs at warmer temperatures (Oliver, 2013).

Strains of *V. vulnificus* are classified into three biotypes based on their biochemical characteristics and host range difference. Biotype 1 produces indole and ornithine decarboxylase, exhibits several immunologically distinct lipopolysaccharide (LPS) types, and is responsible for the majority of human infections. Biotype 2 is negative for indole and ornithine decarboxylase production, expresses a common LPS type, and is primarily eel pathogens. A recently identified biotype 3 is shown to possess biochemical properties of both biotype 1 and biotype 2 and to cause human wound infection. While biotype 3 does cause human infections, these have to date been limited to Israel and to persons handing fish (Jones and Oliver, 2009; Strom and Paranjpye, 2000).

I-1-1. Disease caused by *V. vulnificus*

Consumption of raw or uncooked seafood containing *V. vulnificus* may cause a severe, fulminant systemic infection. Most patients who suffer from *V. vulnificus* infection have underlying predisposing factors, including liver damage, excess levels of iron, and immunocompromised conditions (Strom and Paranjpye, 2000). The infection results in illness ranging from fever, chills, nausea, gastroenteritis to primary septicemia (Horseman and Surani, 2011; Strom and Paranjpye, 2000). The symptoms are typically observed within 36 hours to 10 days. The mortality rate from primary septicemia is very high (>50%) and death can occur within one to two days after the first signs of illness (Horseman and Surani, 2011; Jones and Oliver, 2009; Strom and Paranjpye, 2000). The majority of primary septicemia cases by *V. vulnificus* has been reported in males over the age of 50. Although the reason for age being a risk factor is not known, estrogen, the major female hormone, appears to be protective after exposure to endotoxin (Merkel *et al*., 2001).

In addition, *V. vulnificus* can cause serious wound infections that result from contact of open wounds with water containing the bacterium and/or shellfish contaminated

with the bacterium (Oliver, 2005). In most cases, infections result from wounds that are acquired while cleaning shellfish, or from pre-existing wounds coming into contact with seawater containing *V. vulnificus.* Symptoms of *V. vulnificus*-induced wound infections include pain, erythema, and edema at the wound site. It can progress rapidly to cellulitis, ecchymoses and bullae which can progress to necrotizing fasciitis at the site of infection. Although the mortality rate for the wound infection, ranging from 20 to 30%, is lower than that for primary septicemia, even healthy people are susceptible to a serious wound infection (Oliver, 2005; Strom and Paranjpye, 2000).

Lastly, the bacterium also produces mild symptoms including diarrhea and abdominal cramps (Horseman and Surani, 2011). As in the case of fatal septicemia, gastroenteritis appears to be associated with ingestion of raw seafood. However, no fatalities from *V. vulnificus* gastroenteritis have been reported (Oliver, 2005b)

In South Korea, the total number of reported *V. vulnificus* infection is 139 from 2015 to 2017, among which 49 resulted in death (35%) (Korea Centers for Disease Control and Prevention (KCDC), http://www.cdc.go.kr/npt/). In Japan, approximately 400

people were estimated to suffer from *V. vulnificus*-induced septicemia annually (Osaka *et al*., 2004). In the United States, an average of 34 cases of *V. vulnificus* infection were reported annually by the U. S. Food and Drug Administration (Jones and Oliver, 2009).

I-1-2. Virulence factors of *V. vulnificus*

Many studies have aimed to investigate the complex phenomenon of *V. vulnificus* infection, and thus a number of bacterial surface factors have been characterized (Jones and Oliver, 2009). The following sections will describe the characteristics of important virulence factors of *V. vulnificus*, such as capsular polysaccharide (CPS), proteins related to iron acquisition, hemolysin (VvhA), MARTX toxin (RtxA1), and factors associated with defense against oxidative stress.

Capsular polysaccharide (CPS)

V. vulnificus is an extracellular pathogen that utilizes CPS to resist against opsonization by complement and subsequent phagocytosis by macrophages. Encapsulation by CPS masks immunogenic structures that would normally activate

nonspecific host response (Linkous and Oliver, 1999; Strom and Paranjpye, 2000). Therefore, CPS allows the *V. vulnificus* cells to be more invasive in subcutaneous tissue, leading to a slower clearance from the bloodstream than unencapsulted cells (Yoshida *et al*., 1985). The presence of a capsule changes the colony morphology; an encapsuled strain is opaque, while an unencapsuled strain is translucent (Wright *et al*., 1999; Yoshida *et al*., 1985). Indeed, unencapsulated mutants exhibited attenuated mortality in mouse models (Simpson *et al*., 1987). Consistently, inactivation of a CPS transport gene (*wza*) of *V. vulnificus* abolished capsule expression and resulted in an decreased mortality (Wright *et al*., 2001).

Lipopolysaccharide (LPS)

LPS from *V. vulnificus* plays a crucial role in the development of severe disease, such as septic shock (Strom and Paranjpye, 2000). Infection by using purified LPS from *V. vulnificus* resulted in a dramatic decline in heart rate and blood pressure of mice, leading to rapid death within 30-60 min (McPherson *et al*., 1991; Jones and Oliver, 2009). Further studies on *V. vulnificus* LPS showed that LPS not only elicits small cytokines response in mice but also stimulates host immune response via nitric oxide

synthesis activity (McPherson *et al*., 1991; Elmore *et al*., 1992). Low density lipoprotein (LDL) cholesterol and estrogen appear to be protective against LPS. Pretreatment of LDL prior to LPS exposure resulted in significantly reduced mortality in mice compared with the control (LPS exposure) (Strom and Pyranjype, 2000)

Multiple systems for iron acquisition

Pathogenesis of *V. vulnificus* is highly associated with elevated serum iron concentration in infected individuals (Wright *et al*., 1981). Iron treatment of mice prior to infection dramatically reduces the intraperitoneal LD_{50} (Stelma *et al*., 1992; Wright *et al*., 1981). Since most iron in human serum is bound to transferrin and other iron-binding compounds (Weinberg, 1978), *V. vulnificus* has developed multiple systems for iron acquisition. Primarily, the organism produces two types of siderophores, a catechol and a hydroxamate (Simpson and Oliver, 1983). The catechol siderophore (vulnibactin) is required for growth in iron-depleted medium and used to scavenge iron from transferrin and holotransferrin (Kim *et al*., 2006). Hydroxamate siderophore has also been shown to be involved in *V. vulnificus*

infection (Alice *et al*., 2008). The expression of genes involved in iron acquisition is primarily regulated by Fur, a ferric uptake regulator. Under iron-limiting conditions, Fur increases the expression of several genes involved in vulnibactin synthesis (*venB*, *vvsAB*, and *vis*) (Alice *et al*., 2008; Kim *et al*., 2006; Webster and Litwin, 2000).

Hemolysin (VvhA) and RtxA1 toxin

VvhA, a secreted hemolysin encoded by *vvhA*, contributes to the virulence of *V. vulnificus*, not only through hemolytic activity but also through other cytotoxic effects (Wright and Morris, 1991). VvhA causes cell death by pore formation in the cellular membrane, followed by an increase of vascular permeability and hypotension (Kim *et al*., 1993). Severe tissue necrosis, fluid accumulation, intestinal irregularities, partial paralysis, and lethality have also been demonstrated to be caused by VvhA (Gray and Kreger, 1987; Lee *et al*., 2005). Other effects of VvhA include apoptosis of endothelial cells and induction of inducible nitric oxide synthase (iNOS) (Kang *et al*., 2002; Kim and Kim, 2002; Kwon *et al*., 2001). However, inactivation of *vvhA* did not affect the mortality of *V. vulnificus* in the mouse model, suggesting that hemolysin is not solely responsible for the lethality and the tissue

damage (Wright and Morris, 1991).

RtxA1 is a multifunctional-autoprocessing RTX toxin (MARTX) encoded by *rtxA1*. MARTX toxins are large single polypeptide toxins produced by various species in the *Vibrio* genus (Satchell, 2015). MARTX toxins are made of repeated structural subunits and form pores in host cellular membranes (Gulig *et al*., 2005). *V. vulnificus* RtxA1 is highly (80% ~ 90%) homologous with *V. cholerae* RtxA, and genetic organization of the two *rtx* clusters of *V. vulnificus* and *V. cholerae* is also similar (Kim *et al*., 2008; Lee *et al*., 2007). Compared to wild type, a strain that was deficient in this toxin was found to be less cytotoxic and showed higher LD_{50} upon intragastric or intraperitoneal injection to mice (Kim *et al*., 2008). RtxA1 is considered to trigger excessive production of reactive oxygen species (ROS) by the host, leading to necrotic cell death and apoptosis (Lee *et al*., 2007). RtxA1 also contributes to host cellular changes, including cytoskeleton rearrangement, bleb formation, and actin aggregation, which lead to cellular necrosis and invasion of *V. vulnificus* into the bloodstream by crossing the intestinal epithelium (Kim *et al*., 2008). Recently, RtxA1 and VvhA have been demonstrated to play an additive role in causing

intestinal tissue damage and inflammation that then promote dissemination of the infecting bacteria to the bloodstream and other organs (Jeong and Satchell, 2012).

Pili and flagella

Attachment and colonization of the host surfaces are important steps in the early phase of most bacterial infections. Pili are proteinaceous fibers that stick out from the cell surface of bacteria and often mediate the initial attachment to the host surface. Likewise, *V. vulnificus* adherence has been demonstrated to correlate with increased piliation (Strom and Paranjpye, 2000). Consistently, the absence of genes required for the biogenesis of type IV pili (*pilA* and *pilD*: genes encoding the pilin structural protein and pre-pillin peptidase, respectively) resulted in a loss of attachment to epithelial cells as well as a slight increase in LD_{50} (Paranjpye *et al*.,1998; Paranjpye and Strom, 2005).

Biofilm

Bacteria have adopted mechanisms for establishing microbial communities known as biofilms, which are embedded in a matrix of extracellular polymeric substance

including polysaccharide, proteins, and nucleic acids (Flemming and Wingender, 2010). Biofilm formation contributes to the survival of microorganisms in an environment niche, and affects the likelihood of contact with a host. This surface-attached state is thought to be the primary means of persistence of bacteria in the environment, providing protection from a variety of stresses (Hall-Stoodly and Stoodly, 2005; Karatan and Watnick, 2009). *V. vulnificus* makes biofilms on various biotic surfaces, such as the eel body surfaces, crab shells, and oyster shells (Marco-Noales *et al*., 2001; Guo *et al*., 2010 and 2011). Diguanylate cyclase protein A (DcpA) has been identified as the regulator of EPS production, biofilm formation, and rugose colony development in *V. vulnificus* (Nakhmachik *et al*., 2008). It has been reported that *brp* gene cluster, which is involved in EPS synthesis, is crucial in biofilm formation. NtrC, which is required for mature biofilm development, is known to regulate the *brp* gene cluster (Kim *et al*., 2009). Another study has demonstrated that the expression of *brp* gene cluster is regulated by c-di-GMP levels and also that BrpT is a putative regulator for *brp* gene cluster (Guo *et al*., 2010).

Defenses against oxidative stress

Pathogenic bacteria are inevitably exposed to ROS that are crucial to host defense for the optimal microcidal activity of neutrophils and other phagocytes (Miller and Britigan, 1997). Therefore, pathogens have evolved sophisticated mechanisms to survive oxidative stress imposed by not only endogenous source but also host defense systems, and such mechanisms are closely linked to their virulence (Janssen *et al*., 2003). Although—like many other pathogenic bacteria—*V. vulnificus* has to cope with oxidative stress in host environments, only a few studies have addressed the molecular mechanisms by which the bacterium can survive under oxidative stresses (Kang *et al*., 2007; Park *et al*., 2004). *V. vulnificus rpoS* has been reported to be indispensable for synthesis and activity of KatG (hydroperoxidase I). *rpoS* is required for exponentially growing *V. vulnificus* to survive in the presence of H_2O_2 (Park *et al*., 2004). In *V. vulnificus*, loss of three superoxide dismutases (CuZnSOD, MnSOD, and FeSOD encoded by *sodC*, *sodA* and *sodB*, respectively) resulted in an increase in LD_{50} when compared to the parent strains. *V. vulnificus soxR* mutant, which is unable to induce MnSOD in response to superoxide, showed significantly diminished virulence in mice (Kang *et al*., 2007). Two distinct 2-Cys peroxiredoxins, Prx1 and Prx2, were identified in *V. vulnificus*. Prx1 was specifically induced by

exogenous H_2O_2. The *prx*1 mutant exhibited less cytotoxicity toward INT-407 epithelial cells *in vitro* and reduced virulence in a mouse model (Baek *et al*., 2009). Because Prx2 is induced by small amounts of H_2O_2, it is constitutively expressed in cells grown aerobically. Kinetic properties indicated that Prx2 effectively scavenges low levels of peroxides because of its high affinity to H_2O_2, whereas Prx1 quickly degrades higher levels of peroxides because of its high turnover rate and more efficient reactivation (Bang *et al*., 2012).

I-2. Oxidative stress and cellular defense mechanisms

I-2-1. Oxidative stress and reactive oxygen and nitrogen species

Oxidative stress has been defined as a disturbance in the normally balanced production of reactive free radical species and antioxidant defense-associated factors. Bacteria are typically exposed to free radicals that are formed in large amounts as an unavoidable byproduct of many biochemical processes or in association with another organism. Reactive oxygen species (ROS) include oxygen radicals as well as certain non-radicals that function as oxidizing agents and/or are easily converted into radicals (e.g. HOCl, HOBr, O_3, $ONOO^-$, $^1O_2$, H_2O_2). During the respiration process of facultative anaerobic bacterium *V. vulnificus*, O_2 is progressively reduced by four electrons to yield water. The incomplete reduction of O_2 leads to the formation of ROS. ROS are generated inevitably by the aerobic metabolism as described above, as well as by the exposure to radiation, metals, redox-active drugs, and host immune system (Storz and Hengge-Aronis, 2000).

Reactive nitrogen species (RNS) include nitric oxide (NO) and nitrogen dioxide

radicals. NO is an important agent of the immune response of the host that is infected with bacteria. Especially pathogens that are ingested may encounter additional NO and RNS as NO forms in the stomach from acidified nitrite and may be synthesized by some of the commensals in the gastrointestinal (GI) tract (Fang, 2004; Sobko *et al*., 2005). Furthermore, Phagocytic cells are among the most important components of the innate immune response, which is the first line of host defense. Two of the most important antimicrobial systems of phagocytic cells are the NADPH oxidase and inducible nitric oxide synthase (iNOS), which are responsible for the generation of ROS and RNS, respectively (Fang, 2004). ROS and RNS avidly damage various biological macromolecules such as nucleic acids, lipids, proteins and carbohydrates, by irreversibly destroying them or altering their functions (Bedard and Krause, 2007; Fang, 2004).

Therefore, pathogens have evolved sophisticated mechanisms to survive oxidative stress imposed by not only endogenous sources but also host defense systems, and the mechanisms are closely linked to their virulence (Fang, 2004).

I-2-2. Previous studies on oxidative stress defense mechanisms of *V. vulnificus*

Superoxide dismutase (SOD) converts $O_2^{\bullet -}$ into H_2O_2. In *V. vulnificus*, three superoxide dismutases (MnSOD, FeSOD, and CuZnSOD, encoded by *sodA*, *sodB* and *sodC*, respectively) have been identified. The loss of the three SODs resulted in an increase in LD_{50} when compared to the parent strains (Kang *et al*., 2007). Transcriptional regulator SoxR has been demonstrated to positively regulate the expression of MnSOD, and the *soxR* mutant also showed significantly diminished virulence in mice (Kang *et al*., 2007).

In the presence of Fe^{2+} cations, H_2O_2 can generate OH•, which is the most destructive species of ROS through Fenton reaction [$H_2O_2 + Fe^{2+} \rightarrow OH^{\bullet} + OH^- + Fe^{3+}$] (Mishra and Imlay, 2012). *V. vulnificus* Prx1 and Prx2 have been identified and studied to degrade H_2O_2. Prx1 and Prx2 were characterized to specifically scavenge exogenous and endogenous H_2O_2, respectively. The purified Prx1 reduced H_2O_2 in the presence of AhpF (alkyl hydroperoxide reductase F) and NADH as an electron donor. The *prx*1 mutant was hypersusceptible to killing by peroxide, and exhibited reduced cytotoxicity toward INT-407 epithelial cells *in vitro* and reduced virulence in a

mouse model than that of parental wild type (Baek *et al*., 2009). Prx2 is a TrxA (thioredoxin A)-dependent peroxidase and is induced by trace amounts of H_2O_2. Kinetic properties indicated that Prx2 effectively scavenges low levels of peroxidase, whereas Prx1 quickly degrades higher levels of peroxides (Bang *et al*., 2012). Another antioxidant enzyme of *V. vulnificus* is KatG (hydroperoxidase I). KatG is a catalase that also degrades H_2O_2 to O_2 and H_2O using heme or manganese cofactors (Mishra and Imlay, 2012). KatG has been demonstrated to contribute to the survival and growth of the bacterium, since *katG* mutant showed reduced survival upon H_2O_2 exposure *in vitro* as well as reduced virulence in mice (Park *et al*., 2004).

I-3. Objective of this study

Reactive oxygen species (ROS) and reactive nitrogen species (RNS) cause oxidative and nitrosative stress in the bacteria. These are implicated in not only diverse physiological processes but also various pathological process. In mammals, specialized enzymes such as NADPH-oxidase and iNOS generate ROS and RNS (Fang, 2004). The controlled generation of ROS and RNS by these enzymes was developed as part of the innate immune system to kill pathogenic bacteria (Fang, 2004). Therefore, pathogenic bacteria including *V. vulnificus* have evolved sophisticated mechanisms to survive oxidative stress, and such mechanisms are closely linked to their virulence as well as the survival under various environmental conditions. For this reason, understanding the strategies of pathogen to survive oxidative and nitrosative stress is critically important for successful control of the pathogen. However, the mechanisms for detoxifying various ranges and sources of ROS and RNS have not been fully characterized in *V. vulnificus* yet. *Vibrio vulnificus* has two OxyRs, central regulators of the antioxidant genes, OxyR1 and OxyR2 (Kim *et al*., 2014). OxyR1 and OxyR2 activate *prx*1 and *prx*2, respectively. Each Prx has

been reported to scavenge distinct ranges of H_2O_2. I further characterized the functions of OxyR2 as a three-state redox switch to tightly regulate production of *prx*2. In addition, the crystal structure of OxyR2 was determined to understand how OxyR2 has a higher sensitivity to low levels of H_2O_2 than other OxyRs do. It was found that the flipped conformation of the peptide bond before the Glu204 residue of OxyR2 and the resulting rigid conformation of His205 side chain had a decisive influence on the high H_2O_2 sensitivity of OxyR2.

To further understand the survival strategies of *V. vulnificus* against nitrosative stress, transcriptomic changes of *V. vulnificus* in response to NO were analyzed by RNA sequencing to identify genes that are likely to play important roles in the survival of *V. vulnificus* under NO stress. Based on the transcriptome analysis, I identified and characterized the gene *VvhmpA*, which encodes an NO-inducible flavohemoglobin, under nitrosative stress in the pathogenesis of *V. vulnificus*.

Chapter II.

Molecular Analysis of Hydrogen Peroxide Hypersensitivity of OxyR2, a Transcriptional Regulator of *Vibrio vulnificus*

II-1. Introduction

Oxygen-derived intermediates (e.g. hydrogen peroxide (H_2O_2) and peroxynitrite 4 respiration processes (Fang, 2004; Stadtman, 2001; Storz and Imlay, 1999). In addition, pathogenic bacteria are inevitably exposed to elevated levels of ROS - imposed by the host immune response system such as neutrophils and other phagocytes during host infection (Fang, 2004). Especially, increased level of hydrogen peroxide (H_2O_2) can damage essential cellular components as it is converted to the hydroxyl radical via the Fenton reaction in the presence of iron or copper ions (Cooke *et al*., 2003; Lemire *et al*., 2013). Many pathogenic bacteria have evolved sophisticated mechanisms to overcome oxidative stress caused by H_2O_2, and such mechanisms are closely linked to their virulence (Fang, 2004; Nathan and Shiloh, 2000). The agents of bacterial defense against H_2O_2 include highly specific and effective antioxidant enzymes such as peroxiredoxins (Prxs) and catalases (Storz and Hengge-Aronis, 2000).

OxyR, a member of the LysR-type transcriptional regulator family, can recognize H_2O_2 above a certain threshold concentration and is a central regulator of the

antioxidant genes including catalase-peroxidase *katG* and peroxiredoxins (*prx*s) in many bacteria. Many LysR-type transcriptional regulators are found in various bacteria, and they are typically homotetramers that contain an N-terminal DNA binding domain (DBD) and C-terminal regulatory domain (RD) (Schell, 1993). OxyR has a DBD for recognizing target gene promoters and an RD containing two conserved cysteine residues (peroxidatic and resolving cysteines) for sensing H_2O_2 (Choi *et al*., 2001). Many crystal structures have been reported since the first descriptions of *E. coli* OxyR structures revealed the redox-state-dependent conformational change of RDs (Choi *et al*., 2001). Recently elucidated full-length OxyR crystal structures from *Pseudomonas aeruginosa* have revealed the homotetrameric arrangement of the protein, where the two dimeric RDs face each other, and the two dimeric DBDs are oriented in the same direction. The crystal structures have also provided insight into how this redox-dependent structural alteration of RDs is propagated to the DBDs, leading to inward or outward motion between dimeric DBDs (Jo *et al*., 2015).

OxyR is a “two-state redox switch” that precisely modulates expression of many antioxidant genes in a H_2O_2-dependent manner. When H_2O_2 is low and within safe

limits, OxyR exists in the reduced state as its two conserved redox-sensitive cysteine residues are present as free thiols separated by an α-helix. The reduced OxyR is converted into oxidized form via two steps when H_2O_2 increases and exceeds safe levels (Lee *et al*., 2004). One of the redox-sensitive cysteines of OxyR, named peroxidatic cysteine, is first oxidized by H_2O_2 to cysteine-sulfenic acid (Cys-SOH), in which the bound H_2O_2 molecule and two water molecules near the peroxidatic cysteine are thought to play crucial roles via a so-called "H_2O_2-driven oxidation mechanism" (Jo *et al*., 2015). Given the high reactivity, the Cys-SOH ultimately forms an intermolecular disulfide bond with another redox-sensitive cysteine, named resolving cysteine, resulting in the formation of the oxidized (or disulfidized) form of OxyR that activates the induction of target genes (Lee *et al*., 2004).

The facultative aerobic pathogen *Vibrio vulnificus* has two different OxyRs (OxyR1 and OxyR2) and two different Prx proteins (Prx1 and Prx2) (Bang *et al*., 2012; Kim *et al*., 2014). OxyR1 has high sequence and functional similarities to the typical OxyR proteins and is oxidized at a certain H_2O_2 concentration (~5 μM) (Kim *et al*., 2014). OxyR2 exhibits limited sequence similarity to other typical OxyR proteins

and is activated by a lower H_2O_2 concentration (~0.5 μM) than OxyR1. OxyR1 and OxyR2 activate *prx*1 and *prx*2, respectively. Each Prx scavenges at distinct concentration ranges of H_2O_2. Prx2 has a higher affinity for H_2O_2 than Prx1 does and thus scavenges at much lower levels of H_2O_2, whereas Prx1 detoxifies higher levels of H_2O_2 more effectively. Prx2 is irreversibly inactivated by overoxidation at one of the catalytic cysteines, peroxidatic cysteine, to S-sulfonated cysteine (Cys-SO_3H) in cells exposed to 30 μM or higher levels of H_2O_2 that exceed its working range (Bang *et al*., 2012). In this study, biochemical and genetic studies found that the sensing cysteine of OxyR2 is overoxidized to Cys-SO_3H when exposed to high levels of H_2O_2 and the overoxidized OxyR2 deters the production of Prx2 that is no longer functional. To understand how OxyR proteins with similar structures exhibit different sensitivities to different levels of H_2O_2, I determined the crystal structures of OxyR2 RD and performed biochemical analysis.

II-2. Experimental procedures

II-2-1. Bacterial Strains, plasmids, and culture media

The strains and plasmids used in this study are listed in Table II-1. The *V. vulnificus* strains were grown in LB medium supplemented with 2.0% (w/v) NaCl (LBS) at 30 ℃. Anaerobic conditions were obtained using an anaerobic chamber with an atmosphere of 90% N_2, 5% CO_2, and 5% H_2 (Coy Laboratory Products, Grass Lake, MI). For anaerobic culture, the media were preincubated in the anaerobic chamber to remove dissolved O_2, which was verified by adding 0.00001% (w/v) resazurin salt (Sigma, St. Louis, MO) to the media as described previously (Kim *et al*., 2014).

Table II-1. Bacterial strains and plasmids used in this study

Strain or plasmid	Relevant characteristics [a]	Reference or source
Bacterial strains		
V. vulnificus		
MO6-24/O	Wild type; clinical isolate; virulent	Laboratory collection
OH0703	MO6-24/O with *oxyR2::nptI*; Km^r	(Kim *et al*., 2014)
DY171	MO6-24/O with Δ*hmpA*	This study
E. coli		
SM10 λ *pir*	*thi thr leu tonA lacY supE recA*::RP4-2-Tc::Mu λ-*pir*; Km^r; host for -requiring plasmids; conjugal donor	(Miller and Mekalanos, 1988)
S17-1 λ*pir, tra*	λ-*pir* lysogen; *thi pro hsdR hsdM*$^+$ *recA* RP4-2 Tc::Mu-Km::Tn7; Tp^r Sm^r; host for π-requiring plasmids; conjugal donor	(Simon *et al*., 1983)
BL21 (DE3)	F^- *ompT hsdS*$_B$ (r_B^- m_B^-) *gal dcm* (DE3)	Laboratory collection
Plasmids		
pPROEX HTa	His_6–tag fusion protein expression vector; Ap^r	Invitrogen
pBANG1408	pPROEX HTa with wild-type *oxyR*2	This study

	regulatory domain; Ap^r	
pPRO-OxyR2RD -E204G	pPROEX HTa with the mutant *oxyR*2 regulatory domain encoding OxyR2-RD-E204G; Ap^r	This study
pPRO-OxyR1RD	pPROEX HTa with the wild-type *oxyR*1 regulatory domain; Ap^r	This study
pDY1703	pPROEX HTa with *VvhmpA*; Ap^r, Cm^r	This study
pJH0311	Broad-host-range vector; Ap^r, Cm^r	(Goo *et al*., 2006)
pBANG1414	pJH0311 with the mutant *oxyR*2 encoding OxyR2-E204G; Ap^r, Cm^r	This study
pBANG1416	pJH0311 with the mutant *oxyR*2 encoding OxyR2-C206D; Apr, Cmr	This study
pDY1025	pJH0311 with wild-type *oxyR*2; Ap^r, Cm^r	(Kim *et al*., 2014)
pDY1607	pJH0311 with the mutant *oxyR*2 encoding OxyR2-E204A; Ap^r, Cm^r	This study
pDY1608	pJH0311 with the mutant *oxyR*2 encoding OxyR2-H205A; Ap^r, Cm^r	This study
pDY1618	pJH0311 with the mutant *oxyR*2 encoding OxyR2-K203D; Ap^r, Cm^r	This study
pDY1701	pJH0311 with *VvhmpA*; Ap^r, Cm^r	This study
pET-21c(+)	Optional C-terminal His_6–tag fusion protein expression vector; Km^r	Invitrogen

pDY1001	pET-28a(+) with wild-type *oxyR*2; Km^r	(Kim *et al*., 2014)
pDY1104	pET-28a(+) with the mutant *oxyR*2 encoding OxyR2-C206S; Km^r	This study
pDY1014	pET-28a(+) with the mutant *oxyR*2 encoding $OxyR2_{5CA}$; Km^r	(Kim *et al*., 2014)
pBANG1501	pET-28a(+) with the mutant *oxyR*2 encoding $OxyR2_{5CA}$-C206D; Km^r	This study
pSH1701	pET-21c(+) with *VvhmpA*; Km^r	This study
pDM4	R6K γ *ori sacB*; suicide vector; *oriT* of RP4; Cm^r	(Milton *et al*., 1996)
pDY1619	pDM4 with Δ*hmpA*	This study

[a] Km^r, kanamycin-resistant; Tp^r, trimethoprim-resistant; Sm^r, streptomycin-resistant; Ap^r, ampicillin-resistant; Cm^r, chloramphenicol-resistant.

Table II-2. Oligonucleotides used in this study

Name	Oligonucleotide Sequence (5'→3')[a, b]	Use
For mutagenesis		
OXYR2C206D-F	GGAAAAAGAGCATGATCTGACTGAACACGCGGTGTCGG	Construction of OxyR2-C206D variant
OXYR2C206D-R	CCGACACCGCGTGTTCAGTCAGATCATGCTCTTTTTCC	
OXYR2C206S-F	GGAAAAAGAGCATAGTCTGACTGAACACGCGGTGTCGGCC	Construction of OxyR2-C206S variant
OXYR2C206S-R	GGCCGACACCGCGTGTTCAGTCAGACTATGCTCTTTTTCC	
OXYR2E204G-F	GTCAGTATTTTTATTGGAAAAAGGGCATTGTCTGACTGAACACGC	Construction of OxyR2-E204G variant
OXYR2E204G-R	GCGTGTTCAGTCAGACAATGCCCTTTTTCCAATAAAATACTGAC	

OXYR2_E204A_F	GAGTCAGTATTTTTATTGGAAAAAGCACATTGTCTG ACTGAACACGCGG	Construction of OxyR2-E204A variant
OXYR2_E204A_R	CCGCGTGTTCAGTCAGACAATGTGCTTTTTCCAATA AAAATACTGACTC	
OXYR2_H205A_F	GTCAGTATTTTTATTGGAAAAAGAGGCATGTCTGAC TGAACACGCGGTGTC	Construction of OxyR2-H205A variant
OXYR2_H205A_R	GACACCGCGTGTTCAGTCAGACATGCCTCTTTTTCC AATAAAAATACTGAC	
OXYR2K203D-F	GTTCAGTCAGACAATGCTCGTCTTCCAATAAAAATA CTGACTCGTCAGG	Construction of OxyR2-K203D variant
OXYR2K203D-R	CCTGACGAGTCAGTATTTTTATTGGAAGACGAGCAT TGTCTGACTGAAC	
For qRT-PCR		
PRX2QRT-F	GTTGCTTTCCGTGGCTCTTTCC	Quantification of *prx*2 expression
PRX2QRT-R	TACTTCGCCGTGCTTCTGGTG	

OXYR2QRT2-F	GCCCAGTCTGAAGCAGTTACACTATC	Quantification of *oxyR*2 expression
OXYR2QRT2-R	GAGAGGACAGCCGATCAACTCTTC	
PRX1QRT-F	TACCCAGCGGACTTCACTTTCG	Quantification of *prx*1 expression
PRX1QRT-R	TGACACTGAGTACACTTCCACACC	
KATGQRT-F	CGTTCCGTTTGCAGCAGGTC	Quantification of *katG* expression
KATGQRT-R	CCAGTTGCGGAAGCCATCTG	
16S-qRT-F	CGGCAGCACAGAGAAACTTG	Quantification of the 16S rRNA expression
16S-qRT-R	CCGTAGGCATCATGCGGTAT	
00248-qRT-F	GGCCGAAACAGGACCAAAAC	Quantification of the VVMO6_00248 expression
00248-qRT-R	TGCGAGTTTGACTTTGCTGC	
03847-qRT-F	GCAAAAGCGGTGTGGTGATT	Quantification of the VVMO6_03847 expression
03847-qRT-R	CAGCCATCAGTTTAGGGGCA	
03846-qRT-F	TCCAGGTACGGGTGTTTGTG	Quantification of the VVMO6_03846 expression
03846-qRT-R	AAGCGCTGCTTTTTCAGTGG	
01967-qRT-F	TAGGCTTTGCTGACTGGACG	Quantification of the VVMO6_01967 expression

01967-qRT-R	ACAGTCCACACAGACGACTT	
00672-qRT-F	AAATTCCCGCTTGGCTGAGA	Quantification of the VVMO6_00672 expression
00672-qRT-R	CAAAGGTAAGTTTGCCGCCC	
01809-qRT-F	GCCGCCGCGTTATTTGTATT	Quantification of the VVMO6_01809 expression
01809-qRT-R	ACGGTGGTGATTTGTTTGCG	
01964-qRT-F	GCTACCGCTGACACTCAACT	Quantification of the VVMO6_01964 expression
01964-qRT-R	CAGCATCAAAACGCCAACCA	
00249-qRT-F	GTTGGAGAGGTTGTGCGAGA	Quantification of the VVMO6_00249 expression
00249-qRT-R	CCAATTCCGCCAAAAAGGCA	
For protein overexpression		
OXYR2-RD-F	GGGCAAGACTCCATGGAACTGGGTAG	Overexpression of OxyR2 RD
OXYR2-RD-R	GTTAGCAGCCGTCGACCTAAAGCAGTTC	
OXYR1-RD-F	GGTCCATGGCAGAGATGGCAAGTGGTCAAAGTG	Overexpression of OxyR1 RD
OXYR1-RD-R	GGTCTCGAGTTACTGCTCTGAACCGCTCAC	
HMPA04-F	CCATGGGCATGCTCAGCGAAAACACCATTAAC	Overexpression of His_6-tagged *Vv*HmpA

HMPA04-R	GTCGACCTAAACCACTTTGTGTGGGCCAAA	
HMPA05-F	GGCAACATATGCTCAGCGAAAACACCATTAC	Overexpression of non-His_6-tagged *Vv*HmpA
HMPA05-R	GGCCTCGAGCTAAACCACTTTGTGTGGGC	
For mutant construction		
HMPA01-F	CTTGTCATCACTCTTCTCTCTTTGAATG	Deletion of *VvhmpA* ORF
HMPA01-R	TATGGATCCTTCAATTCGTTAGTTTGGTA	
HMPA02-F	GAAGGATCCATATTGATCGGCAGTGAT	Deletion of *VvhmpA* ORF
HMPA02-R	GGCTCCTCTATGGTGAAGAAAGTCTAA	
For mutant complementation		
HMPA03-F	GGTACCGGTGGGCTCCTCTATGGTGA	Amplification of *VvhmpA* ORF
HMPA03-R	GAGCTCCTAAACCACTTTGTGTGGGC	

[a] The oligonucleotides were designed using the *V. vulnificus* MO6-24/O genomic sequence (GenBank™ accession number CP002469 and CP002470, www.ncbi.nlm.nih.gov).

[b] Regions of oligonucleotides not complementary to the corresponding genes are underlined.

II-2-2. Site-directed mutagenesis of *oxyR*2

To construct OxyR2 mutant (C206D, E204G, E204A, H205A, and K203D), a QuikChange® site-directed mutagenesis kit (Agilent Technologies, Loveland, CO) was used, following previously described protocols (Kim *et al*., 2014). The complementary mutagenic primers, listed in Table II-2, were used in conjunction with the pDY1025 plasmid (*oxyR*2 cloned into a broad host-range vector pJH0311 under the *lac* promoter) to create pBANG1416, pBANG1414, pDY1607, pDY1608, and pDY1618 (for OxyR2 (C206D, E204G, E204A, H205A, K203D, respectively)). *E. coli* SM10 λ *pir*, *tra* (Miller and Mekalanos, 1988) harboring pJH0311, pDY1025, pBANG1416, pBANG1414, pDY1607, pDY1608, and pDY1618 were used as conjugal donors to the *oxyR*2 mutant (OH0703). The conjugation was conducted as previously described (Kim *et al*., 2014).

II-2-3. *In vivo* alkylation of OxyR2 and Western blotting analysis

The *oxyR*2 mutant OH0703 with pDY1025 expressing *oxyR*2 or *oxyR*2-E204G-expressing pBANG1414 was used for Western blotting analysis of OxyR2 as described previously (Kim *et al*., 2014). OH0703 (pDY1025) was grown

anaerobically to an A_{600} of 0.3, aliquoted to the same volume, and exposed to various concentrations of H_2O_2. To alkylate free thiols in the proteins with 0.5 kDa 4-acetamido-4'-maleimidylstilbene-2,2'-disulfonic acid (AMS; Invitrogen), the cells were immediately precipitated with 10% (w/v) ice-cold TCA, and then the resulting pellets were dissolved in 50 μl of the fresh AMS buffer (15 mM AMS, 1 M Tris, 1 mM EDTA, 0.1% (w/v) SDS, pH 8.0) (Kim *et al*., 2014).

After incubation at 37℃ for 1 h, the same amounts of pelleted total protein were resolved with SDS-PAGE under non-reducing conditions and immunoblotted with either anti-OxyR2 or anti-OxyR2-Cys^{206}-SO_3H antibody as described previously (Kim *et al*., 2014). The anti-OxyR2 polyclonal antibody was prepared previously in a rabbit by using the purified His_6-tagged OxyR2 as an antigen (Kim *et al*., 2014). An *S*-sulfonated peptide corresponding to the active site of OxyR2, EKEHC^{206}(SO_3H)LTEHA, was synthesized and conjugated with keyhole limpet hemocyanin and then used to raise rabbit anti-OxyR2-Cys^{206}-SO_3H polyclonal antibody (AbFrontier, Seoul, South Korea).

II-2-4. ELISA

The Cys^{206}-SH peptide EKEHC^{206}(SH)LTEHA and its *S*-sulfonated form, Cys^{206}-SO_3H peptide EKEHC^{206}(SO_3H)LTEHA, were synthesized (AbFrontier) and used to analyze the binding specificity of anti-OxyR2-Cys^{206}-SO_3H antibody. The microtiter 96-well plates were coated with 100 μl of each of the synthetic peptides (1 μg/ml) for overnight at 4℃ and blocked with the blocking buffer (2% skim milk in PBS with 20 mM 2-mercaptoethanol) for 2 h to prevent nonspecific binding. After the blocking buffer was disposed of, various concentrations of anti-OxyR2-Cys^{206}-SO_3H antibody in 100 μl of the blocking buffer were added to each well to react for 2 h. When needed, the peptides were added to the reaction along with the antibody as binding competitors.

Then the wells were reacted with HRP-conjugated goat anti-rabbit IgG (0.2 μg/ml) (AbFrontier) for 2 h. For the colorimetric development of HRP, 3,3',5,5'-tetramethylbenzidine solution (0.0075% (w/v), Sigma) was added to react for 1 min. The reaction was stopped by adding 100 μl of 2 M H_2SO_4. Absorbance at 450 nm (A_{450}) was recorded to measure the amount of anti-OxyR2-Cys^{206}-SO_3H antibody in

each well using an Infinite™ M200 microplate reader (Tecan, Männedorf, Switzerland). The wells were washed between each step of the reaction either with TBST-M (50 mM Tris, 150 mM NaCl, 0.1% Tween 20, 20 mM 2-mercaptoethanol) before anti-OxyR2-Cys^{206}-SO_3H antibody was added or with TBST (50 mM Tris, 150 mM NaCl, 0.1% Tween 20) after the antibody was added. All reactions were carried out at room temperature.

II-2-5. RNA purification and transcript analysis

Total cellular RNAs from cultures grown anaerobically to an A_{600} of 0.3 or aerobically to an A_{600} of 0.5 were isolated using RNAprotect® bacteria reagent and RNeasy® minikit (Qiagen). When necessary, the cultures were exposed to H_2O_2 with indicated concentrations for 30 sec or 3 min and then harvested. For quantitative real-time PCR, cDNA was synthesized using iScript™ cDNA synthesis kit (Bio-rad), and real-time PCR amplification of the cDNA was performed using Chromo 4 real-time PCR detection system (Bio-rad) with pairs of primers listed in Table II-2. Relative expression levels of the specific transcripts were calculated using the 16S rRNA expression level as the internal reference for normalization (Lim *et al*., 2014).

qRT-PCR data are presented as mean ± standard deviation (S.D.) of three independent experiments.

II-2-6. Expression and purification of proteins

The DNA sequence encoding OxyR2-RD (amino acids 86-301 of OxyR2 (accession code: ADV87476)), was amplified by PCR using the pair of primers described in Table 2. The PCR products were ligated into a His_6-tagged protein expression vector, pPROEX-HTa (Invitrogen) (Table II-1). The expression vector for OxyR2-RD (E204G) was constructed using overlapping PCR technique with the primers listed in Table II-2. His_6-tagged OxyR2-RD and OxyR2-RD (E204G) were expressed in *Escherichia coli* BL21 (DE3) by the addition of 0.5 mM isopropyl-β-D-thiogalactopyranoside for 6 h at 30 °C. The expressed proteins, including the wild type and mutant proteins, were purified using the same procedure previously described for *P. aeruginosa* OxyR RD (Jo *et al*., 2015). Briefly, the overexpressed OxyR2-RDs were purified by Ni-NTA chromatography, anion-exchange chromatography (HiTrapQ, GE Healthcare), and size-exclusion chromatography (HiLoad 26/600 superdex 200 pg, GE Healthcare). All purified proteins were

concentrated to 30 mg/ml and stored at -80 °C until use for crystallization. Expression and purification of OxyR1-RD (accession code: AIL71797, residues 80-299) used the same procedures as used for OxyR2-RD (Table II-1).

II-2-7. Structural determination

Purified OxyR2-RD proteins (wild-type and E204G variants) were crystallized using the hanging-drop vapor diffusion method at 14 °C after mixing 1 μl protein solution with 1 μl precipitation solution. The wild-type OxyR2 RD protein was crystallized at 14 °C in a precipitation solution containing 0.2 M ammonium citrate (pH 6.5), 14% (w/v) PEG 3350, 2 mM TCEP (Tris(2-carboxyethyl)phosphine), and 5 mM DTT. To obtain phase information, we soaked the crystals in 10 mM $ZnCl_2$-supplemented precipitation solution. The native and Zn-soaked crystals were flash-frozen in nitrogen steam at -173 °C for X-ray diffraction using crystallization solution supplemented with 20% glycerol as cryoprotectant. Native and single-wavelength anomalous diffraction (Zn-SAD) data were collected in Pohang Accelerator Laboratory beam lines. Phasing information and the initial model were obtained using a combination of molecular replacement (MR-SAD) and single-wavelength

anomalous diffraction methods with the PHENIX Phaser-EP program and the Zn-SAD dataset (Cha *et al*., 2012; Zwart *et al*., 2008). The final structure was refined with the PHENIX program against the native dataset to a 1.8 Å resolution (Echols *et al*., 2012). +

The E204G variant proteins of OxyR2-RD were also crystallized at 14 °C, in three different conditions. The crystallization of OxyR2-RD (E204G) in the "SO_4-free, high resolution" condition was conducted under the same condition as with the wild-type protein. In the "SO_4-free, P3121" condition, OxyR2-RD (E204G) variant protein was crystallized in the solution containing 0.2 M sodium acetate, 0.1 M Tris-HCl (pH 9.0), 14% PEG 4000, and 2 mM TCEP. In the last condition, "SO_4-bound," structure was grown in the solution containing 0.2 M ammonium sulfate, 0.1 M sodium citrate (pH 5.6), 11% PEG 4000, and 2 mM TCEP. The E204G variant crystals were flash-frozen in liquid nitrogen steam at -173 °C for X-ray diffraction using crystallization solution supplemented with 20% glycerol as a cryoprotectant. All structures of OxyR2 variants were determined by the molecular replacement method using the wild-type OxyR2-RD structure. The MOLREP program in the

CCP4 package (Winn *et al*., 2011) was used for molecular replacement, and COOT (Emsley and Cowtan, 2004) and PHENIX (Echols *et al*., 2012) were used to rebuild and refine the models. I want to express my sincere thanks to Drs. Nam-Chul Ha and Inseong Jo for their instrumental help in determining protein structure.

II-2-8. Competitive kinetics with horseradish peroxidase (HRP)

The purified proteins OxyR2-RD and OxyR1-RD were reduced by incubation in the appropriate buffer (20 mM Tris-Cl (pH 8.0), 150 mM NaCl, 1 mM EDTA, and 1 mM DTT) for 60 min at room temperature. Residual DTT was removed by ultrafiltration using 10 kDa Amicon Ultra Centrifugal Filter Devices (Merck Millipore, Darmstadt, Germany). The reaction mixtures containing 5.84 μM horseradish peroxidase (Sigma) and various concentrations (0-21.9 μM) of the reduced OxyR2-RD or OxyR1-RD were treated with 4 μM H_2O_2 at room temperature in reaction buffer containing 20 mM Tris-HCl (pH 8.0), 150 mM NaCl, and 1 mM EDTA. The concentration of horseradish peroxidase was calculated by measuring the absorbance at 403 nm (ε_{403} = 1.02 X 10^5 M^{-1} cm^{-1}), and the concentrations of other proteins were determined spectrophotometrically based on the molar extinction coefficients at 280

nm. The competitive kinetics of OxyR1 and OxyR2-RD were determined using a previously described procedure (Ogusucu *et al*., 2007; Winterbourn and Peskin, 2016). In brief, the ratio of inhibition of horseradish peroxidase oxidation (F/(1-F)) was calculated by measuring the A_{403} using a Tecan Infinite M200 reader (Tecan, Mannedorf, Switzerland). The second-order rate constants (k) of OxyR1-RD and OxyR2-RD were determined from the slope of the plot, $((F/(1-F))k_{HRP}[HRP]/$ [OxyR1-RD or OxyR2-RD] ($k_{HRP} = 1.7 \times 10^7\ M^{-1}\ s^{-1}$).

II-3. Results

II-3-1. Overoxidation of OxyR2 in *V. vulnificus* Cells Exposed to H_2O_2

To ascertain whether the overoxidation of OxyR2 at the sensing cysteine occurs by cellular H_2O_2 in *V. vulnificus* as in the case of Prx2, *oxyR*2 mutant OH0703 with pDY1025 expressing *oxyR*2 was grown aerobically and then exposed to various concentration of H_2O_2. To determine the number of free thiol in the cellular OxyR2 proteins, the cells were treated with AMS, which specifically reacts with a free thiol group. AMS linking would cause upshifts in the protein bands when visualized with SDS-PAGE because alkylation of a free thiol in the proteins with AMS adds 0.5 kDa of molecular mass. The total cellular proteins were resolved with non-reducing SDS-PAGE and immunoblotted with anti-OxyR2 rabbit antibody. Without exposure to H_2O_2, OxyR2 in the cells existed in the reduced state in which all seven cysteine residues present in OxyR2 were alkylated with AMS (7AMS control). An OxyR2 band containing pentuply alkylated cysteine residues coexisted with the heptuply alkylated OxyR2 band when cells were exposed to 10 μM H_2O_2, indicating that a portion of OxyR2 was oxidized to form a disulfide bond. More importantly, a portion of OxyR2 in the cells exposed to H_2O_2 exceeding 30 μM appeared to have sextuply

alkylated cysteine residues, indicating that one of the seven cysteine residues of OxyR2 had a single modification, such as an oxidation, that could prevent alkylation by AMS. When determined based on band intensities, relative amounts of OxyR2 with the single cysteine modification (or sextuply alkylated) increased gradually by exposure to higher levels of H_2O_2 (Fig. II-1A).

To examine whether the OxyR2 with a single cysteine modification, as observed in the cells exposed to H_2O_2 exceeding 30 μM, is the OxyR2 with overoxidized Cys^{206}, the total cellular proteins were resolved with non-reducing SDS-PAGE and immunoblotted with the anti-OxyR2-Cys^{206}-SO_3H antibody. To determine the specificity of the anti-OxyR2-Cys^{206}-SO_3H antibody by ELISA, the antibody was tested to react with the Cys^{206}-SO_3H or Cys^{206}-SH peptides that were synthesized and attached to the microtiter 96-well plates. The results showed that the antibody specifically bound to the Cys^{206}-SO_3H peptide. Furthermore, the binding of the antibody to the attached Cys^{206}-SO_3H peptide was effectively inhibited when extra Cys^{206}-SO_3H peptide was added to the reaction as a competitor. In addition, the antibody was shown to slightly bind Cys^{206}-SH, and when the Cys^{206}-SH peptide was

added as a competitor, it also could marginally inhibit the antibody reaction to the Cys^{206}-SO_3H peptide attached to the microtiter 96-well plates, reflecting that Cys^{206}-SH peptide could be oxidized to Cys^{206}-SO_3H peptide in an aerobic condition that we tested. The results indicated that the anti-OxyR2-Cys^{206}-SO_3H antibody that we used is specific to the OxyR2 with Cys^{206}-SO_3H (Fig. II-1B, C). The OxyR2 protein with overoxidized Cys^{206} was specifically detected in cells exposed to H_2O_2 exceeding 30 μM and increased gradually in cells exposed to higher levels of H_2O_2. The results suggested that the sensing cysteine of OxyR2 becomes overoxidized *in vivo* when the *V. vulnificus* cells are exposed to high levels of H_2O_2, as was demonstrated *in vitro*.

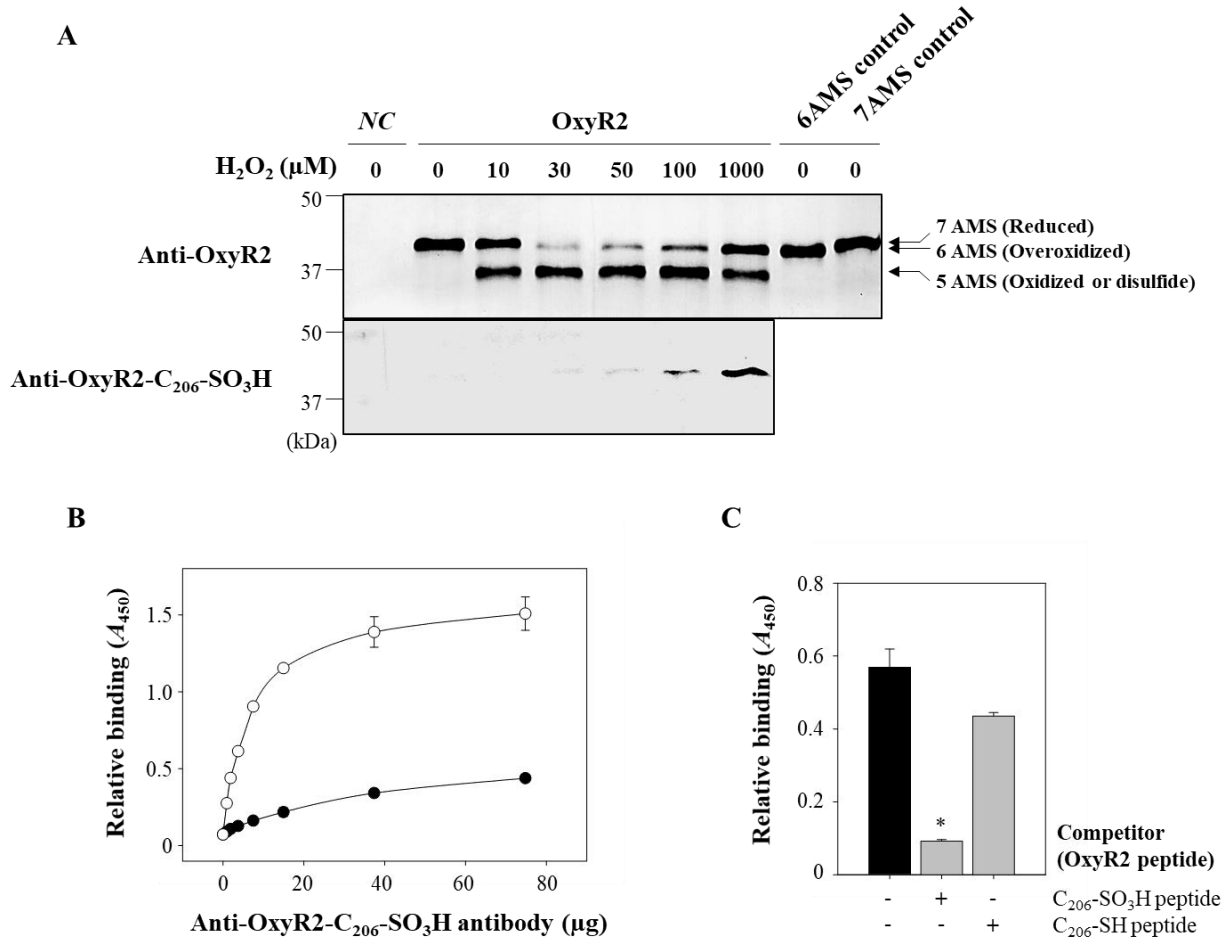
A
NC
OxyR2
6AMS control
7AMS control
H2O2 (μM)
0
0
10
30
50
100
1000
0
0
50
37
Anti-OxyR2
7 AMS (Reduced)
6 AMS (Overoxidized)
5 AMS (Oxidized or disulfide)
50
37
Anti-OxyR2-C206-SO3H
(kDa)
B
Relative binding (A450)
1.5
1.0
0.5
0
0
20
40
60
80
Anti-OxyR2-C206-SO3H antibody (μg)
C
Relative binding (A450)
0.8
0.6
0.4
0.2
0
*
Competitor
(OxyR2 peptide)
- + -
C206-SO3H peptide
- - +
C206-SH peptide

Figure II-1. Overoxidation of OxyR2 Cys206 in *V. vulnificus* cells exposed to various levels of H_2O_2

A, OH0703(pDY1025) was grown anaerobically to an A_{600} of 0.3 and exposed to various H_2O_2 concentrations for 3 min. Cellular proteins were precipitated with TCA and alkylated with fresh AMS buffer for 1 h at 37 °C. Proteins (3.5 μg for the top panel and 7 μg for the bottom panel) were resolved by non-reducing SDS-PAGE and immunoblotted using anti-OxyR2 antibody (top) or anti-OxyR2-Cys^{206}-SO_3H antibody (bottom). The predicted numbers of AMS that alkylated each OxyR2 molecule and the redox states of the protein complexes are indicated at the ends of the gel. Negative control (NC) was OH0703 (pJH0311), 6AMS control was OH0703 (pBANG1416), and 7AMS control was OH0703 (pDY1025). *B*, the specificity of anti-OxyR2-Cys^{206}-SO_3H antibody to overoxidized and reduced OxyR2 was determined using ELISA. The microtiter 96-well plates were coated with 0.1 μg of synthetic peptides corresponding to either OxyR2 active site with overoxidized (*S*-sulfonated) Cys^{206} (EKEHC^{206}(SO_3H)LTEHA) (○) or with reduced Cys^{206} (EKEHC^{206}(SH)LTEHA) (●), and the peptides were reacted with various concentrations of the antibody as indicated. *C*, the *S*-sulfonated OxyR2 peptide (0.1

μg) was attached to the microtiter 96-well plates and then reacted with 4 μg of anti-OxyR2-Cys^{206}-SO_3H antibody. As a binding competitor, either *S*-sulfonated or reduced OxyR2 peptides (12.5 ng) was added to the reaction with the antibody as indicated. Black bar, control where no competitor was added. Relative binding of the antibody to the specific peptides is presented in A_{450}. All data in *B* and *C* represent mean ± S.D. (*error bars*). *, statistically significant difference ($p < 0.05$) between groups.

II-3-2. Overoxidized State of OxyR2 Turns Off the *prx*2 Promoter

To examine the transcriptional activity of OxyR2 in the overoxidized state, the expression of *prx*2 was monitored in the wild-type *V. vulnificus* cells. The expression of *prx*2 was significantly induced when the anaerobically grown cells were exposed to H_2O_2, indicating that OxyR2 was oxidized to the disulfide state under this condition to activate the *prx*2 promoter (P_{prx2}). However, the level of *prx*2 transcript gradually decreased with increasing concentrations of H_2O_2 (> 30 μM), which would lead to increased portion of overoxidized OxyR2. The changes in *prx*2 expression were dependent on OxyR2 activity, but not on *oxyR*2 transcript expression level. The transcript expression level of *oxyR*2 was not significantly induced by increasing concentrations of H_2O_2 (< 1 mM) (Fig. II-2A). These combined results suggested that the shift of OxyR2 to overoxidized state deters further expression of *prx*2 transcript. Because it has been reported that Prx2 is overoxidized and inactivated by H_2O_2 exceeding 30 μM (Bang *et al*., 2012), this deterrence of the *prx*2 expression may prevent the production of Prx2 that would not be functional in the environments of high H_2O_2.

However, it was still possible that H_2O_2 over 30 μM may also detrimentally affect other transcription factors, such as components of RNA polymerase or other transcriptional factors, to finally deter *prx*2 expression. To rule out this possibility, OH0703 containing pBANG1416 expressing OxyR2-C206D was grown aerobically without exogenously added H_2O_2, and the *prx*2 expression was compared with that of OH0703 expressing wild-type OxyR2. It has been reported that properties of aspartic acid such as its size and polarity are comparable with those of the overoxidized cysteine residues (Cys-SO_2H and Cys-SO_3H), and therefore OxyR2-C206D was anticipated to mimic the overoxidized state of OxyR2. OH0703 producing wild-type OxyR2 expressed almost 13-fold greater *prx*2 than the negative control strain lacking OxyR2. This supported our previous observation that wild-type OxyR2 activates the *prx*2 expression under aerobic conditions. In contrast, the *prx*2 expression level of the strain producing OxyR2-C206D was almost the same as that of the negative control strain (Fig II-2B). The results indicated that the deterrence of the *prx*2 expression in response to H_2O_2 exceeding 30 μM is caused mainly, if not solely, by overoxidation of OxyR2 and further confirmed that OxyR2-C206D is functionally similar to the overoxidized OxyR2.

A

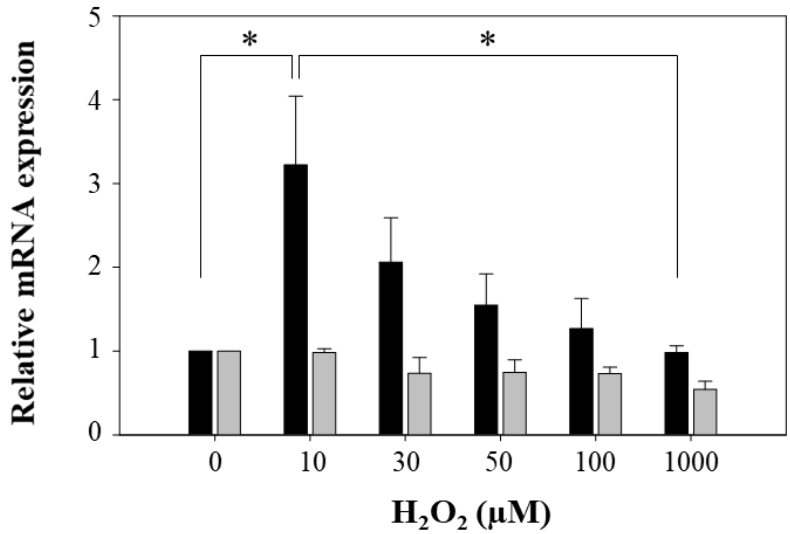
Relative mRNA expression
5
4
3
2
1
0
*
*
0
10
30
50
100
1000
H2O2 (μM)

B

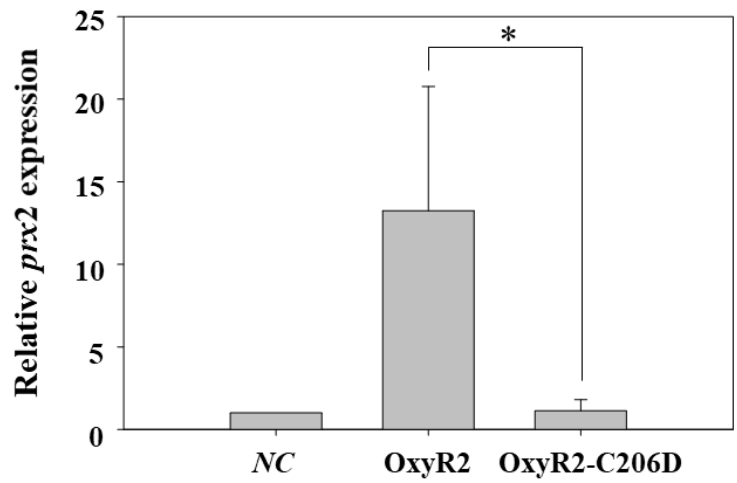
Relative prx2 expression
25
20
15
10
5
0
*
NC
OxyR2
OxyR2-C206D

Figure II-2. Expression levels of *prx*2 in response to various levels of H_2O_2

A, wild-type *V. vulnificus* was grown anaerobically to an A_{600} of 0.3 and exposed to various concentrations of H_2O_2 as indicated for 3 min. Total RNAs were isolated, and the relative levels of *prx*2 (black bars) and *oxyR*2 (gray bars) transcripts were determined by quantitative real-time PCR analyses. The level of each transcript from wild type unexposed to H_2O_2 is presented as 1. *, statistically significant difference ($p < 0.05$) between groups. *B*, transcriptional activity of OxyR2-C206D. Cultures were grown aerobically to an A_{600} of 0.5, total RNAs were isolated, and the relative levels of *prx*2 transcript were determined by quantitative real-time PCR analyses. The level of transcript from negative control (NC) is presented as 1. Negative control was OH0703 (pJH0311). OxyR2, OH0703 (pDY1025); OxyR2-C206D, OH0703 (pBANG1416). All data in *A* and *B* represent mean ± S.D. (*error bars*).

II-3-3. OxyR2 regulates *prx*2 as a three-state redox switch in response to H_2O_2

Fig. II-3 represents the operating model of OxyR2 that regulates the expression of *prx*2 as a three state redox switch. OxyR2 adopts three distinct redox states (reduced, disulfide, and overdoxidized states) in an H_2O_2 concentration-dependent manner. So far in the widely accepted mechanism of OxyR proteins, OxyR, upon reaction with H_2O_2, shifts from being in the reduced state to the disulfide state and activates the expression of *prx*2. However, when exposed to H_2O_2 exceeding the working range for Prx2, OxyR2 moves to an overoxidized state, a third redox state, and turns off the expression of *prx*2. I propose that OxyR2 is able to prevent production of unnecessary Prx2 and thus save valuable cellular resources by working as a three-state redox switch.

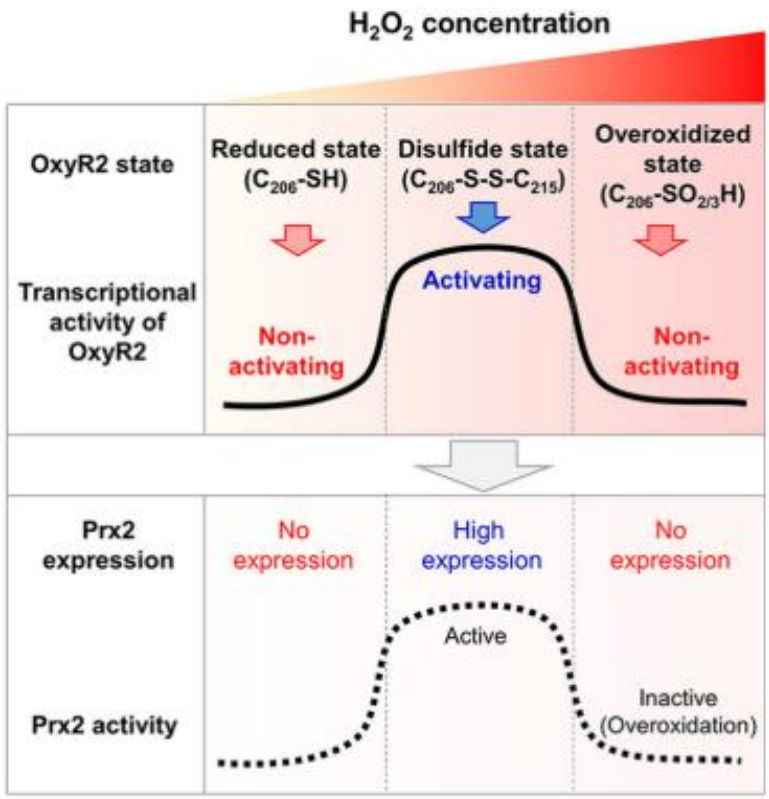

Figure II-3. A working model for OxyR2 as a three-state redox switch

OxyR2 exhibits three different redox states, revealing different transcriptional activities in response to various levels of H_2O_2 in cells (solid line) as indicated. Concurrently, the *prx*2 expression (dotted line) varies, depending on the redox states of OxyR2. C_{206}-$SO_{2/3}$H, overoxidized Cys206 with either Cys_{206}-SO_2H or Cys_{206}-SO_3H.

II-3-4. Structural analysis of OxyR2-RD

To investigate the relationship between the structural features of *V. vulnifcus* OxyR2 and the protein's higher H_2O_2 sensitivity, the crystal structures of wild-type OxyR2-RD (residues 86-301) grown under reduced conditions were determined using the Zn-anomalous signals from a $ZnCl_2$-soaked crystal. The structural determination was carried out by Drs. Nam-Chul Ha and Inseong Jo. The resulting electron-density maps were of sufficient quality to allow us to build an almost complete model. The structure was refined against the 1.6-Å-resolution dataset. Like other OxyR-RDs, the protomer consists of two subdomains (RD-I and RD-II; Fig. II-4A). Two notable dimers generated by the crystallographic 2-fold axis were found in the crystal, where each protomer individually participated in dimer formation. These observations indicate that OxyR2 is also a dimer in solution, like other OxyR proteins. The overall structure of OxyR2-RD was similar to other OxyR-RD structures previously determined in the reduced state (Fig. II-4A and B). The two conserved cysteine residues (Cys206 and Cys215) remained in free thiol forms separated by the inter-cysteine helix (residues 206-215). The relative orientation between the dimers is similar to those of other reduced OxyR proteins from *Escherichia coli*, *Neisseria*

meningitidis, *Pseudomonas aeruginosa*, and *Porphyromonas gingivalis* (Choi *et al*., 2001; Jo *et al*., 2015; Sainsbury *et al*., 2010; Svintradze *et al*., 2013). Thus, it was concluded that OxyR2-RD exhibited the typical reduced conformation of OxyR.

To further analyze the structure in more detail, the OxyR2-RD structure was superposed onto *P. aeruginosa* OxyR (*Pa*OxyR) in the reduced state (Fig. II-4 B). While the RD-I subdomain exhibited minimal deviation among the structures, the RD-II subdomain had a particular variation in the location of the resolving cysteine (Cys215 in OxyR2, Cys208 in *Pa*OxyR) (Fig. II-4C). Compared with cysteine positions in other OxyR proteins, the resolving cysteine Cys215 is buried in the interior of the RD-II subdomain along with the inter-cysteine α-helix. However, the peroxidatic cysteine is located at the same position as in other OxyR proteins (Fig. II-4).

OxyR2 has a noncanonical conformation of the peptide bond between Lys203 and Glu204. Notably, the structural superposition of OxyR2 with other OxyR proteins revealed large conformational differences at the peptide bond (or peptide flipping)

between Lys203 and Glu204 (Fig. II-4C). However, neither the Lys203 nor Glu204 side chains was involved in an interaction with other residues or the bound H_2O_2 and water molecules near the peroxidatic cysteine residue. Sequence alignment revealed that Glu204 of OxyR2 was replaced with a Gly residue in most other OxyR proteins. The conserved Gly residue is known to provide conformational flexibility to the adjacent peptide bonds (Fig. II-4D). Thus, Glu204 of OxyR2 is more likely than the Lys203 residue to be responsible for the noncanonical conformation of the peptide bond.

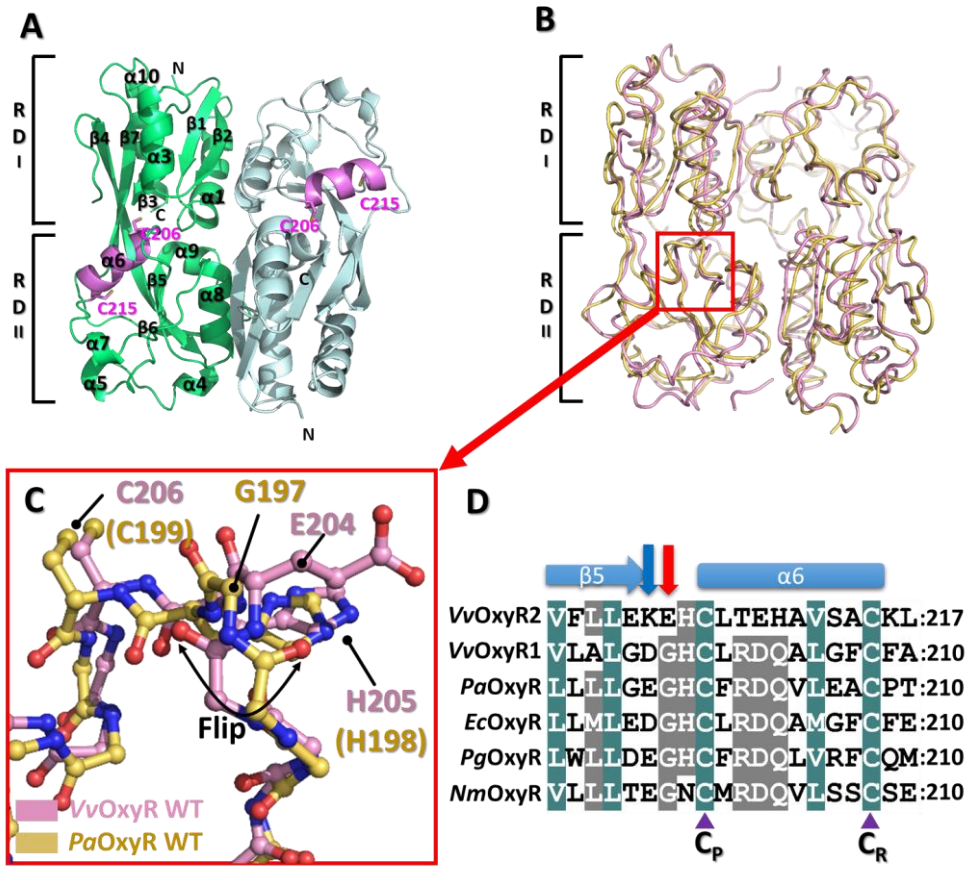
A
RDI
RDII
α10
N
β4
β7
β1
β2
α3
β3
C
α1
C215
C206
C206
α6
α9
β5
α8
C215
β6
α7
α5
α4
N
B
RDI
RDII
C
C206
(C199)
G197
E204
H205
(H198)
Flip
VvOxyR WT
PaOxyR WT
D
β5
α6
VvOxyR2 VFLLEKEHCLTEHAVSACKL:217
VvOxyR1 VLALGDGHCLRDQALGFCFA:210
PaOxyR LLLLGEGHCFRDQVLEACPT:210
EcOxyR LLMLEDGHCLRDQAMGFCFE:210
PgOxyR LWLLDEGHCFRDQLVRFCQM:210
NmOxyR VLLLTEGNCMRDQVLSSCSE:210
CP
CR

Figure II-4. Structure of the wild-type OxyR2-RD

A, The dimeric assembly of wild-type OxyR2-RD under reduced conditions: Protomers are highlighted in green or light blue, except in the inter-cysteine α-helical regions (pink). The conserved cysteines (Cys206 and Cys215) are represented as sticks. Secondary structural elements and the subdomains RD-I and RD-II are labeled. *B*, Comparison of OxyR2-RD dimers (pink) with *P. aeruginosa* OxyR-RD in the reduced state (yellow, PDB code 4Y0M): The red box indicates the region near the peroxidatic cysteine (Cys206) and the Glu204-containing loop. *C*, A close-up view of the region indicated by the red box in *B*: The regions near the peroxidatic cysteine of OxyR2-RD (pink) and *Pa*OxyR-RD (yellow) are represented in ball-and-stick. The flipped peptide bond is indicated with a double-headed arrow. *D*, A sequence alignment of OxyR2 with other OxyRs, focusing on the region containing the conserved cysteine residues (*Vv* for *V. vulnificus*; *Pa* for *P. aeruginosa*; *Nm* for *N. meningitidis*): The secondary structures are displayed above the sequence. The red arrow indicates Glu204 and its equivalent residues, and the blue arrow indicates Lys203 and its equivalent residues. Two conserved cysteine residues (peroxidatic cysteine C_P, resolving cysteine C_R) are indicated by purple triangle marks. The

strictly conserved amino acid residues are indicated by cobalt blue boxes, and the moderately conserved amino acid residues are indicated by gray boxes. The structural determination was carried out by Drs. Nam-Chul Ha and Inseong Jo.

II-3-5. Glu204 is involved in the hypersensitivity of OxyR2 to H_2O_2

To examine the role of Glu204, I generated a mutant strain of *V. vulnificus* that harbors E204G substitution on *oxyR*2 instead of wild-type *oxyR*2 and then measured the minimum concentrations of H_2O_2 required for oxidation of OxyR2 in a bacterial cell. The bacterial strains expressing either the wild-type OxyR2 or the OxyR2 (E204G) variant were grown anaerobically and then were exposed to various concentrations of H_2O_2. To estimate the oxidation state of OxyR2, the cells were treated with AMS, and all cellular proteins were then resolved with non-reducing SDS-PAGE and immunoblotted using anti-OxyR2 antibody to visualize the OxyR2 protein bands. Oxidation of wild-type OxyR2 occurred within 30 seconds after exposure to 0.5 μM H_2O_2 (Fig. II-5A, upper panel). In contrast, the OxyR2 (E204G) variant was not oxidized until exposed to 5 μM H_2O_2 (Fig. II-5B, upper panel), indicating that mutation of the 204th residue from Glu to Gly resulted in a significant increase in the threshold H_2O_2 level that can be sensed by OxyR2.

To assess the transcriptional activities of wild-type OxyR2 and the OxyR2 (E204G) variant, I measured the transcript level of *prx*2, using quantitative real-time PCR.

The results demonstrated that *prx*2 expression was activated by OxyR2 when exposed to H_2O_2 exceeding concentrations of 0.5 μM (Fig. II-5A, lower panel). In contrast, the OxyR2 (E204G) variant insufficiently activated *prx*2 expression until being exposed to 5 μM H_2O_2 (Fig. II-5B, lower panel). Collectively, these results indicate that Glu204 of OxyR2 is an important residue for sensitivity to H_2O_2.

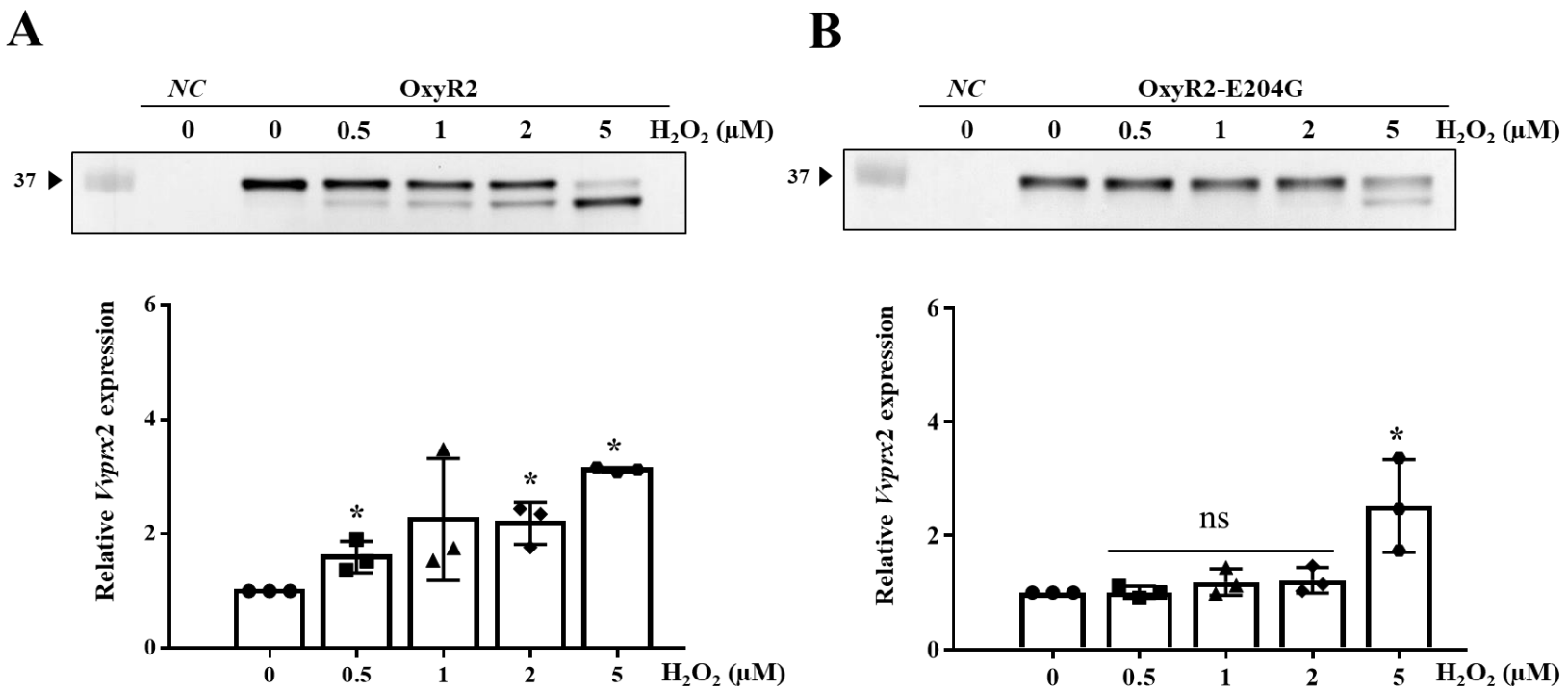
A
NC
OxyR2
0
0
0.5
1
2
5
H2O2 (μM)
37
Relative Vprx2 expression
6
4
2
0
*
*
*
0
0.5
1
2
5
H2O2 (μM)
B
NC
OxyR2-E204G
0
0
0.5
1
2
5
H2O2 (μM)
37
Relative Vprx2 expression
6
4
2
0
ns
*
0
0.5
1
2
5
H2O2 (μM)

Figure II-5. Effects of the Glu204 mutation and transition to Gly on H_2O_2 sensing at low levels in OxyR2

The *oxyR*2 mutants containing plasmids expressing OxyR2 (*A*) or OxyR2 (E204G), in which Glu204 was mutated to Gly (*B*), were grown anaerobically to A_{600} of 0.3 and exposed to various concentrations of H_2O_2, as indicated, for 30 sec (top panels) or 3 min (bottom panels) before harvesting. The cells (top panels) were then precipitated with TCA and alkylated with fresh AMS buffer for 1 h at 37 °C. Alkylated OxyR2 proteins were resolved by non-reducing SDS-PAGE and immunoblotted using anti-OxyR2 antibody. The two redox states for each OxyR2 (reduced and oxidized) are shown with arrows. The negative control (NC) is an *oxyR2* mutant expressing an empty vector. Total RNAs (bottom panels) were isolated, and the relative *prx*2 transcript levels were estimated by qRT-PCR analyses. The *prx*2 mRNA level under anaerobic conditions (0 μM H_2O_2) was set to 1. *Error bars* from three independent experiments represent S.D. *, statistically significant difference ($p < 0.05$) between control (0 μM H_2O_2) and groups. ns, not statistically significant.

II-3-6. Crystal structures of the E204G variant

Three crystal structures of the OxyR2-RD (E204G) variants were determined to confirm the structural role of Glu204. Of these, the crystal structure grown under similar crystallization condition to the wild-type protein exhibited the same space group (*C*2221) and packing constraints at the resolution of 1.55 Å, resulting in a "SO_4-free, high resolution" structure. Another structure was determined in a different space group (*P*3121) at a moderate resolution (2.3 Å). Additionally, another crystal structure was determined at 1.5 Å resolution, designated the "SO_4-bound form", because it contains a sulfate ion near the peroxidatic cysteine residue. The overall structures of the variants were very similar to those of the wild-type protein except for the region around Gly204 (Fig. II-6A and B).

In the "SO_4-free, high-resolution" structure of the E204G variant, the peptide bond at the mutated region exhibited a dual conformation of both the noncanonical conformation as observed in wild-type OxyR2 and the typical conformation observed in most OxyR proteins (Fig. II-6B and C). The other structures ("SO_4-free P3121" and "SO_4-bound" forms) of the variant presented only the typical

conformation or the flipped conformation compared with the wild-type OxyR2 structure (Fig. II-6B and C). Taken together, our finding suggests that the substitution to a glycine residue provides structural flexibility favoring the typical conformation at the peptide bond between the 203rd and 204th residues.

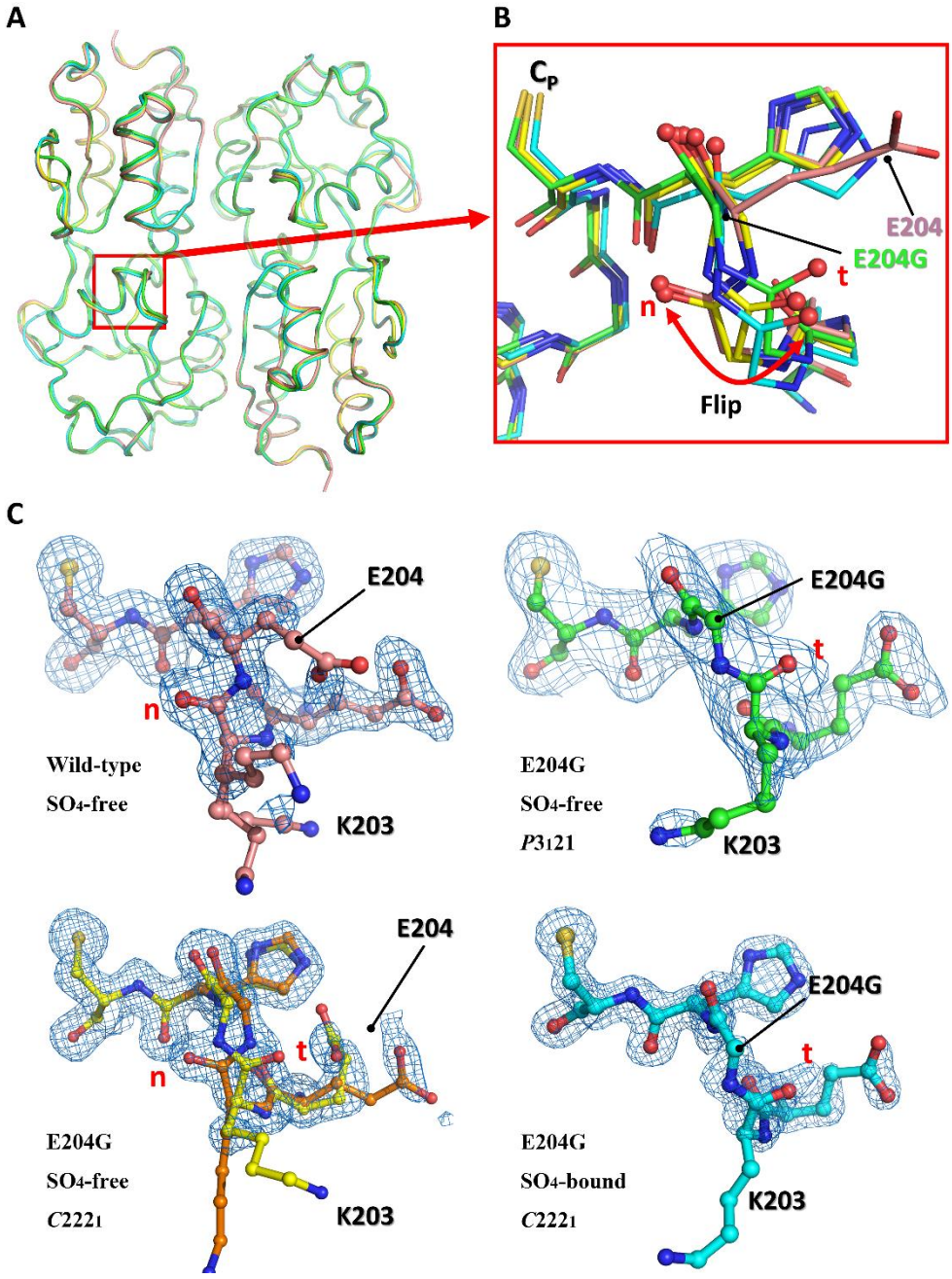
A
B
C_P
E204
E204G
t
n
Flip
C
E204
n
Wild-type
SO4-free
K203
E204G
t
E204G
SO4-free
P3121
K203
E204
t
n
E204G
SO4-free
C2221
K203
E204G
t
E204G
SO4-bound
C2221
K203

Figure II-6. Structural comparison of the wild-type OxyR-RD and the OxyR2-RD (E204G) variant

A, Structural superposition of the wild-type OxyR2-RD (pink) and the three OxyR2-RD (E204G) variants, which are named "SO_4-free *P*3121" (green), "SO_4-free, high resolution" (yellow and orange), and "SO_4-bound" (cyan). Regions containing the peroxidatic cysteine and the Glu204-containg loop are indicated by a red box. *B*, A close-up view of the red boxed region in (*A*): All residues are drawn in ball-and-stick representations. A flipped peptide bond is indicated with a double-headed arrow. The "t" and "n" letters in red indicate the typical conformation observed in the most OxyR proteins and the noncanonical conformation only observed in the wild-type OxyR2, respectively. *C*, 2*F*o-*F*c electron density maps (blue mesh) around the Glu204-containing of the wild-type (left top, pink), "SO_4-free high resolution" E204G (left bottom, yellow and orange), "SO_4-free *P*3121" E204G (right top, green) and "SO_4-bound" E204G variant (right bottom, cyan) are contoured at 1.0 σ. The "t" and "n" letters in red indicate the typical conformation observed in the most OxyR proteins and the noncanonical conformation only observed in the wild-type OxyR2, respectively. The structural determination was carried out by Drs. Nam-Chul Ha and

Inseong Jo.

II-3-7. The peptide bonds around Glu204 are structurally linked to the environment of the active site

To analyze the structural role of Glu204 in OxyR2, I generated a *V. vulnificus* mutant strain harboring an *oxyR*2 (E204A) that would allow the role of the side chain to be excluded. This E204A variant OxyR2 was expected to have a similar peptide conformation to the wild-type OxyR2 with Glu204, because only a glycine residue endows flexibility to the peptide bonds in proteins. As shown in Fig. II-7A, this substitution exhibited an expression profile of *prx*2 similar to that of the wild-type strain. The *prx*2 transcript expression was induced by the mutant OxyR2 when treated with H_2O_2 exceeding concentrations of 0.5 μM, as observed with wild-type OxyR2 (Fig. II-5A). This observation indicates that the peptide bond conformation of Glu204 is responsible for the hypersensitivity of OxyR2 rather than the side chain of the Glu204. Next, the role of the positive charge at Lys203, which, like Glu204, seems to be unique in OxyR2 (Fig. II-4D blue arrow). When the lysine residue was changed to a negatively charged Asp, a similar *prx*2 expression profile was observed (Fig. II-7C).

I examined the structures of OxyR2 by focusing on the interactions involved in the peptides around Glu204 or Gly204. I noted that the carbonyl group of the peptide bond after Glu204 or Gly204 interacts directly with a chloride ion, which corresponds to the H_2O_2 molecule in the H_2O_2-bound *Pa*OxyR C199D structure (Jo *et al*., 2015). More importantly, the peptide bond after Gly204 exhibited a minor conformational duality, due to the dual conformation of the peptide bond before Gly204 in the SO_4-free high-resolution E204G structure that has the same packing constraints as the wild-type protein (Fig. II-6C). The backbone carbonyl group of Gly204 (or the carbonyl group of the peptide bond between Gly204 and His205) exhibited a 0.7 Å difference between the two conformations. This observation indicates that the motion or positional uncertainty of 0.7 Å in the carbonyl group is involved with the binding of H_2O_2 near the peroxidatic cysteine residue (Fig. II-6B). The conformational duality or flexibility in this carbonyl group contributes to the lower H_2O_2 sensitivity of E204G variant OxyR2. In other words, the wild-type OxyR2 has a higher sensitivity to H_2O_2 due to the more rigid conformation resulting from employing Glu204 instead of Gly with its intrinsic conformational flexibility.

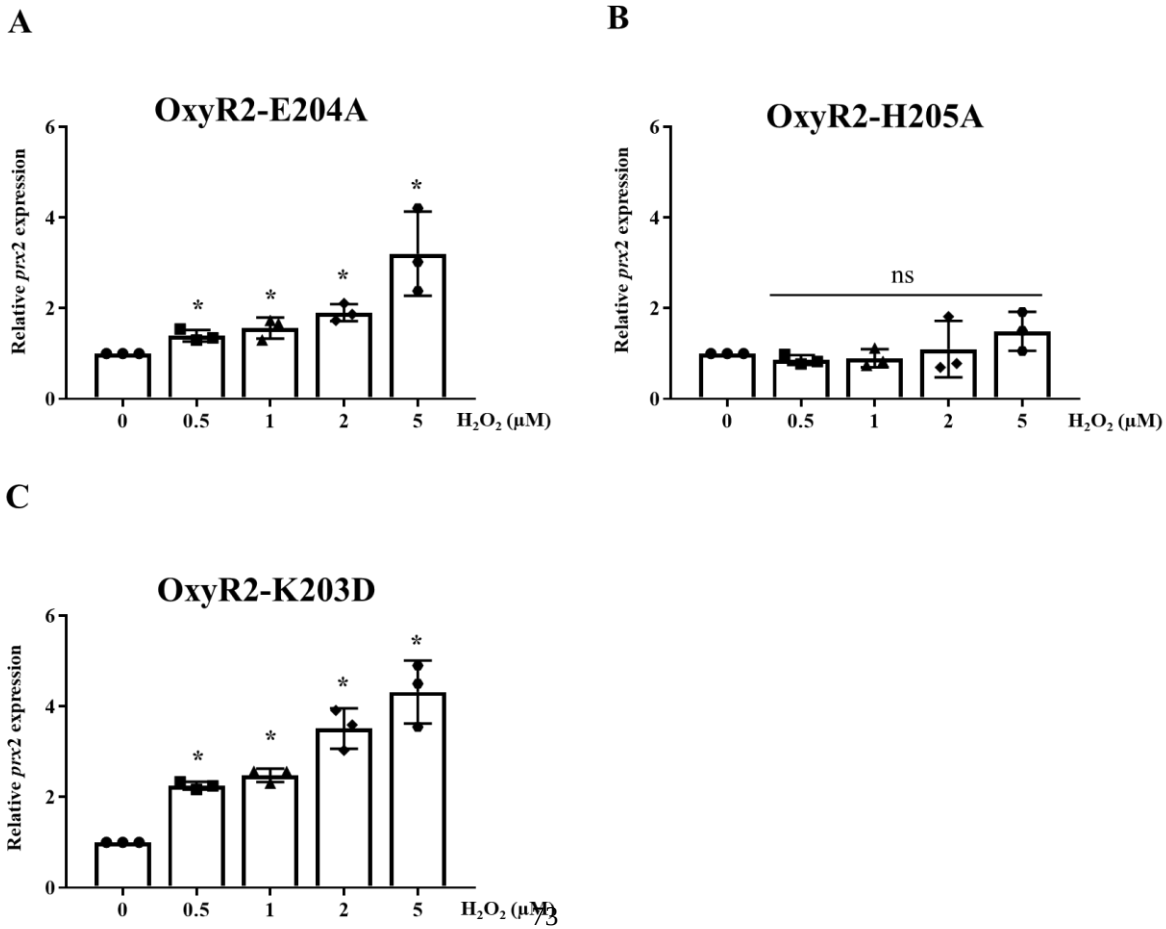
A
OxyR2-E204A
Relative prx2 expression
0
2
4
6
*
*
*
*
0
0.5
1
2
5
H2O2 (μM)
B
OxyR2-H205A
Relative prx2 expression
ns
C
OxyR2-K203D
Relative prx2 expression

Figure II-7. Effects of the Glu204 and His205 mutations on H_2O_2 sensing at low levels in OxyR2

The *oxyR*2 mutants containing plasmids expressing OxyR2 (E204A) (*A*), OxyR2 (H205A) (*B*), and OxyR2 (K203D) (*C*) were grown anaerobically to an A_{600} of 0.3 and exposed to various concentrations of H_2O_2, as indicated, for 3 minutes. Total RNA isolation and quantitative real-time PCR analyses were performed as previously described. The *prx*2 mRNA level under anaerobic conditions (H_2O_2 = 0 uM) was set as 1. *Error bars* from three independent experiments represent S.D. *, statistically significant difference ($p < 0.05$) between control (0 μM H_2O_2) and groups. ns, not statistically significant.

II-3-8. His205 is important in sensing H_2O_2

Due to the structural variation of the peptide bond after Glu204 or between Glu204 and His205, the position of the side chain of His205 was also affected by the conformation of the peptide bond. I thus investigated the role of the side chain of His205. A *V. vulnificus* mutant strain harboring the *oxyR*2 (H205A) failed to express *prx*2 at the indicated concentrations of H_2O_2, demonstrating an important role of His205 in sensing H_2O_2 (Fig. II-7B). Since His205 interacts with an invariant water molecule, this conformational variation at the side chain of His205 also contributes to the sensitivity of OxyR2.

II-3-9. OxyR2 has a second-order reaction rate constant that is two times higher than that of OxyR1

To obtain mechanistic insight into the relationship between the structural variations of OxyR2 and the sensitivity to H_2O_2, I measured the second-order reaction rate constants of OxyR2-RD and OxyR1-RD by analyzing competition kinetics with horseradish peroxidase-like peroxiredoxins (Ogusucu *et al*., 2007). As the control, BSA, which is known to have 35 cysteine residues (one of which is a free cysteine

residue), was used. As shown in Fig. II-8, both OxyR proteins exhibited constants of 10^7 $M^{-1}s^{-1}$, while BSA displayed a negligible value. The rate constants for the OxyR RDs were similar to those for peroxiredoxins, indicating that the peroxidatic cysteines of OxyRs are oxidized to Cys-SOH by H_2O_2 at a rate similar to that of peroxiredoxins. Noticeably, OxyR2-RD was about two times faster than OxyR1-RD, which may account for the higher sensitivity of OxyR2 than OxyR1. The faster reaction rate indicates that the activation energy of the reaction is lower and that the reaction occurs even at very low concentration of H_2O_2.

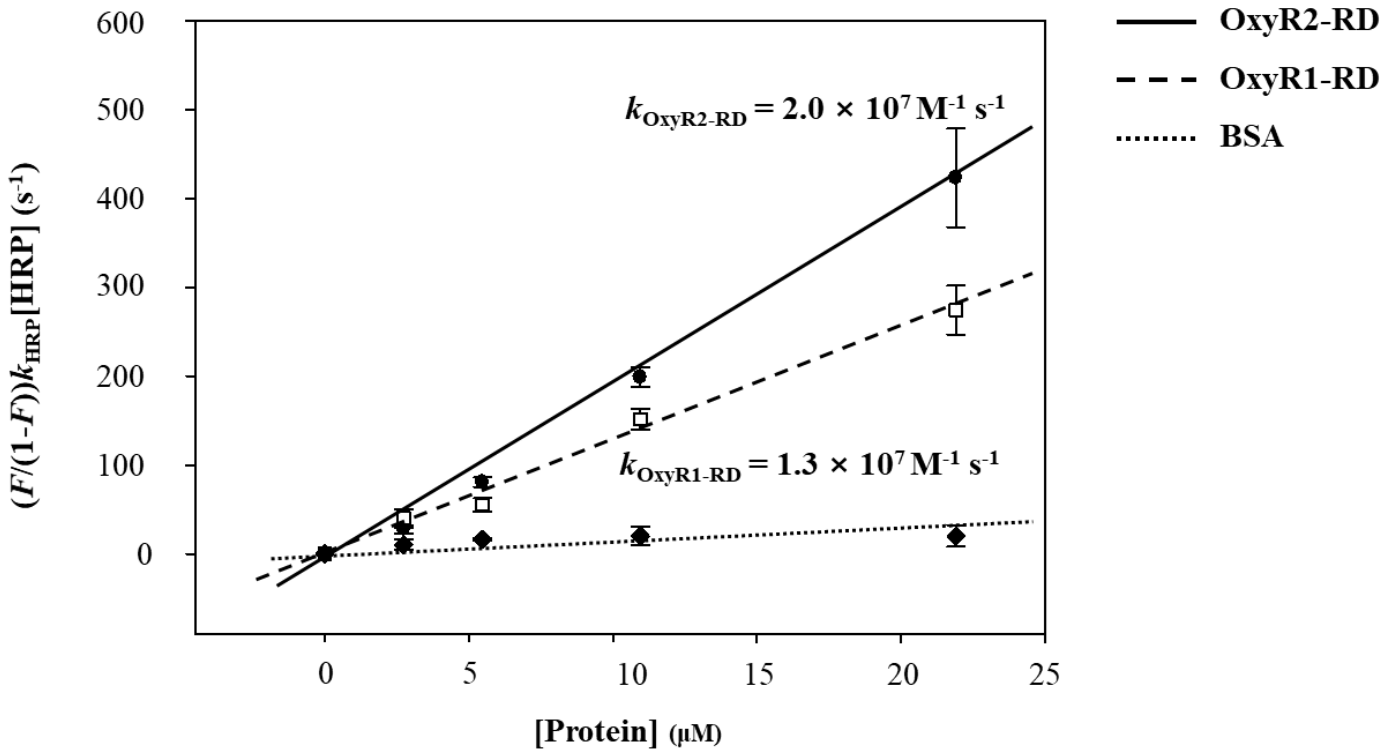
600
500
400
300
200
100
0
0
5
10
15
20
25
$(F/(1-F))k_{HRP}[HRP]$ (s^{-1})
[Protein] (μM)
$k_{OxyR2-RD} = 2.0 \times 10^7 M^{-1} s^{-1}$
$k_{OxyR1-RD} = 1.3 \times 10^7 M^{-1} s^{-1}$
OxyR2-RD
OxyR1-RD
BSA

Figure II-8. Determination of the second-order rate constants of OxyR2- RD and OxyR1-RD

Reaction mixtures containing HRP and various concentrations of OxyR2-RD (●) or OxyR1-RD (□) (0 – 21.9 μM) were exposed to H_2O_2. BSA (◆) was used as a negative control. The ratio of HRP oxidation was determined by measuring the absorbance at 403 nm. $k_{OxyR1\text{-}RD}$ and $k_{OxyR2\text{-}RD}$ were determined as the slope from the equation, $(F/(1-F))k_{HRP}$[HRP] against [OxyR1-RD or OxyR2-RD]. The fitting lines were calculated by the least square methods. *Error bars* from three independent experiments represent S.D.

II-4. Discussion

OxyR2 from *V. vulnificus* has a distinctive amino acid sequence and a higher sensitivity to H_2O_2 compared with other OxyRs from different bacterial species. *V. vulnificus* OxyR2 functions as a three state redox switch to regulate the expression of *prx*2. When OxyR2 encountered H_2O_2 exceeding the range in which Prx2 is functional, the peroxidatic cysteine of OxyR2 was overoxidized to Cys^{206}-SO_3H.

In many ways, OxyRs share the binding and reaction mechanisms of peroxiredoxins, or the peroxide-decomposing enzymes. Both OxyRs and peroxiredoxins have two invariant cysteine residues, which rapidly form a disulfide bond when exposed to H_2O_2. An H_2O_2 molecule is specifically bound near the peroxidatic cysteine (Hall *et al*., 2009; Jo *et al*., 2015). Two-step oxidation mechanisms were proposed for both proteins. During the first step, disulfide formation in the proteins begins with the nucleophilic attack on the peroxide by the thiolate moiety in the peroxidatic cysteine residue, resulting in the Cys-SOH form (Hall *et al*., 2009; Jo *et al*., 2015; Lee *et al*., 2004). During the second step, the Cys-SOH form at the peroxidatic cysteine establishes a disulfide bond with the resolving cysteine in both proteins.

In addition to these reduced and oxidized (disulfide) states, the overoxidized state is the third and unique redox state of OxyR2, and in this state, the protein turns off the transcription of *prx*2 in environments with high H_2O_2, where Prx2 is no longer functional. At low levels of H_2O_2 below the sensing levels of OxyR2, OxyR2 is maintained in the reduced state. Under the Prx2 working range of H_2O_2, the sensing cysteine in OxyR2 is oxidized and results in Cys-SOH intermediate that forms a disulfide bond with the other redox-sensitive cysteine, leading to activation of the target genes. However, when H_2O_2 levels exceed the Prx2 working range, the Cys-SOH intermediate that would normally be making an intermolecular disulfide bond is instead rapidly overoxidized to Cys-SO_3H or Cys-SO_2H by the high levels of H_2O_2. The resulting overoxidized OxyR2 turns off unnecessary Prx2 production. Thus, the overoxidized OxyR2 prevents production of useless Prx2 and saves valuable cellular resources. Therefore, the overoxidized OxyR2 is not simply an expired or perished form of OxyR2 but rather plays a crucial role in the survival of *V. vulnificus* during pathogenesis.

To investigate the structural basis of the higher sensitivity of the OxyR2, the crystal

structures of wild type and an E204G variant of OxyR2-RD were determined. In particular, I have identified an OxyR2-specific residue Glu204 near the peroxidatic cysteine residue. The plane of the peptide bond that occurs before Glu204 was rotated compared with the other OxyR proteins with glycine residue at the Glu204 site. Further analyses revealed that the OxyR2 variant harboring an E204G mutation showed decreased sensitivity to H_2O_2 in *V. vulnificus*, comparable to those of other OxyR proteins. Structural comparisons of the wild type and the E204G variant OxyR2s provided a reasonable structural explanation for high sensitivity of OxyR2. The E204G mutation has provided significant conformational flexibility in the region of Gly204 and His205. The carbonyl group of the peptide bond between His205 and Gly204 is involved in binding a H_2O_2 molecule, and the imidazole ring of His205 interacts with the invariant water molecule near the peroxidatic cysteine. Thus, our study suggests that the OxyR proteins regulate their sensitivity to H_2O_2 by altering the overall structural constraints around Glu204, which affect the binding of H_2O_2 and a water molecule.

The higher sensitivity to H_2O_2 could be explained by the high affinity for H_2O_2 and

the water molecules at the site near the peroxidatic cysteine residue. Unfortunately, I was not able to measure the binding constant of H_2O_2 due to the rapid reaction of H_2O_2 with peroxidatic cysteine residue of the OxyR proteins. Instead, the reaction rate constant for the formation of Cys-SOH at the peroxidatic cysteine residue, where H_2O_2 reacts, was measured. The results indicated that the structural alteration of OxyR2 may be related to the increased reaction rate constant for decomposition of the H_2O_2 molecule, as the structural alteration caused by Glu204 provides a more favorable local environment and thus reduced activation energy for the oxidation of the peroxidatic cysteine residue.

The higher second-order reaction rate constant also has implications for the high propensity for overoxidation of OxyR2. The Cys-SOH form at the peroxidatic cysteine has an alternative reaction pathway for overoxidation of the peroxidatic cysteine. H_2O_2 could enter the H_2O_2 binding site even when the peroxidatic cysteine residue is oxidized to Cys-SOH, suggesting a reaction rate constant similar to k_1. Thus, our finding suggests that the more sensitive OxyR with the higher k_1 value is more likely to enter the pathway leading to the overoxidation state instead of the

oxidized state with the disulfide bond. A similar explanation can also be applied to peroxiredoxins. In terms of gene regulation, the common mechanistic properties of relying on the cellular H_2O_2 level are important for maintaining targeted sensitivity for optimal gene expression of peroxiredoxins by OxyRs. Furthermore, the pathways leading to overoxidation of OxyR2 and Prx2 are also important for the fine regulation of gene expression.

This study shows that the thiol-based sensor OxyR regulates sensitivity to H_2O_2 by modulating the conformation of the residues required for binding of an H_2O_2 molecule. The OxyR2 strategy has implications for engineering other thiol-based sensor proteins with different sensitivities.

Acknowledgements

I would like to thank Drs. Nam-Chul Ha and Inseong Jo for help in structure determination and the discussions that followed.

Chapter III.

Identification and Characterization of *Vv*HmpA, a Nitric Oxide Dioxygenase of *Vibrio vulnificus*

III-1. Introduction

Reactive nitrogen species (RNS) including nitric oxide (NO) and its derivatives are among the most important components of the host innate immune system, which is the first line of defense against infecting pathogens (Fang, 2004). Under infectious conditions, NO is produced by inducible nitric oxide synthase (iNOS) which is expressed in phagocytes, especially in macrophages (Nathan and Shiloh, 2000). NO produced by iNOS in macrophages can subsequently be converted to additional RNS such as nitrogen dioxide (NO_2), peroxynitrite ($ONOO^-$), and dinitrogen trioxide (N_2O_3) (Fang, 2004; Stern and Zhu, 2014). Furthermore, pathogens that are ingested may encounter additional NO and RNS in the gastrointestinal tract as NO forms from acidified nitrite in the stomach and may be synthesized by some of the commensals in the host (Davies *et al*., 2011; Sobko *et al*., 2005), which provides a formidable antimicrobial barrier to ingested enteric pathogens (Fang, 2004). Because NO is a small uncharged molecule, it can quickly permeate across the cell membrane and lead to the damage of cellular components, including metal centers of proteins, membrane lipids and nucleotide bases, and thereby inhibit respiration and interfere with DNA replication of pathogens (Fang, 1999; Forrester and Foster, 2012; Nathan

and Shiloh, 2000). Therefore, pathogens have evolved sophisticated mechanisms to overcome nitrosative stress caused by the increased level of RNS, and such mechanisms are closely linked to their virulence (Bang *et al*., 2006; Richardson *et al*., 2006; Stern *et al*., 2012).

To protect themselves from nitrosative stress, pathogens rely on a variety of detoxifying enzymes such as NO dioxygenase, flavorubredoxin and associated oxidoreductase, cytochrome *c* nitrite reductase, *S*-nitrosoglutathione reductase, and peroxynitrite reductase (Bryk *et al*., 2000; Fang, 2004; Karlinsey *et al*., 2012; Liu *et al*., 2001). Among these, NO dioxygenases are a family of flavohemoglobin (Hmp) composed of N-terminal globin domain with the heme-binding site and C-terminal oxidoreductase domain containing nicotinamide adenine dinucleotide (NAD)- and flavin adenine dinucleotide (FAD)-binding sites (Bonamore and Boffi, 2008). Although some NO dioxygenases reduce NO to N_2O in the absence of oxygen (Mills *et al*., 2008), typical NO dioxygenases detoxify the potentially harmful NO by oxidizing it to a non-toxic metabolite NO_3^- under aerobic environments (Hausladen *et al*., 2001). Under conditions where O_2 is not limiting, the N-terminal ferrous-oxy

(Fe^{2+}-O_2) heme of the NO dioxygenase reacts with NO to yield NO_3^- and ferric-deoxy (Fe^{3+}) heme, in which both atoms of O_2 are incorporated into NO_3^- (Forrester and Foster, 2012; Gardner *et al*., 2006). The C-terminal oxidoreductase domain reduces the heme in the ferric state by reacting with $FADH_2$ and the resulting FAD^+ is then reduced to $FADH_2$ by utilizing the reducing power of cellular NADH (Forrester and Foster, 2012).

The opportunistic human pathogen, *Vibrio vulnificus*, is a causative agent of life-threatening septicemia and necrotizing fasciitis in individuals with predisposing conditions, such as liver damage and kidney failure (Gulig *et al*., 2005; Oliver, 2015). It is a reasonable assumption that *V. vulnificus* has to cope with nitrosative stress imposed by immune systems to survive in the host environments and in turn to ensure developing illness. Nevertheless, no definitive analysis on the mechanisms of *V. vulnificus* to survive under nitrosative stress at molecular levels and thereby to develop illness has been reported until now (Elgaml and Miyoshi, 2015). Accordingly, I initiated a transcriptome analysis and identified *V. vulnificus hmpA* (*VvhmpA*), a homologue of *E. coli hmp*, which is the most preferentially expressed

in *V. vulnificus* cells exposed to NO. The biochemical and kinetic properties of *V. vulnificus* HmpA (*Vv*HmpA), the product of *hmpA*, were verified experimentally. Construction of the isogenic *hmpA* mutant and evaluation of its phenotypes provided strong evidence that *Vv*HmpA contributes to the survival and thus virulence of *V. vulnificus* during infection.

III-2. Experimental procedures

III-2-1. Strains, plasmids, and culture conditions

The strains and plasmids used in this study are listed in Table II-1. Unless otherwise noted, the *V. vulnificus* MO6-24/O (wild type), *Vv*hmpA mutant, and *Vv*hmpA-complemented strain were grown aerobically in Luria-Bertani (LB) medium supplemented with 2.0% (w/v) NaCl (LBS) at 30 °C, and their growth was monitored spectrophotometrically at 600 nm (A_{600}). The RAW 264.7 murine macrophage cells were obtained from Korean Cell Line Bank (Seoul, Korea) and grown in Dulbecco's modified Eagle's medium (DMEM) containing 10% fetal bovine serum (FBS) and appropriate antibiotics (100 units/ml penicillin G and 100 μg/ml streptomycin (Gibco-BRL, Gaithersburg, MD)) in air supplemented with 5% CO_2 at 37 °C.

III-2-2. RNA purification and transcriptome analysis

Total RNAs were isolated from *V. vulnificus* MO6-24/O, grown aerobically to A_{600} of 0.5 in M9 minimal media supplemented with 0.4% (w/v) glucose (M9G) and exposed to different types of NO donors for 10 min. As NO donors, excess amounts of either NO-releasing poly(lactic-*co*-glycolic acid)-polyethylenimine nanoparticles

(NO/PPNPs, releasing NO with $t_{1/2}$ = 24 h at 37 °C) or Spermine NONOate (Cayman Chemical, Ann Arbor, MI, releasing NO with $t_{1/2}$ = 39 min at 37 °C) were used (Bang *et al*., 2006; Nurhasni *et al*., 2015). The RNAs were further purified by removing DNA using TURBO DNase (Ambion, Austin, TX), and mRNA was selectively enriched by depleting rRNA using a Ribo-Zero rRNA removal kit (Epicentre, Madison, WI) according to the manufacturer's procedure.

The cDNA libraries were constructed using a TruSeq Stranded mRNA Sample Prep kit (Illumina, San Diego, CA). Strand-specific paired-end 100-bp sequences were read from each cDNA library using HiSeq 2500 (Illumina) as described previously (Kim *et al*., 2018). The raw sequencing reads were analyzed using CLC Genomics Workbench 5.5.1 (CLC Bio, Aarhus, Denmark) and mapped on to the *V. vulnificus* MO6-24/O genome sequence (GenBank™ accession numbers: CP002469 and CP002470). The expression level of each gene was defined using the number of fragments per kilobase of transcript per million mapped reads (FPKM) (Conesa *et al*., 2016). Quantile-normalized FPKM values were then statistically analyzed by t-tests to identify the genes expressed differentially (fold change ≥ 2; p value of < 0.05)

in the *V. vulnificus* exposed to NO/PPNPs.

III-2-3. qRT-PCR

One microgram of the total RNA was used to synthesize cDNA with the iScript™ cDNA synthesis kit (Bio-Rad, Hercules, CA), and real-time PCR amplification of the cDNA was performed by using the Chromo 4 real-time PCR detection system (Bio-Rad) with pairs of specific primers (Table II-2) as described previously (Jang *et al*., 2017). Relative expression levels of the *VvhmpA* mRNA in the same amounts of total RNA were calculated by using the 16S rRNA expression level as the internal reference for normalization (Jang *et al*., 2017).

III-2-4. Generation and complementation of the *Vv*hmpA mutant

The *VvhmpA* gene was inactivated *in vitro* by deletion of the *VvhmpA* ORF (660-bp of 1,185-bp) using the PCR-mediated linker-scanning mutation method as described previously (Kim *et al*., 2014). Briefly, two pairs of primers HMPA01-F and -R (for amplification of the 5' amplicon) and HMPA02-F and -R (for amplification of the 3' amplicon) were designed and used (Table II-2). The *VvhmpA* gene with the 660-bp

deletion was amplified by PCR using the mixture of both amplicons as the template and HMPA01-F and HMPA02-R as primers. The resulting *ΔhmpA* was ligated into SpeI-SphI-digested pDM4 to form pDY1618 (Table II-1). *E. coli* S17-1 λ*pir*, *tra* (Simon *et al*., 1983) strain containing pDY1618 was used as a conjugal donor to *V. vulnificus* MO6-24/O to generate the *VvhmpA* mutant, DY171 (Table II-1). The conjugation and isolation of the transconjugant were conducted using the method described previously (Lim and Choi, 2014).

To complement the *VvhmpA* mutation, the upstream region and ORF of *VvhmpA* were amplified by PCR using HMPA03-F and HMPA03-R as primers (Table II-2). The amplified *VvhmpA* was cloned into the broad-host-range vector pJH0311 (Goo *et al*., 2006) to create pDY1701 (Table II-1). Either pJH0311 or pDY1701 was transferred into DY171 by conjugation as described above.

III-2-5. Western blot analysis

The ORF of *VvhmpA* was amplified by PCR using a pair of primers, HMPA04-F and -R (Table II-2), digested with NcoI and SalI, and then ligated into pPROEX HTa

(Invitrogen) to result in pDY1703 (Table II-1). The His_6-tagged *Vv*HmpA was expressed in *E. coli* BL21 (DE3) containing pDY1703 and purified by using affinity chromatography (Qiagen) according to the manufacturer's procedure, and used to raise rabbit anti-*Vv*HmpA polyclonal antibody (AbFrontier, Seoul, Korea) (Jang *et al*., 2017).

For Western blot analysis, *V. vulnificus* MO6-24/O grown to A_{600} of 0.5 in M9G was exposed either to Spermine NONOate as described above or to M9G (negative control) and then harvested to isolate total cellular proteins. To detect *Vv*HmpA, the total cellular proteins (20 μg) were resolved on SDS-PAGE under reducing conditions and immunoblotted using the rabbit anti-*Vv*HmpA antibody as described previously (Jang *et al*., 2017). A mouse antibody to *E. coli* DnaK was purchased (Enzo Lifescience, Farmingdale, NY) and used to detect *V. vulnificus* DnaK (*Vv*DnaK, a loading control) (Jang *et al*., 2017).

III-2-6. Purification of *Vv*HmpA and absorption spectra of the reduced, NO-bound, and oxidized *Vv*HmpA

The *VvhmpA* ORF was amplified by PCR using a pair of primers, HMPA05-F and -R (Table II-2), digested with NdeI and XhoI, and then ligated into pET-21c(+) (Invitrogen) to result in pSH1701 (Table II-1). The non-His_6-tagged *Vv*HmpA was expressed in *E. coli* BL21 (DE3) containing pSH1701 and purified by using a HiTrap Q anion-exchange column (GE Healthcare, Chicago, IL) and then a HiLoad Superdex 16/60 200 column (GE Healthcare) as described previously (Ahn *et al*., 2018). The purified *Vv*HmpA was quantitated using the Bradford method (Bradford, 1976) and dissolved in the buffer with 20 mM Tris-HCl (pH 8.0) and 0.25 M NaCl at 4 °C until use.

To obtain reduced *Vv*HmpA, the purified *Vv*HmpA (10 μM) was mixed with sodium hydrosulfite powder (Sigma, 1 μM) under anaerobic conditions (Ioannidis *et al*., 1992). Immediately, the residual sodium hydrosulfite was removed by using Ultracell-10K centricon (Millipore, Burlington, MA) in the anaerobic chamber with an atmosphere of 90% N_2, 5% CO_2, and 5% H_2 (Coy Laboratory Products, Grass Lake, MI) (Kim *et al*., 2014). The reduced *Vv*HmpA (10 μM) was incubated under anaerobic conditions with 40 μM Diethylamine NONOate sodium salt hydrate

(Sigma) for 10 min to obtain the NO-bound *Vv*HmpA, or under aerobic conditions for 20 min to obtain the oxidized *Vv*HmpA. The UV-vis absorption spectra of the *Vv*HmpA proteins were recorded by using Shimadzu UV-1800 UV/VIS spectrophotometer (Shimadzu, Kyoto, Japan) at room temperature.

III-2-7. Reconstitution of *Vv*HmpA with heme and FAD and quantitation of the cofactors

To reconstitute *Vv*HmpA with heme *in vitro*, 10 μM of the purified *Vv*HmpA was gradually mixed with stoichiometric excess of hemin (1 mM in 0.01 M NaOH) and then incubated for 40 min at 4 °C (Gardner *et al*., 2000a). After the residual hemin aggregates were removed by centrifugation, the *Vv*HmpA saturated with heme was further purified using a HiPrep^{TM} 26/10 column (GE Healthcare). Similarly, 10 μM of the purified *Vv*HmpA was incubated with 80 μM of FAD for an hour at room temperature, and then residual FAD was removed from the resulting reconstituted *Vv*HmpA using Ultracell-10K centricon (Fang *et al*., 2017). The contents of the heme and FAD in *Vv*HmpA both before and after the reconstitution with each of the cofactor were determined using the pyridine hemochromagen assay (Barr and Guo,

2015) and FAD fluorometric assay (Hirano and Namihira, 2017), respectively, as described previously.

III-2-8. Kinetic analysis

Fresh NO stock solution was prepared daily as described previously (Poole *et al*., 1996) with modifications. Briefly, NO gas was formed by reacting 0.25 g sodium nitrite with 5 ml acidic ferrous sulfate solution, and purified by passing through 1 M NaOH solution and then degassed distilled water. The purified NO gas was collected and then dissolved in degassed distilled water to form the NO stock solution of approximately 500 μM, which was serially diluted to appropriate concentrations immediately before use.

To determine the kinetic properties of *Vv*HmpA, 10 μl of the distilled water containing varying concentrations of NO and 10 μl of the purified and heme-reconstituted *Vv*HmpA (1 μM) were delivered via separate syringes to 980 μl of the reaction buffer (50 mM potassium phosphate (pH 7.8) with 100 μM EDTA, 1 μM FAD and 100 μM NADH) that is pre-incubated at either 37 °C or 30 °C (Gardner *et*

al., 2000a). The initial rates of NO decomposition were obtained by measuring the residual NO in the reaction mixture amperometrically using an ISO-NOP electrode (World Precision Instruments, Sarasota, FL) and plotted against the concentrations of NO. K_M was determined as the NO concentration at which *Vv*HmpA decomposes NO at half the rate of its V_{max} (Smagghe *et al*., 2008) and the k_{cat} was determined through the Lineweaver-Burk plotting. Presuming only *Vv*HmpA molecules containing heme are active, the k_{cat} was expressed relative to heme.

III-2-9. NO-decomposition activity and survival of *V. vulnificus*

The *V. vulnificus* strains grown to A_{600} of 0.5 in M9G were pre-incubated with 50 μM Spermine NONOate for 30 min to induce *Vv*HmpA. The *V. vulnificus* cells were harvested with centrifugation, washed twice using PBS, and resuspended with 10 ml PBS. The PROLI NONOate (Cayman Chemical) was administered to the resuspended *V. vulnificus* cells to achieve 2 μM NO at a final concentration, and their NO-decomposition activities were determined by measuring the residual NO using the ISO-NOP electrode.

To examine the effect of *Vv*HmpA on the survival of *V. vulnificus* under nitrosative stress, equal numbers (approximately 10^7 cells/ml) of the *V. vulnificus* strains were used to inoculate the M9G containing 0.15 mg/ml NO/PPNPs at a final concentration. The resulting cultures were further incubated aerobically with shaking and the viable cells were counted at time intervals.

III-2-10. Cytotoxicity and survival of *V. vulnificus* infecting immune cells

The macrophage RAW 264.7 cells were resuspended in fresh DMEM containing 500 ng/ml *E. coli* O111:B4 lipopolysaccharide (Sigma) and 1 mM L-arginine (Sigma) to induce NO production (Walker *et al*., 1997) either with or without L-NG-monomethyl arginine citrate (L-NMMA, Sigma), which is a known NO synthase inhibitor (Nathan and Hibbs, 1991). The RAW 264.7 cells were seeded into 24-well culture dishes at a concentration of 5×10^5 cells per well, and infected with the *V. vulnificus* strains at a multiplicity of infection (MOI) of 1. The cytotoxicities of the *V. vulnificus* strains were determined by measuring the LDH activity released into the supernatant as described previously (Lim and Choi, 2014), and expressed using the LDH activity released from the RAW 264.7 cells completely lysed by 1.5%

Triton X-100 (Sigma) as 100%. To determine the survival of the *V. vulnificus* strains under the nitrosative stress derived from the RAW 264.7 cells, the culture dishes were washed two times to remove bacteria nonadherent to the macrophages as described previously (Lim and Choi, 2014). Following the last wash, the RAW 264.7 cells were broken with 0.1% Triton X-100 treatment for 20 min, and the recovered bacterial cells were enumerated as cfu per well (Lim and Choi, 2014). Statistical significance was determined by the Student's t test.

III-2-11. Mouse lethality assay

The *V. vulnificus* strains grown to A_{600} of 0.5 were harvested and resuspended in PBS to 1.0×10^7 cfu/ml. To determine mouse lethality, 100 μl of the suspension of either the wild type or *VvhmpA* mutant was used for intraperitoneal infection of the 7-week-old Institute of Cancer Research (ICR) female mice (specific-pathogen-free, Seoul National University) (n = 5 for each infection). The infection experiments were performed three times with the mice (total n = 15) to ensure reproducibility and survival percentages of the mice were recorded for 24 h. Statistical significance was determined by the log-rank test. All manipulations for mouse lethality assay were

approved by the Animal Care and Use Committee at Seoul National University.

III-2-12. Data analyses and transcriptome data accession number

Averages and standard deviations (S.D.) were calculated from at least three independent experiments. Statistical analyses were performed using GraphPad Prism 7.0 (GraphPad Software). All raw transcriptome data were deposited in SRA (https://www.ncbi.nlm.nih.gov/sra) under accession number PRJNA513463.

III-3. Results

III-3-1. Effects of NO on *V. vulnificus* transcriptome

To investigate the response of *V. vulnificus* to NO stress, The *V. vulnificus* MO6-24/O cells exposed to NO/PPNPs (Nurhasni *et al*., 2015) were harvested and their transcriptomes were analyzed. The NO/PPNPs were chosen as they have been reported to release NO in a sustained manner over 6 days without any burst release (Nurhasni *et al*., 2015). To minimize the effects of the NO-derived molecules that could be generated by reaction of NO in a rich medium, and to characterize early response of *V. vulnificus* to NO stress, I chose to use M9G and to have a relative short incubation time of 10 min. Transcriptome analysis revealed 551 genes that were differentially expressed (fold change ≥ 2; p value < 0.05) upon exposure to NO; 320 genes were upregulated and 231 genes were downregulated (data were deposited in Sequence Read Archive (SRA, https://www.ncbi.nlm.nih.gov/sra, under accession number PRJNA513463). The differentially expressed genes were involved with functions such as nitrosative and oxidative stress tolerance, inorgarnic ion transport, molecular chaperone, secretion, and chemotaxis (Tables III-1, 2). Among the genes upregulated upon exposure to NO, eight genes potentially involved in nitrosative

stress defense were selected (Fig. III-1). Six of the genes are predicted to encode proteins involved in the defense against nitrosative stress: NO dioxygenase, nitrite reductase large subunit, nitrite reductase small subunit, NrfA (cytochrome *c* nitrite reductase subunit c_{552}), NnrS (putative heme- and copper-containing transmembrane protein), and NrfD (cytochrome *c* nitrite reductase subunit). The other two genes are predicted to encode transcriptional regulators that control the expression of the genes involved in nitrosative stress defense: NorR (NO reductase transcriptional regulator) and NsrR (nitrite-sensitive transcriptional repressor).

Expression of the eight genes in *V. vulnificus* exposed to NO/PPNPs was reevaluated by using qRT-PCR analyses, further confirming that NO exposure induced transcription of the genes (Fig. III-1). Since the expression of the VVMO6_00248 gene, predicted to encode an NO dioxygenase, increased the most upon exposure to NO (Fig. III-1), the gene was selected for further study. To verify that the induction of the VVMO6_00248 gene is not confined to a specific NO donor, expression of the gene upon exposure of *V. vulnificus* to Spermine NONOate as an alternate NO donor was determined. As shown in Fig. III-2, exposure to Spermine NONOate

increased the levels of the gene product as well as the transcript of VVMO6_00248 as determined by Western blot analysis and qRT-PCR, respectively. The combined results confirmed that the expression of the VVMO6_00248 gene in *V. vulnificus* is induced upon exposure to NO.

Table III-1. Selected genes that showed increased transcript levels in wild-type *V. vulnificus* after 10 min of exposure to 0.15 mg/ml NO/PPNPs

Locus tag	Annotation from NCBI	Fold change	*p* value
1. Nitrosative and oxidative stress tolerance			
VVMO6_00248	Nitric oxide dioxygenase	65.2	1.28×10^{-197}
VVMO6_03847	Nitrite reductase large subunit	49.7	1.73×10^{-175}
VVMO6_03846	Nitrite reductase small subunit	44.6	1.01×10^{-79}
VVMO6_01967	Cytochrome *c* nitrite reductase subunit c_{552}, NrfA	21.3	1.48×10^{-208}
VVMO6_00672	Putative heme- and copper-containing transmembrane protein, NnrS	19.1	4.99×10^{-86}
VVMO6_01809	Nitric oxide reductase transcription regulator, NorR	14.4	2.93×10^{-110}
VVMO6_01964	Cytochrome c nitrite reductase subunit NrfD	10.1	7.96×10^{-42}
VVMO6_00249	Nitrite-sensitive transcriptional repressor, NsrR	3.1	2.48×10^{-31}
2. Fe transport and metabolism			
VVMO6_02185	Ferrous iron transporter B	30.8	1.18×10^{-205}
VVMO6_02186	Ferrous iron transport protein A	28.3	1.46×10^{-202}

VVMO6_02184	Iron transporter FeoC	14.6	2.28×10^{-53}
VVMO6_RS16865	Energy transducer TonB	11.3	1.36×10^{-72}
VVMO6_03377	Hemin ABC transporter substrate-binding protein	11.2	8.41×10^{-94}
VVMO6_03376	Iron ABC transporter permease	10.4	1.51×10^{-96}
VVMO6_03378	Biopolymer transporter ExbD	9.7	4.32×10^{-77}
VVMO6_03382	Putative heme utilization radical SAM enzyme HutW	9.3	8.69×10^{-82}
VVMO6_03379	Biopolymer transporter ExbB	8.9	6.92×10^{-79}
VVMO6_03768	TonB-dependent receptor	8.2	1.19×10^{-52}
3. Inorganic ion transport and metabolism			
VVMO6_03845	Formate transporter	31.0	1.72×10^{-38}
VVMO6_01148	Dihydroorotate dehydrogenase	29.2	6.49×10^{-163}
VVMO6_00672	Short-chain dehydrogenase	19.1	4.99×10^{-86}
VVMO6_01834	Manganese transporter 11 TMS	13.1	4.89×10^{-64}
4. Molecular chaperone and related functions			
VVMO6_00610	Protease	39.9	1.71×10^{-186}
VVMO6_00609	U32 family peptidase	25.0	6.09×10^{-73}
VVMO6_03996	Peptidase T	24.9	3.38×10^{-178}
VVMO6_01724	Peptidase M20	13.6	5.51×10^{-90}

5. Secretion, motility, and chemotaxis

VVMO6_03848	Chemotaxis protein	4.3	1.82×10^{-48}
VVMO6_00940	Methyl-accepting chemotaxis protein	2.6	1.71×10^{-29}
VVMO6_04557	Chemotaxis protein CheA	2.3	5.23×10^{-13}
VVMO6_03840	Flagellar motor protein MotA	2.3	2.35×10^{-18}

6. Energy production and conversion

VVMO6_03472	L-threonine dehydrogenase	41.5	1.27×10^{-206}
VVMO6_01660	Qinol dehydrogenase ferredoxin subunit NapH	20.0	1.74×10^{-171}
VVMO6_00219	Fmarate reductase flavoprotein subunit	19.7	4.69×10^{-147}
VVMO6_01810	Hydroxylamine reductase	19.6	8.14×10^{-165}
VVMO6_01661	Ferredoxin-type protein NapG	19.5	3.43×10^{-175}
VVMO6_01811	Hybrid-cluster NAD(P)-dependent oxidoreductase	17.7	2.80×10^{-104}
VVMO6_02043	Bifunctional acetaldehyde-CoA/alcohol dehydrogenase	11.6	1.97×10^{-91}
VVMO6_03816	Anaerobic ribonucleoside triphosphate reductase	11.3	1.38×10^{-73}
VVMO6_03887	Anaerobic C4-dicarboxylate transporter DcuC	7.5	8.49×10^{-35}

VVMO6_00218	Succinate dehydrogenase/fumarate reductase iron-sulfur subunit	5.2	3.38×10^{-30}

Table III-2. Selected genes that showed decreased transcript levels in wild-type *V. vulnificus* after 10 min of exposure to 0.15 mg/ml NO/PPNPs

Locus tag	Annotation from NCBI	Fold change	*p* value
1. Secretion, motility, and chemotaxis			
VVMO6_04219	Hemolysin D	0.112	9.31×10^{-75}
VVMO6_02863	Type II secretion system protein GspL	0.330	1.34×10^{-39}
VVMO6_04387	HlyD family secretion protein	0.337	6.51×10^{-4}
VVMO6_02861	General secretion pathway protein GspN	0.339	1.14×10^{-29}
VVMO6_02868	Type II secretion system protein GspG	0.341	3.05×10^{-36}
VVMO6_02871	Type II secretion system protein GspD	0.343	2.21×10^{-29}
VVMO6_02869	Type II secretion system protein GspF	0.350	4.37×10^{-30}
VVMO6_02870	Type II secretion system protein GspE	0.360	2.37×10^{-28}
VVMO6_02864	General secretion pathway protein GspK	0.363	3.18×10^{-27}
VVMO6_02865	Type II secretion system protein GspJ	0.408	2.86×10^{-18}
VVMO6_02867	Type II secretion system protein GspH	0.420	1.48×10^{-18}
VVMO6_02866	Type II secretion system protein GspI	0.432	3.74×10^{-17}

2. Cell wall structures and biogenesis

VVMO6_04218	TolC family protein	0.185	1.07×10^{-53}
VVMO6_00583	Outer membrane protein U, OmpU	0.300	3.49×10^{-39}
VVMO6_03275	OmpV family protein	0.408	3.88×10^{-8}

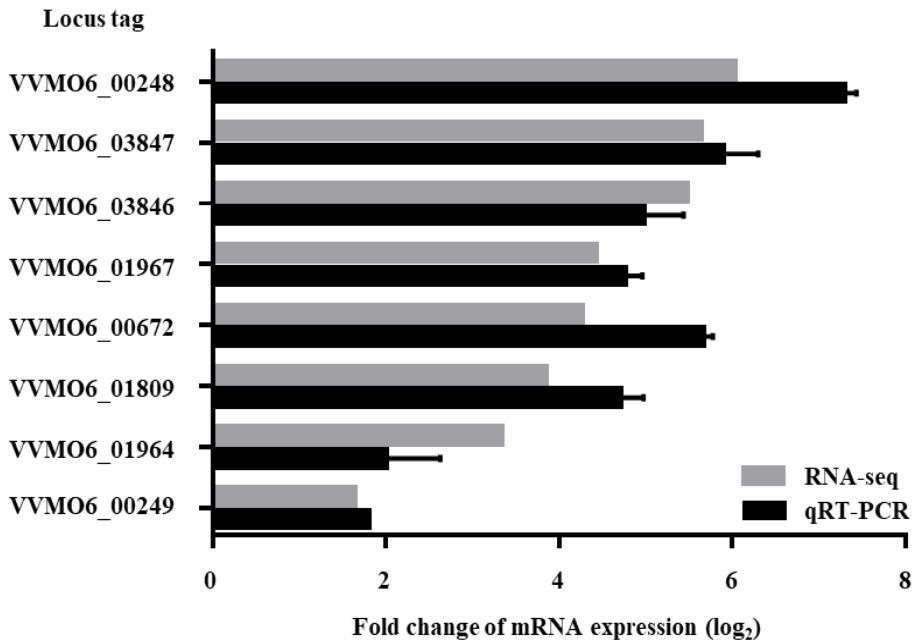

Gene product
Nitric oxide dioxygenase
Nitrite reductase large subunit
Nitrite reductase small subunit
Cytochrome *c* nitrite reductase subunit c_{552}, NrfA
Putative heme- and copper-containing transmembrane protein, NnrS
Nitric oxide reductase transcription regulator, NorR
Cytochrome *c* nitrite reductase subunit, NrfD
Nitrite-sensitive transcriptional repressor, NsrR

Figure III-1. Genes upregulated by NO exposure and possibly involved in nitrosative stress defense

Among the NO-upregulated genes (fold change ≥ 2; *p* value of < 0.05) identified by transcriptome analysis, eight genes potentially involved in nitrosative stress defense were selected and their upregulation was confirmed by qRT-PCR. Each column represents the mRNA expression level of *V. vulnificus* MO6-24/O exposed to NO/PPNPs relative to that exposed to PPNPs (negative control). *Error bars* represent the S.D. Locus tags are based on the *V. vulnificus* MO6-24/O genome sequence (GenBank™ accession numbers: CP002469 and CP002470) and the products of the genes are presented on the right. *NO/PPNPs*, NO-releasing poly(lactic-*co*-glycolic acid)-polyethylenimine nanoparticles; *PPNPs*, poly(lactic-*co*-glycolic acid)-polyethylenimine nanoparticles.

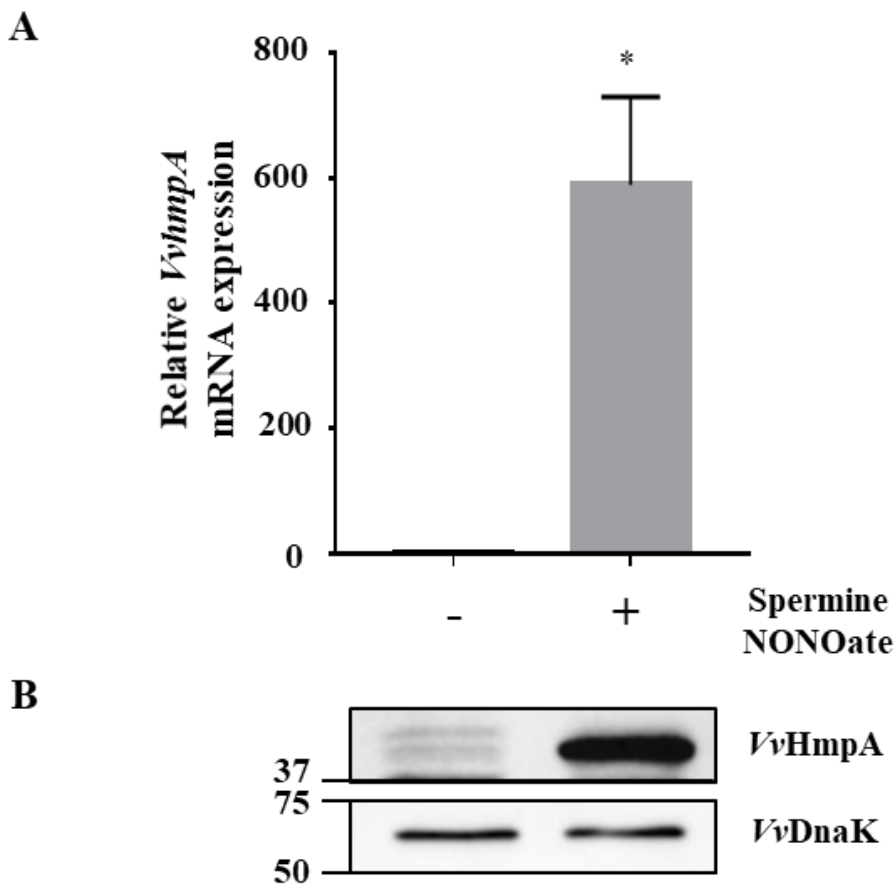
A
800
600
400
200
0
*
Relative Vvhmp A mRNA expression
-
+
Spermine NONOate
B
37
75
50
VvHmpA
VvDnaK

Figure III-2. Expression of *VvhmpA* under nitrosative stress

RNAs and proteins were extracted from *V. vulnificus* MO6-24/O exposed either to Spermine NONOate or M9G (negative control). *A*, the *VvhmpA* mRNA levels were determined by qRT-PCR analyses, and expressed using the *VvhmpA* mRNA level of the culture unexposed to NO as 1. *Error bars* represent the S.D. *B*, total proteins of the cultures were resolved on reducing SDS-PAGE, and *Vv*HmpA and *Vv*DnaK were immunoblotted using the rabbit anti-*Vv*HmpA antibody and the mouse anti-DnaK antibody, respectively. The protein size markers (Bio-Rad) on the left are in kilodaltons. *, statistically significant difference ($p < 0.05$) between control (0 μM Spermine NONOate) and Spermine NONOate treated group.

III-3-2. Identification and sequence analysis of *Vv*HmpA

The amino acid sequence deduced from the nucleotide sequence of the VVMO6_00248 gene revealed a putative protein, composed of 394 amino acids with a theoretical molecular mass of 44.3 kDa and a pI of 5.21. The deduced amino acid sequence of VVMO6_00248 was 62%, 61%, and 51% identical to known NO dioxygenases such as *E. coli* Hmp (*Ec*Hmp), *Salmonella enterica* serovar Typhimurium Hmp (*St*Hmp), and *V. cholerae* HmpA (*Vc*HmpA) (Fig. III-3), respectively. These findings led us to assume that the protein is an NO dioxygenase of *V. vulnificus* and thus named it *Vv*HmpA. Amino acid sequence analysis of *Vv*HmpA further revealed that the protein possesses the highly conserved heme-binding domain of known NO dioxygenases (Bonamore and Boffi, 2008) (Fig. III-3). Moreover, *Vv*HmpA contains the putative NAD- and FAD-binding domains, which are also conserved in NO dioxygenases (Bonamore and Boffi, 2008) (Fig. III-3). The combined results proposed that *Vv*HmpA is a multidomain NO dioxygenase that possibly contains heme and FAD as its cofactors.

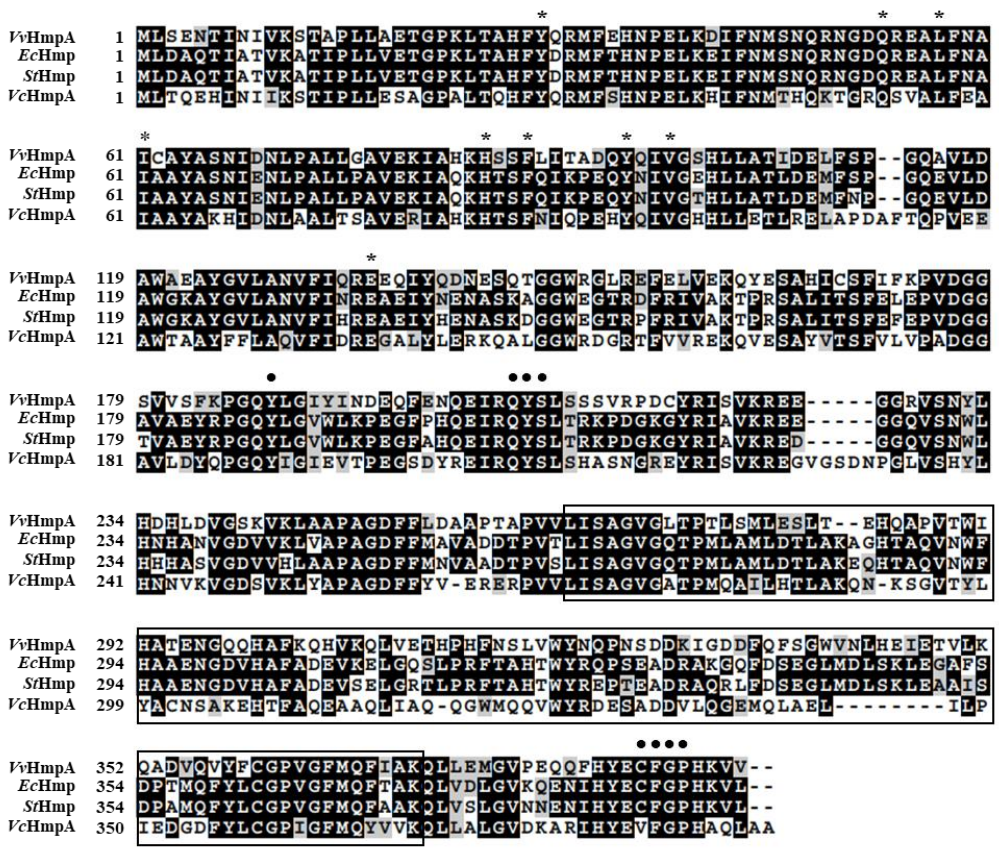
VvHmpA 1 MLSENTINIVKSTAPLLAETGPKLTAHFYQRMFEHNPELKDIFNMSNQRNGDQREALFNA
EcHmp 1 MLDAQTIATVKATIPLLVETGPKLTAHFYDRMFTHNPELKEIFNMSNQRNGDQREALFNA
StHmp 1 MLDAQTIATVKATIPLLVETGPKLTAHFYDRMFTHNPELKEIFNMSNQRNGDQREALFNA
VcHmpA 1 MLTQEHINIIKSTIPLLESAGPALTQHFYQRMFSHNPELKHIFNMTHQKTGRQSVALFEA
VvHmpA 61 ICAYASNIDNLPALLGAVEKIAHKHSSFLITADQYQIVGSHLLATIDELFSP--GQAVLD
EcHmp 61 IAAYASNIENLPALLPAVEKIAQKHTSFQIKPEQYNIVGEHLLATLDEMFSP--GQEVLD
StHmp 61 IAAYASNIENLPALLPAVEKIAQKHTSFQIKPEQYNIVGTHLLATLDEMFNP--GQEVLD
VcHmpA 61 IAAYAKHIDNLAALTSAVERIAHKHTSFNIQPEHYQIVGHHLLETLRELAPDAFTQPVEE
VvHmpA 119 AWAEAYGVLANVFIQREEQIYQDNESQTGGWRGLREFELVEKQYESAHICSFIFKPVDGG
EcHmp 119 AWGKAYGVLANVFINREAEIYNENASKAGGWEGTRDFRIVAKTPRSALITSFELEPVDGG
StHmp 119 AWGKAYGVLANVFIHREAEIYHENASKDGGWEGTRPFRIVAKTPRSALITSFEFEPVDGG
VcHmpA 121 AWTAAYFFLAQVFIDREGALYLERKQALGGWRDGRTFVVREKQVESAYVTSFVLVPADGG
VvHmpA 179 SVVSFKPGQYLGIYINDEQFENQEIRQYSLSSSSVRPDCYRISVKREE-----GGRVSNYL
EcHmp 179 AVAEYRPGQYLGVWLKPEGFPHQEIRQYSLTRKPDGKGYRIAVKREE-----GGQVSNWL
StHmp 179 TVAEYRPGQYLGVWLKPEGFAHQEIRQYSLTRKPDGKGYRIAVKRED-----GGQVSNWL
VcHmpA 181 AVLDYQPGQYIGIEVTPEGSDYREIRQYSLSHASNGREYRISVKREGVGSDNPGLVSHYL
VvHmpA 234 HDHLDVGSKVKLAAPAGDFFLDAAPTAPVVLISAGVGLTPTLSMLESLT--EHQAPVTWI
EcHmp 234 HNHANVGDVVKLVAPAGDFFMAVADDTPVTLISAGVGQTPMLAMLDTLAKAGHTAQVNWF
StHmp 234 HHHASVGDVVHLAAPAGDFFMNVAADTPVSLISAGVGQTPMLAMLDTLAKEQHTAQVNWF
VcHmpA 241 HNNVKVGDSVKLYAPAGDFFYV-ERERPVVLISAGVGATPMQAILHTLAKQN-KSGVTYL
VvHmpA 292 HATENGQQHAFKQHVKQLVETHPHFNSLVWYNQPNSDDKIGDDFQFSGWVNLHEIETVLK
EcHmp 294 HAAENGDVHAFADEVKELGQSLPRFTAHTWYRQPSEADRAKGQFDSEGLMDLSKLEGAFS
StHmp 294 HAAENGDVHAFADEVSELGRTLPRFTAHTWYREPTEADRAQRLFDSEGLMDLSKLEAAIS
VcHmpA 299 YACNSAKEHTFAQEAAQLIAQ-QGWMQQVWYRDESADDVLQGEMQLAEL--------ILP
VvHmpA 352 QADVQVYFCGPVGFMQFIAKQLLEMGVPEQQFHYECFGPHKVV--
EcHmp 354 DPTMQFYLCGPVGFMQFTAKQLVDLGVKQENIHYECFGPHKVL--
StHmp 354 DPAMQFYLCGPVGFMQFAAKQLVSLGVNNENIHYECFGPHKVL--
VcHmpA 350 IEDGDFYLCGPIGFMQYVVKQLLALGVDKARIHYEVFGPHAQLAA

Figure III-3. Sequence analysis of *V. vulnificus* HmpA (*Vv*HmpA), *E. coli* Hmp (*Ec*Hmp), *S.* Typhimurium Hmp (*St*Hmp), and *V. cholerae* HmpA (*Vc*HmpA)

The amino acid sequences retrieved from the NCBI protein database (accession numbers: WP_013570994.1 for *Vv*HmpA, NP_417047.1 for *Ec*Hmp, WP_000883146.1 for *St*Hmp, and WP_000957477.1 for *Vc*HmpA) were aligned using the Clustal Omega program. Identical (black boxes), conserved (gray boxes), and missing (dashes) sequences are indicated. The conserved amino acid residues potentially involved in the binding of heme and FAD are indicated above the amino acid sequences by asterisks and dots, respectively. The putative NAD-binding domain is boxed by a black line.

III-3-3. *Vv*HmpA is a flavohemoglobin

Absorption spectra of *Vv*HmpA in solution were characterized to reveal physical properties of the protein. A narrow intense band centered at approximately 433 nm, referred to as the Soret band and characteristic of heme proteins (Anderson and Robertson, 1995), was observed in the absorption spectrum of the reduced *Vv*HmpA (Fig. III-4A). The 433 nm Soret peak of the reduced *Vv*HmpA was altered to the 420 nm and 404 nm Soret peaks of the NO-bound and oxidized *Vv*HmpAs, respectively (Fig. III-4A). These Soret peak alterations most probably resulted from the changes in the physical state of iron in the heme protein, as demonstrated previously with a heme protein *Ec*Hmp which showed Soret peaks at 431.5 nm, 419 nm, and 403.5 nm in its reduced, NO-bound, and oxidized states, respectively (Anderson and Robertson, 1995; Gardner *et al*., 2000a; Ioannidis *et al*., 1992). Therefore, it is reasonable to propose that *Vv*HmpA is also a heme protein, in which iron can exist in either reduced, NO-bound, or oxidized state.

Measurement of heme content revealed that the overexpressed and purified *Vv*HmpA contains 0.06 molecules of heme per *Vv*HmpA monomer (Fig. III-4B). It was

possible that the amount of heme provided in the condition used for the overexpression and purification of the *Vv*HmpA protein is not sufficient to saturate the protein. To examine the possibility, the purified *Vv*HmpA was saturated with excess hemin *in vitro* (Gardner *et al*., 2000a), and then the content of heme in the reconstituted *Vv*HmpA was determined. Following the reconstitution, the content of heme in the *Vv*HmpA increased to 0.93±0.04 molecules of heme per *Vv*HmpA monomer (Fig. III-4B). These findings suggested that holo-*Vv*HmpA contains approximately one molecule of heme per protein monomer.

FAD fluorometric assay was carried out in order to determine the FAD content of the purified *Vv*HmpA. Prior to saturation with excess FAD *in vitro*, the purified *Vv*HmpA contained 0.24 molecules of FAD per *Vv*HmpA monomer (Fig. III-4B). After saturation with excess FAD *in vitro*, the content of FAD in the reconstituted *Vv*HmpA increased to 0.92±0.12 molecules of FAD per *Vv*HmpA monomer (Fig. III-4B), suggesting that the holo-*Vv*HmpA contains approximately one molecule of FAD per protein monomer. The combined results proposed that the holo-*Vv*HmpA protein is a flavohemoglobin that contains equimolar amounts of heme and FAD as cofactors.

A

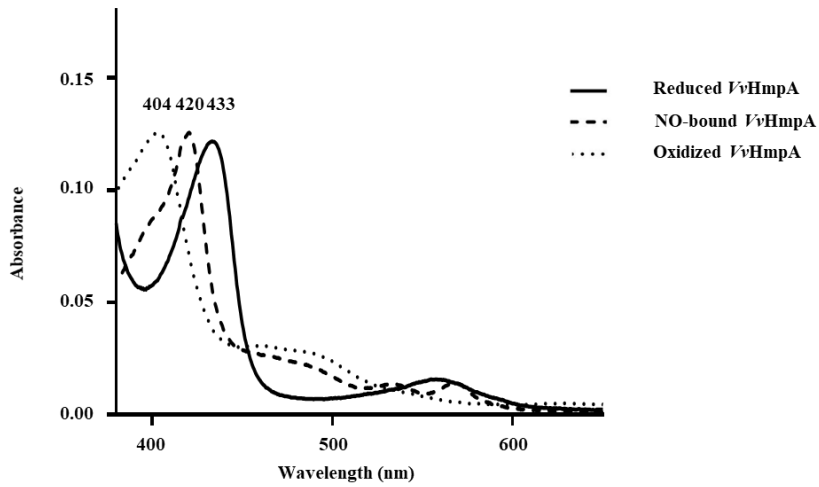

B

Protein	Heme	FAD
	Ratio	
Purified *Vv* HmpA	0.06	0.24
Reconstituted *Vv* HmpA	0.93±0.04	0.92±0.12

Figure III-4. Absorption spectra and cofactors of *Vv*HmpA

A, the absorption spectra of the purified *Vv*HmpA in the reduced (*solid line*), NO-bound (*dashed line*), and oxidized (*spotted line*) states were measured using a UV-vis spectrophotometer. The numbers above the peaks indicate the wavelengths of the observed Soret peaks. *B,* the ratios of heme and FAD per one molecule of purified and reconstituted *Vv*HmpA.

III-3-4. Kinetic properties of *Vv*HmpA for NO decomposition

To determine the kinetic properties of *Vv*HmpA, the initial rates of NO decomposition were measured at different concentrations of NO using an NO-sensitive electrode. Also, the kinetic analysis was conducted with purified non-His_6-tagged HmpA to eliminate interference of other facters such as His_6-tag. At the concentrations of NO exceeding 0.15 μM, which are most probably encountered in the human immune system (Toledo and Augusto, 2012), the NO-decomposition rate of *Vv*HmpA was higher at 37 °C rather than at 30 °C (Fig. III-5A). The V_{max} of *Vv*HmpA for NO, obtained from the Michaelis-Menten plot, was approximately 110.1±6.1 nM s^{-1} at 37 °C and the NO-decomposition rate at the concentration of 1 μM NO was approximately 80% of the V_{max} value (Fig. III-5A). In contrast, the V_{max} of *Vv*HmpA for NO at 30 °C was about 47±1.5 nM s^{-1} and the NO-decomposition rate at the concentration of 1 μM NO was approximately 90% of the V_{max} value (Fig. III-5A). The K_M values of *Vv*HmpA for NO were 0.3±0.04 μM and 0.1±0.01 μM at 37 °C and 30 °C, respectively (Fig. III-5B). The k_{cat} values of *Vv*HmpA for NO were 21.4±1.2 s^{-1} and 9.1±0.2 s^{-1} at 37 °C and 30 °C, respectively (Fig. III-5B). Considering that *V. vulnificus* is a pathogen infecting humans with the body

temperature of 37 °C, the results indicated that *Vv*HmpA is more efficient at decomposing high levels of toxic NO in the host than in the natural environment.

A

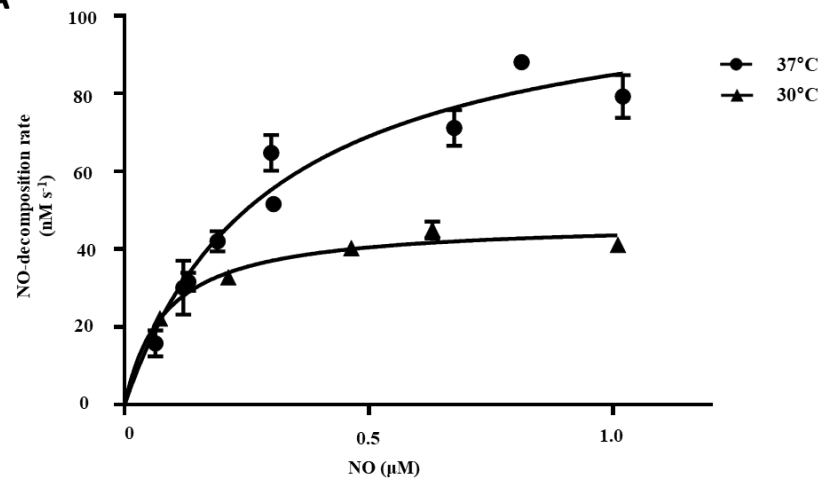

B

Temperature	V_{max}	K_M	k_{cat}
	$nM\ s^{-1}$	μM	s^{-1}
37°C	110±6.1	0.3±0.04	21.4±1.2
30°C	47.1±1.5	0.1±0.01	9.1±0.2

Figure III-5. Kinetic analysis of *Vv*HmpA

A, the *Vv*HmpA protein and various concentrations of NO were delivered into the reaction buffer. The initial rates of NO decomposition were determined by measuring the residual NO in the reaction mixture and plotted against the corresponding initial concentrations of NO. *Error bars* represent the S.D. *B,* V_{max}, K_M and k_{cat} values for NO were determined by fitting the curve (*A*) to a classical Michaelis-Menten enzyme kinetic equation. The turnover rate (k_{cat}) is expressed relative to heme.

III-3-5. *Vv*HmpA is essential for the survival of *V. vulnificus* under nitrosative stress *in vitro*

To evaluate the role of *Vv*HmpA in *V. vulnificus* encountering nitrosative stress, an isogenic mutant lacking functional *VvhmpA* gene and the *VvhmpA*-complemented strain, which achieved by adding the *VvhmpA*-expressing plasmid to the aforementioned isogenic mutant (Table II-1), and then the NO-decomposition activities of the *V. vulnificus* strains were compared (Fig. III-6A). When NO was administered to the *V. vulnificus* wild-type culture, the NO concentration decreased rapidly in the culture and the residual NO was not detectable after 100 s, indicating that the *V. vulnificus* wild type effectively decomposes NO *in vitro*. In contrast, the decreasing rate of NO levels in the *VvhmpA* mutant culture was much slower than that in the wild-type culture (Fig. III-6A). The decreasing rate of NO levels in the *VvhmpA* mutant culture was close to that in the medium without bacterial inoculation (control, PBS), indicating that the NO-decomposition activity of the *VvhmpA* mutant was significantly impaired (Fig. III-6A). By complementation of the *VvhmpA* gene, the impaired NO-decomposition activity of the *VvhmpA* mutant was restored to a level even higher than that of the wild type (Fig. III-6A). The results suggested that

the NO-decomposition activity of *V. vulnificus* is mostly dependent on *Vv*HmpA *in vitro*.

To examine the effects of *Vv*HmpA on the survival of *V. vulnificus* under nitrosative stress *in vitro*, the growth of *V. vulnificus* strains in M9G was compared in the presence of NO (Fig. III-6B). The growth of the *VvhmpA* mutant was significantly delayed compared with that of the wild type. That is, the *VvhmpA* mutant did not enter the exponential phase until 7 h post-inoculation, which is delayed for approximately 2 h compared with the wild type. The delayed growth of the *VvhmpA* mutant was restored in the *VvhmpA*-complemented strain (Fig. III-6B), indicating that *Vv*HmpA is able to effectively decompose toxic NO to the level at which *V. vulnificus* can manage to grow. The combined results led us to conclude that *Vv*HmpA detoxifies NO effectively *in vitro*, which in turn ensures survival of the pathogen under nitrosative stress.

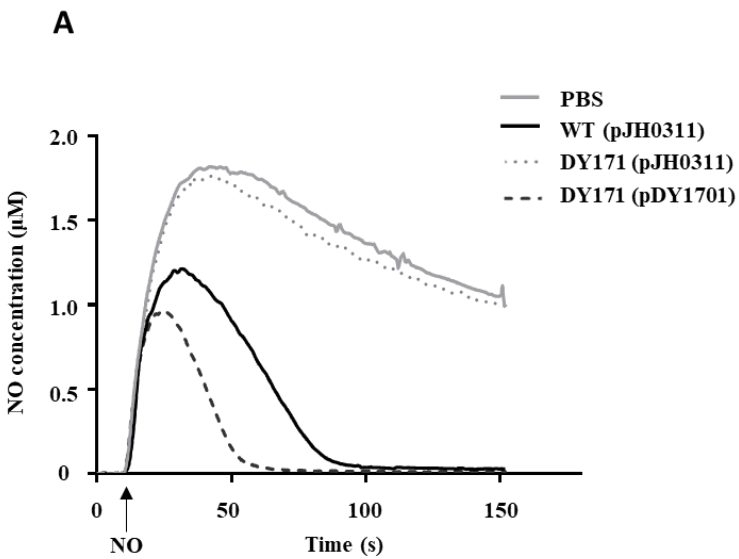
A
PBS
WT (pJH0311)
DY171 (pJH0311)
DY171 (pDY1701)
NO concentration (μM)
2.0
1.5
1.0
0.5
0
0
50
100
150
NO
Time (s)

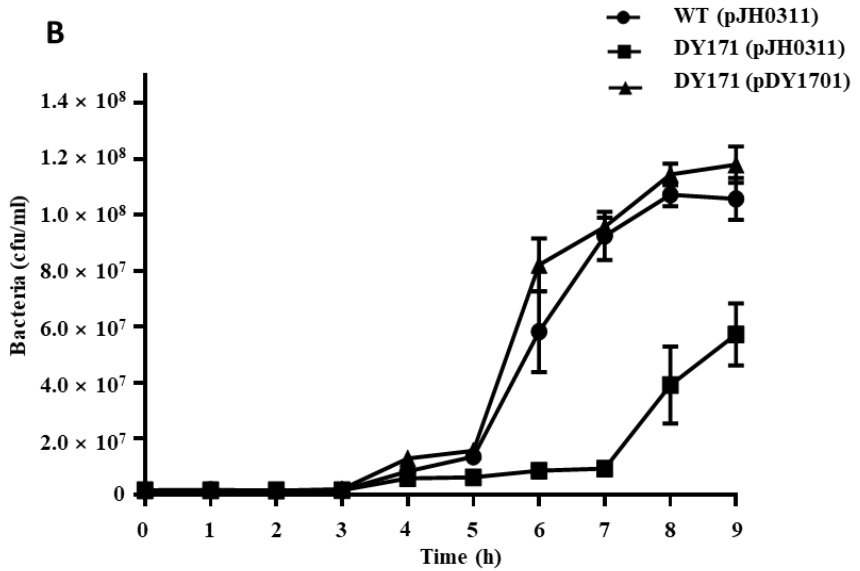
B
WT (pJH0311)
DY171 (pJH0311)
DY171 (pDY1701)
Bacteria (cfu/ml)
1.4 × 10^8
1.2 × 10^8
1.0 × 10^8
8.0 × 10^7
6.0 × 10^7
4.0 × 10^7
2.0 × 10^7
0
0
1
2
3
4
5
6
7
8
9
Time (h)

Figure III-6. NO decomposition and survival of the *V. vulnificus* strains under nitrosative stress

A, the *V. vulnificus* strains were pre-exposed to Spermine NONOate to induce *Vv*HmpA, and then 2 μM of NO was administered to the strains at the time designated by *an arrow*. The residual NO in the mixtures was measured to determine the NO decomposition. *B,* survival of the *V. vulnificus* strains exposed to excess NO was monitored by counting viable cells at time intervals. *Error bars* represent the S.D. *PBS*, control; *WT (pJH0311)*, wild type; *DY171 (pJH0311), VvhmpA* mutant; *DY171 (pDY1701), VvhmpA*-complemented strain.

III-3-6. *Vv*HmpA is essential for the virulence of *V. vulnificus ex vivo*

To examine the role of *Vv*HmpA in the virulence of *V. vulnificus ex vivo*, the activities of lactate dehydrogenase (LDH) released from the NO-producing murine macrophage RAW 264.7 cells infected with the *V. vulnificus* strains were determined. As shown in Fig. III-7A, the *VvhmpA* mutant exhibited significantly lower LDH-releasing activity compared with those of the wild type or the *VvhmpA*-complemented strain. In contrast, when the NO production from the RAW 264.7 cells was inhibited by the NO synthase inhibitor L-NMMA, the wild type, *VvhmpA* mutant, and *VvhmpA*-complemented strain exhibited comparable levels of LDH-releasing activity (Fig. III-7B). These results indicated that *Vv*HmpA contributes to the virulence of *V. vulnificus* by coping with NO released from the host immune cells.

To gain further insight into how the *VvhmpA* mutant showed the lower virulence *ex vivo* compared with the wild type, the numbers of the *V. vulnificus* cells adherent to the RAW 264.7 cells were measured. The numbers of the *VvhmpA* mutant were significantly lower than those of the wild type and *VvhmpA*-complemented strain (Fig. III-7C), indicating that *Vv*HmpA is required for *V. vulnificus* to survive in

proximity to the NO-producing macrophages. Accordingly, when the NO production from the RAW 264.7 cells was inhibited by L-NMMA, the numbers of the wild type, *VvhmpA* mutant, and *VvhmpA*-complemented strain adherent to the RAW 264.7 cells were comparable (Fig. III-7D). The results indicated that *Vv*HmpA is crucial for *V. vulnificus* to overcome nitrosative stress imposed by the host immune cells and thereby survive during infection.

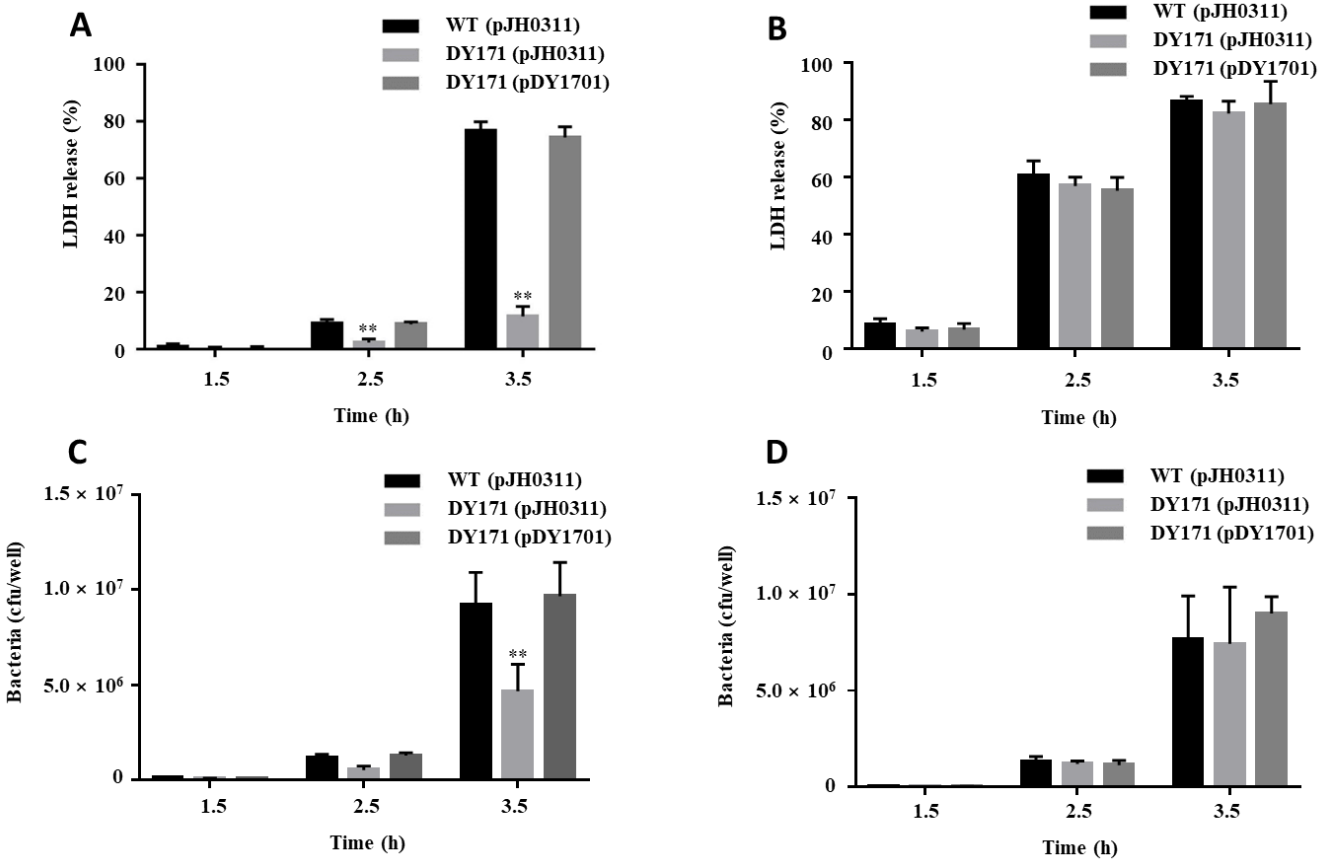
A
WT (pJH0311)
DY171 (pJH0311)
DY171 (pDY1701)
LDH release (%)
100
80
60
40
20
0
**
**
1.5
2.5
3.5
Time (h)
B
WT (pJH0311)
DY171 (pJH0311)
DY171 (pDY1701)
LDH release (%)
100
80
60
40
20
0
1.5
2.5
3.5
Time (h)
C
WT (pJH0311)
DY171 (pJH0311)
DY171 (pDY1701)
Bacteria (cfu/well)
1.5 × 10^7
1.0 × 10^7
5.0 × 10^6
0
**
1.5
2.5
3.5
Time (h)
D
WT (pJH0311)
DY171 (pJH0311)
DY171 (pDY1701)
Bacteria (cfu/well)
1.5 × 10^7
1.0 × 10^7
5.0 × 10^6
0
1.5
2.5
3.5
Time (h)

Figure III-7. Cytotoxicity and survival of the *V. vulnificus* strains infecting the RAW 264.7 cells

The NO-producing RAW 264.7 cells were infected with the *V. vulnificus* strains at the MOI of 1 for various incubation times in the absence (*A* and *C*) or presence (*B* and *D*) of the NO synthase inhibitor, L-NMMA. *A* and *B*, the cytotoxicity was expressed using the total LDH activity of the RAW 264.7 cells completely lysed by 1.5% Triton X-100 as 100%. *C* and *D*, the *V. vulnificus* cells adherent to the RAW 264.7 cells were enumerated in cfu per well at each time point after infection. *Error bars* represent the S.D. **, $p < 0.005$ relative to groups infected with the wild type at each incubation time. *WT (pJH0311)*, wild type; *DY171 (pJH0311)*, *VvhmpA* mutant; *DY171 (pDY1701)*, *VvhmpA*-complemented strain.

III-3-7. *Vv*HmpA is essential for the pathogenesis of *V. vulnificus in vivo*

The importance of *Vv*HmpA in the *V. vulnificus* pathogenesis was further investigated in a mouse model. As shown in Fig. III-8, the survival time of mice infected with the *VvhmpA* mutant was consistently prolonged (*p* value of 0.0420, log-rank test) compared with that of mice infected with the wild type. At 24 h post-infection, percentages of mice that survived after challenge with the *VvhmpA* mutant or the wild type were 66.6 and 33.3%, respectively, indicating that the deletion of *VvhmpA* attenuated the virulence of *V. vulnificus* in mice. Taken together, the combined results suggest that *Vv*HmpA is essential for NO decomposition, survival adjacent to NO-producing immune cells, and thereby the pathogenesis of *V. vulnificus*.

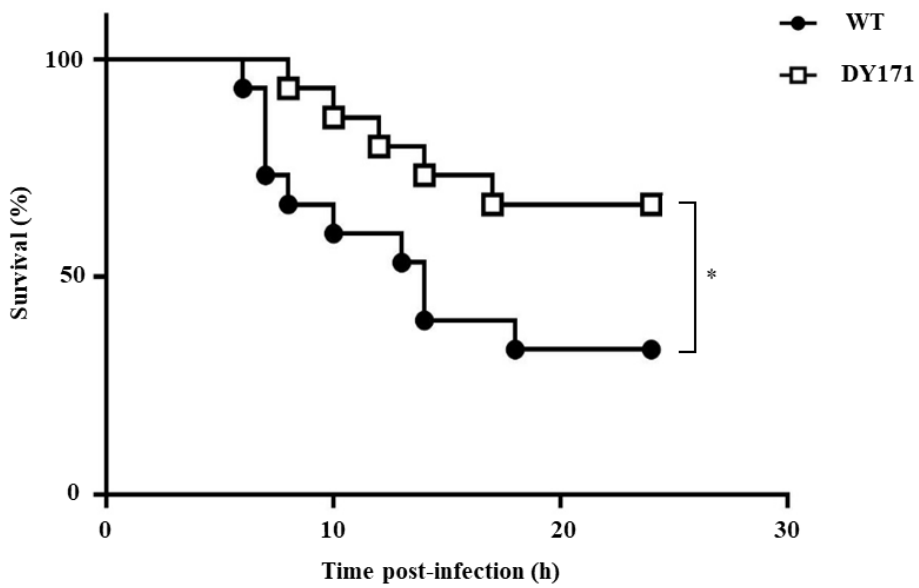

Figure III-8. Mouse lethality of the *V. vulnificus* strains

Groups (n = 15) of 7-week-old specific pathogen-free female ICR mice were intraperitoneally infected with either the wild type or the *VvhmpA* mutant of *V. vulnificus* at doses of 1.0×10^6 cfu. Mouse survival percentage was monitored for 24 h. *, $p < 0.05$; *WT*, wild type; *DY171, VvhmpA* mutant.

III-4. Discussion

In order to establish infection successfully, pathogens need to overcome nitrosative stresses that originate from the host immune system (Fang, 2004). In addition to the 8 genes, whose expression was further confirmed by qRT-PCR analysis in the present study (Figs. III-1 and III-2), transcriptome analysis of *V. vulnificus* identified 551 genes that are differentially expressed upon exposure to NO (Table III-1, 2). Among the genes, *VvhmpA* was the most greatly induced and thus its gene product *Vv*HmpA was selected for further study. It should be noted that the expression burst of *Vv*HmpA occurs in response to only 10 min of NO stress. This rapid response may benefit the bacteria by quickly decomposing the NO and preventing cellular damage from NO. The deduced amino acid sequence revealed that *Vv*HmpA is a multidomain NO dioxygenase consisting of the N-terminal globin domain with the heme-binding site and the C-terminal oxidoreductase domain with NAD- and FAD-binding sites (Fig. III-3). As well appreciated in a multidomain *Ec*Hmp, the N-terminal ferrous-oxy heme reacts with NO to yield NO_3^- and ferric-deoxy heme, and then the C-terminal domain transfers electrons from NAD(P)H to the ferric heme via FAD (Gardner *et al*., 2000a). This endogenous electron transfer could allow for an

efficient regeneration of the ferrous heme, which is ready for another catalytic cycle of NO decomposition. In contrast, single-domain NO dioxygenases found in some pathogens such as *Campylobacter jejuni* lack the C-terminal domain and rely on an exogenous redox partner(s) to regenerate ferrous heme, resulting in less efficient NO decomposition (Shepherd *et al*., 2011). Therefore, *V. vulnificus* seems to adopt the fast-paced and multidomain *Vv*HmpA to efficiently overcome nitrosative stress during infection.

Biochemical and kinetic analyses of *Ec*Hmp proposed two possible reaction mechanisms to initiate NO decomposition, namely dioxygenation and nitrosylation (Forrester and Foster, 2012; Gardner *et al*., 2000a; Hausladen *et al*., 2001). Dioxygenation begins with O_2 binding to the ferrous heme to result in ferrous-oxy heme, most probably under conditions where O_2 is not limiting. The ferrous-oxy heme reacts with NO to form a transient Fe-$ONOO^-$ intermediate which releases NO_3^- as described above. In contrast, nitrosylation involves initial reaction of the ferrous heme with NO to form a ferrous-nitrosyl heme, converting transiently to a ferric-nitrosyl heme which in turn reacts with O_2 to release NO_3^- under O_2 limiting

conditions. Regardless of which mechanistic pathway predominates, they both result in rapid enzymatic turnover of NO to NO_3^-. Although the exact NO detoxification mechanisms of *Vv*HmpA have not been yet clarified, the similarities found in the amino acid sequences and absorption spectra of *Ec*Hmp and *Vv*HmpA (Figs. III-3 and III-4A) led us to postulate that *Vv*HmpA also could convert NO to NO_3^- through one of the two pathways depending on O_2 availability. Supporting this postulation, the kinetic values of *Vv*HmpA for NO decomposition under aerobic conditions (Fig. III-5) are also comparable to those of *Ec*Hmp, in which the k_{cat} and K_M values are 10-670 s^{-1} and 0.25 μM for NO, respectively (Gardner, 2005; Gardner *et al*., 2000b).

After infection, pathogenic bacteria probably encounter increased levels of NO due to the expression of iNOS in cells of the immune system and must overcome the nitrosative stress for successful pathogenesis (Bang *et al*., 2006; Richardson *et al*., 2006; Stern *et al*., 2012). The NO concentration in humans and experimental animals increases to the micromolar range under infectious and inflammatory conditions (Toledo and Augusto, 2012). It is noteworthy that the K_M and k_{cat} values of *Vv*HmpA for NO at 37 °C, the temperature to which *V. vulnificus* is inevitably exposed in the

host, are greater than those at 30 °C (Fig. III-5). This kinetic property indicates that *Vv*HmpA expressed in the host may be more optimized for acting on the large amounts of NO and decomposing them rapidly to a safe level during infection, before the increased nitrosative stress impairs cellular components of *V. vulnificus*. Accordingly, it is reasonable to hypothesize that *Vv*HmpA could provide an evolutionary advantage for *V. vulnificus* to survive in the host rather than in nature, where lower concentration of NO may be occasionally encountered. Supporting this hypothesis, loss of *Vv*HmpA led *V. vulnificus* to show significantly reduced survival adjacent to the NO-producing macrophage cells (Fig. III-7C and D), lower cytotoxicity to the immune cells (Fig. III-7A and B), and lastly attenuated virulence in mice (Fig. III-8).

It has been reported that the Hmp proteins of serval pathogenic bacteria including *V. cholerae*, *S.* Typhimurium and *Staphylococcus aureus* were responsible for NO detoxification and thus required for their survival under nitrosative stress and successful pathogenesis (Bang *et al*., 2006; Richardson *et al*., 2006; Stern *et al*., 2012). However, little has been known about the biochemical and kinetic properties

of the Hmp proteins of the pathogens until now. In the present study, absorption spectral and biochemical analyses revealed that *Vv*HmpA is a flavohemoglobin containing equimolar amounts of heme and FAD as cofactors. Kinetic properties of *Vv*HmpA to have greater K_M and k_{cat} values at 37 °C than at 30 °C indicated that *Vv*HmpA is optimized to act on and decompose large amounts of NO more effectively in the host. Reduced NO-decomposition activity and growth rate of the *VvhmpA* mutant in the presence of NO, along with the attenuated virulence observed both in the cell culture and mouse models, indicated that *Vv*HmpA contributes to the survival of *V. vulnificus* under nitrosative stress, and thereby plays a crucial role in the pathogenesis of the pathogen. Therefore, *Vv*HmpA could be a promising target for development of new antibacterial agents.

Chapter IV.

Conclusion

A successful infection by *V. vulnificus* primarily depends on its ability to survive within the hostile environment of the host. The key challenges that *V. vulnificus* encounters during the infection are ROS and RNS produced by host innate immune system. Therefore, rapid response against ROS and RNS is crucial for successful infection as well as survival of *V. vulnificus*. *V. vulnificus* OxyR is a transcription regulator that can recognize H_2O_2 and it expresses antioxidant genes such as Prxs and KatG. *V. vulnificus* has two OxyRs, OxyR1 and OxyR2. These two OxyRs differ in the concentration of H_2O_2 that they sense, and OxyR2 is known to sense a lower concentration of H_2O_2 than OxyR1 does. OxyR2, via its two redox-sensitive cysteine residues, regulates the expression of the antioxidant gene *prx*2. Through *in vivo* alkylation assay, the Cys206, a peroxidatic cysteine of OxyR2, was overoxidized to OxyR2-Cys^{206}-SO_3H at high concentrations of H_2O_2. It was also revealed that overoxidized OxyR2 turns off the transcription of *prx*2. There is evidence that OxyR2 regulates the expression of *prx*2 through three distinct redox states (reduced, disulfide, and overoxidized states). The overoxidized OxyR2, by repressing the expression of *prx*2 at high concentrations of H_2O_2, is repressing production of Prx2 that would not be effective at the high H_2O_2 concentrations and thus saving valuable

cellular resources.

The crystal structures of OxyR2 and OxyR2 (E204G) variant revealed that the high H_2O_2 sensitivity of OxyR2 results from the conformational difference in the peptide bond between Lys203 and Glu204 near the peroxidatic cysteine residue. OxyR2 variant harboring an E204G mutation revealed decreased sensitivity to H_2O_2. The E204G mutation has provided significant conformational flexibility in the region of Gly204 and His205. Further analysis revealed that the rigid peptide bond conformation of Glu204 affects the side chain conformation of the His205 residue and this finally results in the high H_2O_2 sensitivity of OxyR2. These findings suggest that OxyR2 has a relatively higher sensitivity to H_2O_2 due to its rigid conformation and this rigidity results from employing glutamic acid as the 204th residue, instead of the usual glycine as in other OxyRs.

From the transcriptome analysis via RNA-seq, 551 genes were identified whose expressions were differentially expressed in *V. vulnificus* that was exposed to NO. Among the identified genes, *VvhmpA* is the most greatly induced gene at the

transcription level. Characterization of *Vv*HmpA showed that it is an NO-inducible flavohemoglobin containing equimolar amounts of heme and FAD. The kinetic properties of *Vv*HmpA indicated that the protein sufficiently decomposes physiological levels of NO. *Vv*HmpA is also more efficient at decomposing higher levels of NO at 37 °C, the temperature encountered in the host, than at 30 °C, which is known to be the most optimal temperature for the bacteria's growth. Also, *Vv*HmpA is crucial for the survival of *V. vulnificus* in the presence of NO *in vitro*. The *VvhmpA* mutant exhibited a significantly reduced cytotoxicity toward activated murine macrophage cells as well as attenuated virulence in mice. The combined results suggest that *Vv*HmpA plays an important role in *V. vulnificus* pathogenesis by contributing to the survival of the pathogen during infection. Thus, *Vv*HmpA can be a promising target for development of new antibacterial agents.

In conclusion, the present study uncovered the complicated defense mechanisms against oxidative and nitrosative stresses and showed that such mechanisms are crucial for survival of *V. vulnificus* in the host. This report contributes to our collective understanding of bacterial survival strategies and may aid with achieving

successful control of *V. vulnificus* in the future.

REFERENCE

Ahn, J., Jang, K.K., Jo, I., Nurhasni, H., Lim, J.G., Yoo, J.W., Choi, S.H., and Ha, N.C. 2018. Crystal structure of peroxiredoxin 3 from *Vibrio vulnificus* and its implications for scavenging peroxides and nitric oxide. IUCrJ *5*, 82-92.

Alice, A.F., Naka, H., and Crosa, J.H. 2008. Global gene expression as a function of the iron status of the bacterial cell: influence of differentially expressed genes in the virulence of the human pathogen *Vibrio vulnificus*. Infect. Immun. *76*, 4019-4037.

Anderson, A.B., and Robertson, C.R. 1995. Absorption spectra indicate conformational alteration of myoglobin adsorbed on polydimethylsiloxane. Biophys. J. *68*, 2091-2097.

Baek, W.K., Lee, H.S., Oh, M.H., Koh, M.J., Kim, K.S., and Choi, S.H. 2009. Identification of the *Vibrio vulnificus ahpCl* gene and its influence on survival under oxidative stress and virulence. J. Microbiol. *47*, 624-632.

Bang, I.S., Liu, L., Vazquez-Torres, A., Crouch, M.L., Stamler, J.S., and Fang, F.C. 2006. Maintenance of nitric oxide and redox homeostasis by the salmonella flavohemoglobin *hmp*. J. Biol. Chem. *281*, 28039-28047.

Bang, Y.J., Oh, M.H., and Choi, S.H. 2012. Distinct characteristics of two 2-Cys peroxiredoxins of *Vibrio vulnificus* suggesting differential roles in detoxifying oxidative stress. J. Biol. Chem. *287*, 42516-42524.

Barr, I., and Guo, F. 2015. Pyridine Hemochromagen Assay for Determining the Concentration of Heme in Purified Protein Solutions. Bio. Protoc. *5*.

Bedard, K., and Krause, K.H. 2007. The NOX family of ROS-generating NADPH oxidases: physiology and pathophysiology. Physiol. Rev. *87*, 245-313.

Bonamore, A., and Boffi, A. 2008. Flavohemoglobin: structure and reactivity. IUBMB Life *60*, 19-28.

Bradford, M.M. 1976. A rapid and sensitive method for the quantitation of microgram quantities of protein utilizing the principle of protein-dye binding. Anal. Biochem. *72*, 248-254.

Bryk, R., Griffin, P., and Nathan, C. 2000. Peroxynitrite reductase activity of bacterial peroxiredoxins. Nature *407*, 211-215.

Cha, S.S., An, Y.J., Jeong, C.S., Kim, M.K., Lee, S.G., Lee, K.H., and Oh, B.H. 2012. Experimental phasing using zinc anomalous scattering. Acta. Crystallogr. D. Biol. Crystallogr. *68*, 1253-1258.

Choi, H., Kim, S., Mukhopadhyay, P., Cho, S., Woo, J., Storz, G., and Ryu, S.E. 2001. Structural basis of the redox switch in the OxyR transcription factor. Cell *105*, 103-113.

Conesa, A., Madrigal, P., Tarazona, S., Gomez-Cabrero, D., Cervera, A., McPherson, A., Szczesniak, M.W., Gaffney, D.J., Elo, L.L., Zhang, X., *et al.* 2016. A survey of best practices for RNA-seq data analysis. Genome Biol. *17*, 13.

Cooke, M.S., Evans, M.D., Dizdaroglu, M., and Lunec, J. 2003. Oxidative DNA damage: mechanisms, mutation, and disease. FASEB J. *17*, 1195-1214.

Davies, B.W., Bogard, R.W., Dupes, N.M., Gerstenfeld, T.A., Simmons, L.A.,

and Mekalanos, J.J. 2011. DNA damage and reactive nitrogen species are barriers to *Vibrio cholerae* colonization of the infant mouse intestine. PLoS Pathog. *7*, e1001295.

Echols, N., Grosse-Kunstleve, R.W., Afonine, P.V., Bunkoczi, G., Chen, V.B., Headd, J.J., McCoy, A.J., Moriarty, N.W., Read, R.J., Richardson, D.C., *et al.* 2012. Graphical tools for macromolecular crystallography in PHENIX. J. Appl. Crystallogr. *45*, 581-586.

Elgaml, A., and Miyoshi, S. 2015. Presence of Nitric Oxide-Sensing Systems in the Human Pathogen *Vibrio vulnificus*. Biocontrol Sci. *20*, 199-203.

Elmore, S.P.,Watts, J.A., Simpson, L.M., and Oliver, J.D. 1992. Reversal of hypotension induced by *Vibrio vulnificus* lipopolysaccharide in the rat by inhibition of nitric oxide synthesis. Microb. Pathog. *13*, 391-397

Emsley, P., and Cowtan, K. 2004. Coot: model-building tools for molecular graphics. Acta. Crystallogr. D. Biol. Crystallogr. *60*, 2126-2132.

Fang, F.C. 1999. *Nitric Oxide and Infection* (New York: Kluwer Academic/Plenum Publishers).

Fang, F.C. 2004. Antimicrobial reactive oxygen and nitrogen species: concepts and controversies. Nat. Rev. Microbiol. *2*, 820-832.

Fang, X., Liang, P., Raba, D.A., Rosas-Lemus, M., Chakravarthy, S., Tuz, K., and Juarez, O. 2017. Kinetic characterization of *Vibrio cholerae* ApbE: Substrate specificity and regulatory mechanisms. PLoS One *12*, e0186805.

Flemming, H.-C. and Wingender, J. 2010. The biofilm matrix. Nat. Rev. Microbiol. *8*, 623-633

Forrester, M.T., and Foster, M.W. 2012. Protection from nitrosative stress: a central role for microbial flavohemoglobin. Free Radic. Biol. Med. *52*, 1620-1633.

Gardner, A.M., Martin, L.A., Gardner, P.R., Dou, Y., and Olson, J.S. 2000a. Steady-state and transient kinetics of *Escherichia coli* nitric-oxide dioxygenase (flavohemoglobin). The B10 tyrosine hydroxyl is essential for dioxygen binding and catalysis. J. Biol. Chem. *275*, 12581-12589.

Gardner, P.R. 2005. Nitric oxide dioxygenase function and mechanism of flavohemoglobin, hemoglobin, myoglobin and their associated reductases. J. Inorg. Biochem. *99*, 247-266.

Gardner, P.R., Gardner, A.M., Brashear, W.T., Suzuki, T., Hvitved, A.N., Setchell, K.D., and Olson, J.S. 2006. Hemoglobins dioxygenate nitric oxide with high fidelity. J. Inorg. Biochem. *100*, 542-550.

Gardner, P.R., Gardner, A.M., Martin, L.A., Dou, Y., Li, T., Olson, J.S., Zhu, H., and Riggs, A.F. 2000b. Nitric-oxide dioxygenase activity and function of flavohemoglobins. Sensitivity to nitric oxide and carbon monoxide inhibition. J. Biol. Chem. *275*, 31581-31587.

Goo, S.Y., Lee, H.J., Kim, W.H., Han, K.L., Park, D.K., Lee, H.J., Kim, S.M., Kim, K.S., Lee, K.H., and Park, S.J. 2006. Identification of OmpU of *Vibrio vulnificus* as a fibronectin-binding protein and its role in bacterial pathogenesis. Infect. Immun. *74*, 5586-5594.

Gray, L.D., and Kreger, A.S. 1987. Mouse skin damage caused by cytolysin from *Vibrio vulnificus* and by *V. vulnificus* infection. J. Infect. Dis. *155*, 236-241.

Gulig, P.A., Bourdage, K.L., and Starks, A.M. 2005. Molecular Pathogenesis of *Vibrio vulnificus*. J. Microbiol. *43 Spec No*, 118-131.

Guo, Y. and Rowe-Magnus, D.A. 2010. Identification of a c-di-GMP-regulated polysaccharide locus governing stress resistance and biofilm and rugose colony formation in *Vibrio vulnificus*. Infect. Immun. *78*, 1390-1402.

Guo, Y. and Rowe-Magnus, D.A. 2011. Overlapping and unique contributions of two conserved polysaccharide loci in governing distinct survival phenotypes in *Vibrio vulnificus*. Environ. Microbiol. *13*, 2888-2990.

Hall, A., Karplus, P.A., and Poole, L.B. 2009. Typical 2-Cys peroxiredoxins--structures, mechanisms and functions. FEBS J. *276*, 2469-2477.

Hall-Stoodley, L. and Stoodley, P. 2005. Biofilm formation and dispersal and the transmission of human pathogens. Trends Microbiol. *13*, 7-10

Hausladen, A., Gow, A., and Stamler, J.S. 2001. Flavohemoglobin denitrosylase catalyzes the reaction of a nitroxyl equivalent with molecular oxygen. Proc. Natl. Acad. Sci. U. S. A. *98*, 10108-10112.

Hirano, K., and Namihira, M. 2017. FAD influx enhances neuronal differentiation of human neural stem cells by facilitating nuclear localization of LSD1. FEBS Open Bio. *7*, 1932-1942.

Hor, L.I., Gao, C.T., and Wan, L. 1995. Isolation and Characterization of *Vibrio*

vulnificus Inhabiting the Marine Environment of the Southwestern Area of Taiwan. J. Biomed. Sci. *2*, 384-389.

Horseman, M.A., and Surani, S. 2011. A comprehensive review of *Vibrio vulnificus*: an important cause of severe sepsis and skin and soft-tissue infection. Int. J. Infect. Dis. *15*, e157-166.

Ioannidis, N., Cooper, C.E., and Poole, R.K. 1992. Spectroscopic studies on an oxygen-binding haemoglobin-like flavohaemoprotein from *Escherichia coli*. Biochem. J. *288 (Pt 2)*, 649-655.

Jang, K.K., Lee, Z.W., Kim, B., Jung, Y.H., Han, H.J., Kim, M.H., Kim, B.S., and Choi, S.H. 2017. Identification and characterization of *Vibrio vulnificus plpA* encoding a phospholipase A_2 essential for pathogenesis. J. Biol. Chem. *292*, 17129-17143.

Janssen, R., van der Straaten, T., van Diepen, A., and van Dissel, J.T. 2003. Responses to reactive oxygen intermediates and virulence of *Salmonella* Typhimurium. Microbes Infect. *5*, 527-534.

Jeong, H.G., and Satchell, K.J. 2012. Additive function of *Vibrio vulnificu*s MARTX(*Vv*) and VvhA cytolysins promotes rapid growth and epithelial tissue necrosis during intestinal infection. PLoS Pathog. *8*, e1002581.

Jo, I., Chung, I.Y., Bae, H.W., Kim, J.S., Song, S., Cho, Y.H., and Ha, N.C. 2015. Structural details of the OxyR peroxide-sensing mechanism. Proc. Natl. Acad. Sci. U. S. A. *112*, 6443-6448.

Jones, M.K., and Oliver, J.D. 2009. *Vibrio vulnificus*: disease and pathogenesis.

Infect. Immun. *77*, 1723-1733.

Kang, I.H., Kim, J.S., and Lee, J.K. 2007. The virulence of *Vibrio vulnificus* is affected by the cellular level of superoxide dismutase activity. J. Microbiol. Biotechnol. *17*, 1399-1402.

Kang, M.K., Jhee, E.C., Koo, B.S., Yang, J.Y., Park, B.H., Kim, J.S., Rho, H.W., Kim, H.R., and Park, J.W. 2002. Induction of nitric oxide synthase expression by *Vibrio vulnificus* cytolysin. Biochem. Biophys. Res. Commun. *290*, 1090-1095.

Karatan, E. and Watnick, P. 2009. Signals, regulatory networks, and materials that build and break bacterial biofilms. Microbiol. Molec. Biol. Rev. *73*, 310-347

Karlinsey, J.E., Bang, I.S., Becker, L.A., Frawley, E.R., Porwollik, S., Robbins, H.F., Thomas, V.C., Urbano, R., McClelland, M., and Fang, F.C. 2012. The NsrR regulon in nitrosative stress resistance of *Salmonella enterica* serovar Typhimurium. Mol. Microbiol. *85*, 1179-1193.

Kim, B.S., Jang, S.Y., Bang, Y.J., Hwang, J., Koo, Y., Jang, K.K., Lim, D., Kim, M.H., and Choi, S.H. 2018. QStatin, a Selective Inhibitor of Quorum Sensing in *Vibrio* Species. MBio *9*.

Kim, B.S., and Kim, J.S. 2002. Cholesterol induce oligomerization of *Vibrio vulnificus* cytolysin specifically. Exp. Mol. Med. *34*, 239-242.

Kim, C.M., Park, R.Y., Park, J.H., Sun, H.Y., Bai, Y.H., Ryu, P.Y., Kim, S.Y., Rhee, J.H., and Shin, S.H. 2006. *Vibrio vulnificus* vulnibactin, but not metalloprotease VvpE, is essentially required for iron-uptake from human holotransferrin. Biol. Pharm. Bull. *29*, 911-918.

Kim, H.R., Rho, H.W., Jeong, M.H., Park, J.W., Kim, J.S., Park, B.H., Kim, U.H., and Park, S.D. 1993. Hemolytic mechanism of cytolysin produced from *V. vulnificus*. Life Sci. *53*, 571-577.

Kim, H.S., Park, S.-J., and Lee, K.-H. 2009. Role of NtrC-regulated exopolysaccharides in the biofilm formation and pathogenic interaction of *Vibrio vulnificus*. Mol. Microbiol. *74*, 436-453.

Kim, S., Bang, Y.J., Kim, D., Lim, J.G., Oh, M.H., and Choi, S.H. 2014. Distinct characteristics of OxyR2, a new OxyR-type regulator, ensuring expression of Peroxiredoxin 2 detoxifying low levels of hydrogen peroxide in *Vibrio vulnificus*. Mol. Microbiol. *93*, 992-1009.

Kim, Y.R., Lee, S.E., Kook, H., Yeom, J.A., Na, H.S., Kim, S.Y., Chung, S.S., Choy, H.E., and Rhee, J.H. 2008. *Vibrio vulnificus* RTX toxin kills host cells only after contact of the bacteria with host cells. Cell Microbiol. *10*, 848-862.

Kwon, K.B., Yang, J.Y., Ryu, D.G., Rho, H.W., Kim, J.S., Park, J.W., Kim, H.R., and Park, B.H. 2001. *Vibrio vulnificus* cytolysin induces superoxide anion-initiated apoptotic signaling pathway in human ECV304 cells. J. Biol. Chem. *276*, 47518-47523.

Lee, B.C., Kim, S.H., Choi, S.H., and Kim, T.S. 2005. Induction of interleukin-8 production via nuclear factor-kappaB activation in human intestinal epithelial cells infected with *Vibrio vulnificus*. Immunology *115*, 506-515.

Lee, C., Lee, S.M., Mukhopadhyay, P., Kim, S.J., Lee, S.C., Ahn, W.S., Yu, M.H., Storz, G., and Ryu, S.E. 2004. Redox regulation of OxyR requires specific disulfide bond formation involving a rapid kinetic reaction path. Nat. Struct. Mol. Biol. *11*,

1179-1185.

Lee, J.H., Kim, M.W., Kim, B.S., Kim, S.M., Lee, B.C., Kim, T.S., and Choi, S.H. 2007. Identification and characterization of the *Vibrio vulnificus rtxA* essential for cytotoxicity *in vitro* and virulence in mice. J. Microbiol. *45*, 146-152.

Lemire, J.A., Harrison, J.J., and Turner, R.J. 2013. Antimicrobial activity of metals: mechanisms, molecular targets and applications. Nat. Rev. Microbiol. *11*, 371-384.

Lim, J.G., Bang, Y.J., and Choi, S.H. 2014. Characterization of the *Vibrio vulnificus* 1-Cys peroxiredoxin Prx3 and regulation of its expression by the Fe-S cluster regulator IscR in response to oxidative stress and iron starvation. J. Biol. Chem. *289*, 36263-36274.

Lim, J.G., and Choi, S.H. 2014. IscR is a global regulator essential for pathogenesis of *Vibrio vulnificus* and induced by host cells. Infect. Immun. *82*, 569-578.

Linkous, D.A., and Oliver, J.D. 1999. Pathogenesis of *Vibrio vulnificus*. FEMS Microbiol. Lett. *174*, 207-214.

Liu, L., Hausladen, A., Zeng, M., Que, L., Heitman, J., and Stamler, J.S. 2001. A metabolic enzyme for *S*-nitrosothiol conserved from bacteria to humans. Nature *410*, 490-494.

Marco-Noales, E., Milán, M., Fouz, B., Sanjuán, E., Amaro, C. 2001. Transmission to eels, portals of entry, and putative reservoirs of *Vibrio vulnificus* serovar E (biotype 2). Appl. Environ. Microbiol. *67*, 4717-4725.

McPherson, V.L., Watts, J.A.,Simpson. L.M., and Oliver J.D. 1991. Physiological effects of the lipopolysaccharide of *Vibrio vulnificus* on mice and rats. Microbios. *67*, 272-273

Merkel, S.M., Alexander, S., Zufall, E., Oliver, J.D., and Huet-Hudson, Y.M. 2001. Essential role for estrogen in protection against *Vibrio vulnificus*-induced endotoxic shock. Infect. Immun. *69*, 6119-6122.

Miller, R.A., and Britigan, B.E. 1997. Role of oxidants in microbial pathophysiology. Clin. Microbiol. Rev. *10*, 1-18.

Miller, V.L., and Mekalanos, J.J. 1988. A novel suicide vector and its use in construction of insertion mutations: osmoregulation of outer membrane proteins and virulence determinants in *Vibrio cholerae* requires *toxR*. J. Bacteriol. *170*, 2575-2583.

Mills, P.C., Rowley, G., Spiro, S., Hinton, J.C., and Richardson, D.J. 2008. A combination of cytochrome c nitrite reductase (NrfA) and flavorubredoxin (NorV) protects *Salmonella enterica* serovar Typhimurium against killing by NO in anoxic environments. Microbiology *154*, 1218-1228.

Milton, D.L., O'Toole, R., Horstedt, P., and Wolf-Watz, H. 1996. Flagellin A is essential for the virulence of *Vibrio anguillarum*. J. Bacteriol. *178*, 1310-1319.

Mishra, S., and Imlay, J. 2012. Why do bacteria use so many enzymes to scavenge hydrogen peroxide? Arch. Biochem. Biophys. *525*, 145-160.

Nakhamchik, A., Wilde, C., and Rowe-Magnus, D.A. 2008. Cyclic-di-GMP regulates extracellular polysaccharide production, biofilm formation, and rugose colony development by *Vibrio vulnificus*. Appl. Environ. Microbiol. *74*, 4199-4209.

Nathan, C., and Shiloh, M.U. 2000. Reactive oxygen and nitrogen intermediates in the relationship between mammalian hosts and microbial pathogens. Proc. Natl. Acad. Sci. U. S. A. *97*, 8841-8848.

Nathan, C.F., and Hibbs, J.B., Jr. 1991. Role of nitric oxide synthesis in macrophage antimicrobial activity. Curr. Opin. Immunol. *3*, 65-70.

Nurhasni, H., Cao, J., Choi, M., Kim, I., Lee, B.L., Jung, Y., and Yoo, J.W. 2015. Nitric oxide-releasing poly(lactic-*co*-glycolic acid)-polyethylenimine nanoparticles for prolonged nitric oxide release, antibacterial efficacy, and *in vivo* wound healing activity. Int. J. Nanomedicine *10*, 3065-3080.

Ogusucu, R., Rettori, D., Munhoz, D.C., Netto, L.E., and Augusto, O. 2007. Reactions of yeast thioredoxin peroxidases I and II with hydrogen peroxide and peroxynitrite: rate constants by competitive kinetics. Free Radic. Biol. Med. *42*, 326-334.

Oliver, J.D. 2005. Wound infections caused by *Vibrio vulnificus* and other marine bacteria. Epidemiol. Infect. *133*, 383-391.

Oliver, J.D. 2013. *Vibrio vulnificus*: death on the half shell. A personal journey with the pathogen and its ecology. Microb. Ecol. *65*, 793-799.

Oliver, J.D. 2015. The Biology of *Vibrio vulnificus*. Microbiol. Spectr. *3*.

Osaka, K., Komatsuzaki, M., Takahashi, H., Sakano, S., and Okabe, N. 2004. *Vibrio vulnificus* septicaemia in Japan: an estimated number of infections and physicians' knowledge of the syndrome. Epidemiol. Infect. *132*, 993-996.

Paranjpye, R.N., Lara, J.C., Pepe, J.C., Pepe, C.M., and Strom, M.S. 1998. The type IV leader peptidase/N-methyltransferase of *Vibrio vulnificus* controls factors required for adherence to HEp-2 cells and virulence in iron-overloaded mice. Infect. Immun. *66*, 5659-5668.

Paranjpye, R.N. and Strom, M.S. 2005. A *Vibrio vulnificus* type IV pilin contributes to biofilm formation, adherence to epithelial cells, and virulence. Infect. Immun. *73*, 1411-1422.

Park, K.J., Kang, M.J., Kim, S.H., Lee, H.J., Lim, J.K., Choi, S.H., Park, S.J., and Lee, K.H. 2004. Isolation and characterization of *rpoS* from a pathogenic bacterium, *Vibrio vulnificus*: role of sigmaS in survival of exponential-phase cells under oxidative stress. J. Bacteriol. *186*, 3304-3312.

Poole, R.K., Anjum, M.F., Membrillo-Hernandez, J., Kim, S.O., Hughes, M.N., and Stewart, V. 1996. Nitric oxide, nitrite, and Fnr regulation of *hmp* (flavohemoglobin) gene expression in *Escherichia coli* K-12. J. Bacteriol. *178*, 5487-5492.

Richardson, A.R., Dunman, P.M., and Fang, F.C. 2006. The nitrosative stress response of *Staphylococcus aureus* is required for resistance to innate immunity. Mol. Microbiol. *61*, 927-939.

Sainsbury, S., Ren, J., Nettleship, J.E., Saunders, N.J., Stuart, D.I., and Owens, R.J. 2010. The structure of a reduced form of OxyR from *Neisseria meningitidis*. BMC Struct. Biol. *10*, 10.

Satchell, K.J. 2015. Multifunctional-autoprocessing repeat-in-toxin (MARTX)

toxins of *Vibrios*. Microbiol. Spectr. *3*, VE-0002-2014

Schell, M.A. 1993. Molecular biology of the LysR family of transcriptional regulators. Annu. Rev. Microbiol. *47*, 597-626.

Shepherd, M., Bernhardt, P.V., and Poole, R.K. 2011. Globin-mediated nitric oxide detoxification in the foodborne pathogenic bacterium *Campylobacter jejuni* proceeds via a dioxygenase or denitrosylase mechanism. Nitric Oxide *25*, 229-233.

Simon, R., Priefer, U., and Puhler, A. 1983. A Broad Host Range Mobilization System for *In vivo* Genetic-Engineering - Transposon Mutagenesis in Gram Negative Bacteria. Bio-Technol. *1*, 784-791.

Simpson, L.M., and Oliver, J.D. 1983. Siderophore production by *Vibrio vulnificus*. Infect. Immun. *41*, 644-649.

Simpson, L.M., White, V.K., Zane, S.F., and Oliver, J.D. 1987. Correlation between virulence and colony morphology in *Vibrio vulnificus*. Infect. Immun. *55*, 269-272.

Smagghe, B.J., Trent, J.T., 3rd, and Hargrove, M.S. 2008. NO dioxygenase activity in hemoglobins is ubiquitous *in vitro*, but limited by reduction *in vivo*. PLoS One *3*, e2039.

Sobko, T., Reinders, C.I., Jansson, E., Norin, E., Midtvedt, T., and Lundberg, J.O. 2005. Gastrointestinal bacteria generate nitric oxide from nitrate and nitrite. Nitric Oxide *13*, 272-278.

Stadtman, E.R. 2001. Protein oxidation in aging and age-related diseases. Ann. N.

Y. Acad. Sci. *928*, 22-38.

Stelma, G.N., Jr., Reyes, A.L., Peeler, J.T., Johnson, C.H., and Spaulding, P.L. 1992. Virulence characteristics of clinical and environmental isolates of *Vibrio vulnificus*. Appl. Environ. Microbiol. *58*, 2776-2782.

Stern, A.M., Hay, A.J., Liu, Z., Desland, F.A., Zhang, J., Zhong, Z., and Zhu, J. 2012. The NorR regulon is critical for *Vibrio cholerae* resistance to nitric oxide and sustained colonization of the intestines. MBio *3*, e00013-00012.

Stern, A.M., and Zhu, J. 2014. An introduction to nitric oxide sensing and response in bacteria. Adv. Appl. Microbiol. *87*, 187-220.

Storz, G., and Hengge-Aronis, R. 2000. *Bacterial stress responses* (Washington, D.C.: ASM Press).

Storz, G., and Imlay, J.A. 1999. Oxidative stress. Curr. Opin. Microbiol. *2*, 188-194.

Strom, M.S., and Paranjpye, R.N. 2000. Epidemiology and pathogenesis of *Vibrio vulnificus*. Microbes Infect. *2*, 177-188.

Svintradze, D.V., Peterson, D.L., Collazo-Santiago, E.A., Lewis, J.P., and Wright, H.T. 2013. Structures of the *Porphyromonas gingivalis* OxyR regulatory domain explain differences in expression of the OxyR regulon in *Escherichia coli* and *P. gingivalis*. Acta. Crystallogr. D. Biol. Crystallogr. *69*, 2091-2103.

Toledo, J.C., Jr., and Augusto, O. 2012. Connecting the chemical and biological properties of nitric oxide. Chem. Res. Toxicol. *25*, 975-989.

Walker, G., Pfeilschifter, J., and Kunz, D. 1997. Mechanisms of suppression of inducible nitric-oxide synthase (iNOS) expression in interferon (IFN)-gamma-stimulated RAW 264.7 cells by dexamethasone. Evidence for glucocorticoid-induced degradation of iNOS protein by calpain as a key step in post-transcriptional regulation. J. Biol. Chem. *272*, 16679-16687.

Webster, A.C., and Litwin, C.M. 2000. Cloning and characterization of *vuuA*, a gene encoding the *Vibrio vulnificus* ferric vulnibactin receptor. Infect. Immun. *68*, 526-534.

Weinberg, E.D. 1978. Iron and infection. Microbiol. Rev. *42*, 45-66.

Winn, M.D., Ballard, C.C., Cowtan, K.D., Dodson, E.J., Emsley, P., Evans, P.R., Keegan, R.M., Krissinel, E.B., Leslie, A.G., McCoy, A., *et al.* 2011. Overview of the CCP4 suite and current developments. Acta. Crystallogr. D. Biol. Crystallogr. *67*, 235-242.

Winterbourn, C.C., and Peskin, A.V. 2016. Kinetic Approaches to Measuring Peroxiredoxin Reactivity. Mol. Cells *39*, 26-30.

Wright, A.C., Hill, R.T., Johnson, J.A., Roghman, M.C., Colwell, R.R., and Morris, J.G., Jr. 1996. Distribution of *Vibrio vulnificus* in the Chesapeake Bay. Appl. Environ. Microbiol. *62*, 717-724.

Wright, A.C., and Morris, J.G., Jr. 1991. The extracellular cytolysin of *Vibrio vulnificus*: inactivation and relationship to virulence in mice. Infect. Immun. *59*, 192-197.

Wright, A.C., Powell, J.L., Kaper, J.B., and Morris, J.G., Jr. 2001. Identification of a group 1-like capsular polysaccharide operon for *Vibrio vulnificus*. Infect. Immun. *69*, 6893-6901.

Wright, A.C., Powell, J.L., Tanner, M.K., Ensor, L.A., Karpas, A.B., Morris, J.G., Jr., and Sztein, M.B. 1999. Differential expression of *Vibrio vulnificus* capsular polysaccharide. Infect. Immun. *67*, 2250-2257.

Wright, A.C., Simpson, L.M., and Oliver, J.D. 1981. Role of iron in the pathogenesis of *Vibrio vulnificus* infections. Infect. Immun. *34*, 503-507.

Yoshida, S., Ogawa, M., and Mizuguchi, Y. 1985. Relation of capsular materials and colony opacity to virulence of *Vibrio vulnificus*. Infect. Immun. *47*, 446-451.

Zwart, P.H., Afonine, P.V., Grosse-Kunstleve, R.W., Hung, L.W., Ioerger, T.R., McCoy, A.J., McKee, E., Moriarty, N.W., Read, R.J., Sacchettini, J.C., *et al.* 2008. Automated structure solution with the PHENIX suite. Methods Mol. Biol. *426*, 419-435.

국문초록

패혈증 비브리오균은 가벼운 장염에서부터 생명을 위협하는 패혈증까지 유발하는 기회 감염성 병원성 미생물이다. 패혈증 비브리오균의 숙주 감염시, 숙주세포의 내재면역계의 면역반응을 통한 활성산소종 (ROS) 와 활성질소종 (RNS)의 발생에 의하여 유발되는 산화 스트레스는 패혈증 비브리오균의 DNA 및 단백질 등에 손상을 입혀 패혈증 비브리오균의 생존을 위협하게 된다. 그러므로 산화 스트레스를 극복하는 것은 패혈증 비브리오균의 숙주 내 생존뿐만 아니라 성공적인 감염에 매우 중요한 역할을 한다.

본 연구에서는 패혈증 비브리오균이 산화 스트레스에 대응하여 생존하는 전략을 이해하기 위하여, 먼저 낮은 H_2O_2 농도를 인지하는 OxyR2 전사조절자를 분자 수준에서 조절기작 및 구조적인 특성을 분석하였다. 패혈증 비브리오균은 LysR-타입 전사조절자인 OxyR 을 두 개 가지고 있으며, 이 중 OxyR2 는 OxyR1 에 비해 더 낮은 수준의 H_2O_2 를 인지하는 것으로 알려져 있다. OxyR2 는 두 개의 보존된 산화-환원 인지 시스테인 잔기를 가지고 있으며, 이 산화-환원 인지 시스테인 이 H_2O_2

에 의해 산화되면 분자간 이황화결합을 생성하며, 이렇게 활성화된 OxyR2 는 항산화 단백질인 Prx2 를 발현시켜 H_2O_2 를 제거한다. 생화학적 연구를 통해 높은 농도의 H_2O_2 조건에서는 OxyR2 의 산화-환원 인지 시스테인 이 단순 산화로 그치지 않고 과산화(overoxidized) 되어 설폰화 시스테인이 (Cys-SO_3H) 이 된다는 세번째 산화-환원 단계를 가짐을 밝혀내었으며, 이렇게 과산화된 OxyR2 는 *prx2*의 전사를 더 이상 발현시키지 못한다는 것을 알아내었다. 이 발견은 OxyR2 가 세가지의 산화-환원 스위치를 통해 *prx2* 의 발현을 세밀히 조절함으로써 세포 내 과도한 Prx2 의 생성을 막아 세포 내 주요 구성물질의 낭비를 막는다는 사실을 밝혀냄에 큰 의미가 있다. 또한, OxyR2 결정구조 분석을 통해 하여 OxyR2 만이 가지고 있는 특징적인 Glu204 잔기가 다른 OxyR 와는 다른 OxyR2의 높은 H_2O_2 인지능력에 영향을 미침을 확인할 수 있었다. Glu204 주변 펩티드결합의 구성이 H_2O_2 와 직접 상호작용하는 His205 의 구조적인 경직성에 영향을 미쳐 OxyR2 가 다른 OxyR 들이 인지하는 것보다 훨씬 낮은 농도의 H_2O_2 조건에서 OxyR2 의 산화-환원 인지 시스테인이 산화 혹은 과산화 되어 Prx2 의 발현을 조절한다는 사실을 밝혀내었다.

활성질소종 (RNS) 이 유발하는 산화 스트레스에 패혈증 비브리오균이 대응하는 전략을 이해하기 위하여, 패혈증 비브리오균이 일산화질소 (NO) 에 노출되었을 때 전사체의 변화를 RNA-sequencing 기법을 통해 분석 하였다. 각 유전자의 발현량을 비교분석한 결과, 특징적으로 발현이 증가 혹은 감소하는 551 개의 유전자를 동정하였다. 전사체 분석 결과로부터, 가장 발현량이 크게 증가하는 *Vv*HmpA 라는 단백질에 대하여 특성 규명을 진행하였다. 생화학적인 연구를 통하여 *Vv*HmpA 가 FAD 와 heme 을 보조인자로 가지는 NO-inducible flavohemoglobin 임을 확인하였다. *Vv*HmpA 의 효소활성을 측정한 결과 *Vv*HmpA 가 단백질 수준에서 일산화질소를 효과적으로 제거한다는 사실을 밝혀내었고, 특징적으로 패혈증비브리오균 의 최적생장온도인 30 ° C 보다 숙주 내 환경과 유사한 37 ° C 온도조건에서 더 효과적으로 일산화질소를 제거한다는 사실을 알 수 있었다. *Vv*HmpA 의 기능을 더 자세히 살펴보고자 *Vv*hmpA 유전자가 결여된 돌연변이체를 제작하였으며, *VvhmpA* 유전자가 결여된 균주는 외부로부터 제공된 일산화질소를 거의 제거하지 못하였다. 또한 *VvhmpA* 유전자가 결여된 균주는 일산화질소가 존재하는 환경에서 생장이 저해되었다. 이를 통해 *Vv*HmpA 가 패혈증비브리오균

의 일산화질소 방어기작에 상당히 기여함을 알 수 있었다. 더불어, *VvhmpA* 결여 균주는 숙주 면역세포인 대식세포에 대한 세포독성 및 대식세포에 대한 생존률이 유의미하게 저하되는 현상을 보였으며, 쥐 실험을 통해 *VvhmpA* 결여 균주는 정상 균주 대비하여 유의미하게 낮은 병원성을 나타낸다는 사실을 확인하였다. 위 결과들을 종합해 볼 때, *Vv*HmpA 는 패혈증 비브리오균이 숙주 내에서 마주할 수 있는 일산화질소를 제거함으로써 패혈증 비브리오균이 숙주 내에서 생존하고 병원성을 발현하는데 중요한 역할을 하는 것으로 판단할 수 있다.

OxyR2 와 *Vv*HmpA 에 관한 본 연구를 통해 숙주 유래 산화 스트레스를 패혈증 비브리오균이 어떻게 대응하는 지에 대한 이해를 증진시킬 수 있었다. 따라서 본 연구는 이러한 이해를 바탕으로 패혈증 비브리오균의 효과적인 제어 방안을 강구하는데 많은 도움을 줄 수 있을 것이다.